DISTURBANCE ACCOMMODATING CONTROL OF AN AUTOMOTIVE TRANSMISSION TORQUE CONVERTER CLUTCH SYSTEM

by

TODD ADDISON PERKINS

A dissertation submitted in partial fulfillment of the
requirements for the degree of

DOCTOR OF PHILOSOPHY IN ELECTRICAL AND COMPUTER ENGINEERING

2024

Oakland University, Rochester, Michigan

Doctorial Advisory Committee:

Manohar Das, Ph.D., Chair
Chris Kobus, Ph.D.
Richard Olawoyin, Ph.D.
S. Ali Arefifar, Ph.D.
Kasaundra Tomlin, Ph.D.

ACKNOWLEDGMENTS

I want to thank God for giving me the inspiration and gifts to pursue my PhD. And equally important I want to thank my family for their higher education examples, encouragement, and supporting me during this process. To Professor Das and my dissertation committee for their guidance, support, and insights.

I would like to give special thanks to my mother & friends for their editing and my niece Kennedy Perkins for her original illustrations.

Finally, I want to thank my community Dr. Tony Ross, Dr. Sami Oweis, Dr. Samon Omekanda, and Dr. Brinda Lewis.

ABSTRACT

MODELING AND CONTROL OF AN AUTOMOTIVE TRANSMISSION TORQUE CONVERTER CLUTCH SYSTEM

by

TODD ADDISON PERKINS

Adviser: Manohar Das, Ph.D.,

Modern automotive drivelines are facing increasing pressure to improve overall efficiency while maintaining vehicle comfort and performance. This thesis presents several new ways to control the torque converter clutch in an automotive automatic transmission in such a way they improve driveline system efficiency while maintaining its comfort. This efficiency improvement is accomplished by extending the clutch's application conditions to a lower speed where the environment is harsher than is possible with the current class of controllers.

Three new model-based methods are evaluated on their ability to control the simplified model of a torque converter clutch. These controllers include one-step-ahead and complex observe based controller methods. These controllers are applied in the presence of large disturbances that include parameter uncertainties and unmeasured state errors to evaluate their robustness in these environments. The lack of clean sensor measurements highlights the limitations of the one-step-ahead method and are demonstrated by the controller's inability to maintain system regulation in this high noise environment. Because it is not practical to accurately measure the torques and internal speeds of the torque converter system, this research addresses this by estimating them using observers.

Using these new observer-based-control methods, this dissertation presents the simulation results that demonstrate this method provides a significant increase in robustness to disturbances. The precise and smooth tracking of the regulator's setpoints highlights the system's ability to meet the powertrain's comfort and economy targets, while being practical enough to be implemented in current automotive systems.

TABLE OF CONTENTS

TABLE OF CONTENTS – CONTINUED

LIST OF TABLES

LIST OF FIGURES

CHAPTER ONE

INTRODUCTION

Since the introduction of mass-market automobiles in the early 20^{th} century, engineers have been evolving the powertrain's balance between efficiency, performance, and comfort. Second only to the widespread adaptation of electronic fuel injection control of internal combustion engines of the 1990s, the evolution of control of automatic transmissions has had the biggest impact in the automotive powertrain. After their introduction into the market during the 1940s, they have steadily grown in market share and complexity. The term Automatic Transmission refers to an automatically shifting device that connects the engine to the final drive of the vehicle. The main components inside a modern transmission are a torque converter and a planetary fixed ratio transmission as shown in Figure 1.1.

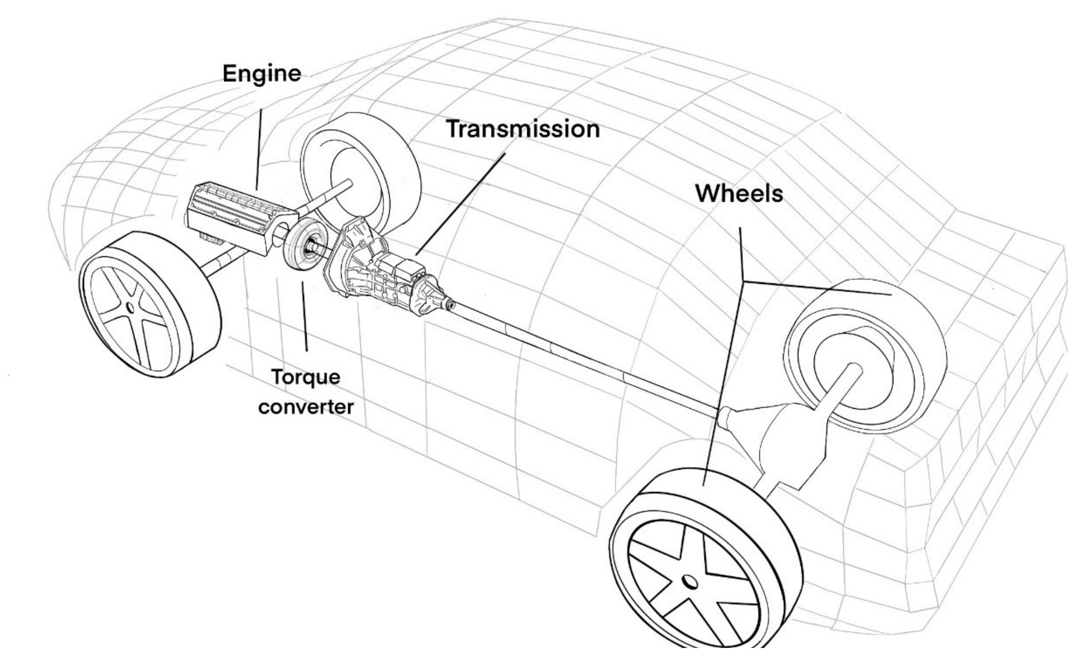

Figure 1.1 - Rear Wheel Drive Vehicle Drive Line

1.1 Torque Converters

Inside the Torque Converter's (TC's) housing, the input torque is directly connected to the impeller in a bath of automatic transmission fluid. For clarity, this impeller, or drive rotor, is often referred to as the TC's pump. The TC's drive rotor, often called the turbine, is directly connected to the case and is driven by the fluid coming from the pump. Rotating along the same axes as the pump and turbine and hydraulically coupled to them, is the stator rotor. Under certain conditions outlined below, the stator redirects the angle pump's hydraulic flow to the turbine to increase the torque acting on the turbine. This hydraulically controlled mechanical clutch directly connects the TC input torque to the case output. This eliminates the torque path, including its damping effects and lower efficiency, through the fluid coupling rotors. For simplification, the drive rotor, driven rotor, and clutch are shown in Figure 1.2.

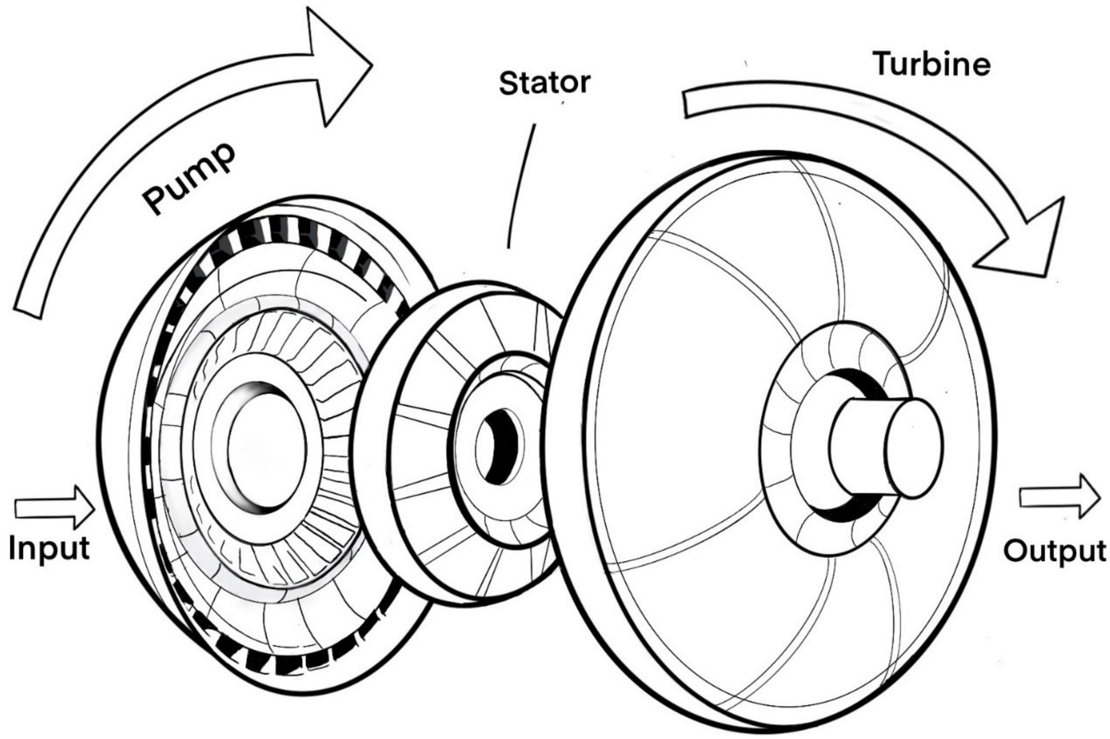

Figure 1.2 - Torque Converter with Lock-up Clutch

Neglecting the small system losses, the TC system's input power is a function of the input torque and pump speed is equal to the output power which is a function of its output torque and turbine speed.

With an understanding of the physical elements, attention can be focused on the TC's four modes of operation. They are torque multiplication, coupled, slip, and locked modes. When the TC is used in reverse, when the speed of the drive rotor is less than the speed of driven rotor, they behave in the same way as when the drive rotor speed is greater than the driven rotor and are not considered in this research.

The first mode, torque multiplication, is defined as when the turbine speed is less than 90% of the pump speed and the Torque Converter Clutch (TCC) is open (not being applied). During this mode, about 90% of the input power is transmitted to the output and the rest is lost to heat. Despite this 10% loss in efficiency, this mode is extensively used during the vehicle's launch because it can multiply the torque input by two to three times to accelerate the vehicle more quickly. This mode provides a high degree of fluid damping that reduces the engine's inherently impulsive torque out from the rest of the vehicle's driveline.

The second mode, coupled, is when the turbine speed of the TC is 90 to 100% of the pump speed and the TCC is not applied. While in coupled mode the TC output's speed and torque of the drive and driven rotors are nearly equal making the system's efficiency to over 95%. This mode still provides a great deal of impulse isolation between the input and output. Before the introduction of TCCs this mode was often used during vehicle cruising to improve efficiency.

The third TC mode is locked when the TCC mechanical couples the drive rotor to the driven rotor. When the input and output speeds are the same, the TC transmits almost all its input power to its output giving it almost 100% efficiency. The minor losses are friction and the small load on the hydraulic pump required to keep the TCC closed. Locked mode saw widespread adoption during the 1980s with the increasing fuel economy requirements of the time. The high efficiency is not without its tradeoffs. It also transmits nearly 100% of the engine's input torque disturbances to the vehicle's drivetrain creating a harsh feel to the vehicle. Because of these disturbances, engineers restrict the implementation of this mode to higher engine speeds and higher transmission gears where the impulses are less pronounced and mechanically dampened by the drivetrain system.

The fourth mode is called slip mode. This mode is similar to the locked mode in that the TCC mechanically couples the input to the output of the TC however the slip mode only partially applies the TCC. This partial application allows the TC's output torque to be carried by both the TCC and the TC fluid coupling. By the proliferation of electronically controlled transmissions in the early 2010's, automotive engineers were able to regulate the TCCs input to output slip speed to a fixed amount. This breakthrough allows the TC, as a system, the high efficiency of the equal input and output speeds while maintaining the input torque pulses dampening effects of a coupled torque converter. This mode is of great interest to this research because it allows for even greater vehicle efficiency by applying slip mode at lower speed and in lower gears than the locked mode was previously available without the harshness penalties. This lower speed application allows for the application of the TCC in great driving conditions though improving the vehicle's overall efficiency.

1.2 Literature Review

Torque Converter Clutch Slip Control has been one of the solutions vehicle manufactures have implemented since the early 2000s to address the ever-increasing demand for improved powertrain efficiency without sacrificing driving comfort of the smaller displacement engines [1], [2], [3]. In response automotive designers introduced a new mode of TCC operation called slip mode. Slip mode is when the TCC is partially applied such that the input and output speeds of the TC are controlled to a set differential speed, $\Delta\omega$ [4], [5], [6], [7], [8], [9], [10]. By allowing 25 to 100 RPM of slip in the TC the torque impulses from the engine can be dampened and not passed on to the rest of the gearbox. Isolating these impulses gives the vehicle a much-improved vehicle feel [11], [12].

Torque converter models are often used for control of the application of their clutches. These models are typically very nonlinear systems with lots of parameter uncertainty and unmodeled disturbances included in their equations [13], [14], [15]. These models generally agree with using a four-state system of equations for the pump speed, stator speed, turbine speed and fluid flow then adding a system input to model the application of the TCC [13], [16]. Additional models examined in this dissertation are based on the publications [17], [18]. The four fundamental mass-inertia ordinary differential equations (ODE)s were well established by Lee and Lee [14] and [19]. The equations from these papers are supplemented by the fundamental friction disk clutch equations introduced by Bai, Maguire and Peng [20].

Many of the physical properties of the TC are difficult to measure and model which makes this control problem more complex. The effects of these unknown modeling parameters are presented in publications by Jang, Lee and Kim [21]; Buechel and Knoll [22] ; and the parametric sensitive paper by Asl, Azad and McPhee [17]. Using these references, the four ODEs created are presented in Chapter 2 of this dissertation.

This dissertation introduces three new methods of TCC slip mode control and compare their reference tracking and robustness to disturbances. In the past, many designers opted for hybrid or switch mode controllers to regulate the TCC slip however these were not further researched because of their computational complexity and hardware system requirements. Those control schemes include switch mode/closed-loop [23], pre-compensator/feedback control [24], predictive control [25], and scheduled servo control based on turbine speed [26]. Other methods include implementations of Kalman Filters [22], [27] and Fuzzy Logic controllers [28] however these require considerable computation resources that may not be practical in today's automotive networks. Other methods include Silva [5] using PI controllers and Hebbale's static models utilizing lookup tables [29]. They are very computationally efficient, however did not show promising results for tracking and robustness to unknown state parameters and disturbances. Hibino's paper [8] provides a comprehensive review of PI, sliding mode, LQR and H_∞ controllers applied to TCC slip control. Other methods included gain scheduling [30] however it did not provide the fidelity necessary to regulate the TCC in slip mode.

This dissertation's research focuses on two basic types of controllers. The first methods were One Step Ahead (OSA) based schemes. They included adaption [31], weighting [32], and prediction control [33]. These controllers relied heavily on the methods presented by Goodwin [34] and Lazar, Poli and Schonberger's contribution on control weighting OSA [35]. Some of the results of this research were published in [36].

A new method of TCC slip control presented in this dissertation uses Disturbance Observer Based Control (DOBC) and an observer to perform active cancelation of the disturbances[27], [37]. This method of control is separated into two types of disturbance observers. The first method, D-DOBC estimates the state $[\hat{x}(t)]$ separately from the disturbances $[\hat{d}(t)]$. This type of controller uses the state observer to model the disturbance then feeds it back into the plant input to cancel the disturbance effects on the system. Johnson [38], [39], [40] called this method of active cancellation Disturbance Accommodating Controller.

The second type of DOBC is called I-DOBC. This method differs from D-DOBC in that the state and disturbances are modeled together as a single observer $[\hat{x} + \hat{d}]$. This method was presented in Trinh's Book [41]. Much of this work can be credited to Darouach who refers to these disturbances as unmodeled inputs [42], [43], [44] or Gomez-Penate who calls them unknow input observers [45]. This method asserts that this control problem can be solved by treating the problem as a system with unknown inputs then applying a reduced order observer to control the plant. One of the advantages of this control scheme is that little information needs to be known about the state disturbance input because it is not separately modeled from the plant output. A tradeoff for this simplicity that will be evaluated is how much care must be taken in designing a noise canceling controller to make it robust enough to counteract these disturbances yet not degrade the desired output.

A larger body of active Disturbance-Observer-Based Control (DOBC) controllers from simple linear system to more complex nonlinear systems is reviewed by Ding [46], Nazari [47], Yang [48] and Tomei [49]. A comprehensive overview was published by Chen, Yang, Guo and Li [50].

Published work done by this researcher include observers, OSA and DOBC observer-based feedback control method for TCC slip control [36], [51], [52].

1.3 Contributions of this Dissertation

The control problem addressed in this dissertation concerns operating an automotive automatic transmission TCC in low engine RPM slip mode. Currently engineers either limit the operation of slip mode to higher speeds to guarantee the TCC does completely close (Locked Mode) where the input and output speeds are the same or the TCC runs away (Coupled Mode) and no longer tracks the desired slip speed delta. The former would cause powertrain harshness and the latter introduces additional powertrain inefficiencies.

The new contributions in this dissertation are as follows:

- The first contribution of this research concerns presentation of simplified linear model of the TC system with integrated TCC and model validation.
- The second contribution is utilization of the TCC's electrically controlled capacity clutch (ECCC) [53] to control the slip of a linear model of a TC. Three types of disturbance accommodating TCC controllers are designed and studied:
    - A disturbance accommodating discrete one step ahead controller (DOPC)
    - A direct disturbance observer-based controller (D-DOBC)
    - An indirect disturbance observer-based controller (I-DOBC)
- Finally, the performance of the above three controllers are compared and their ability to regulate the clutch slip from 25 to 50 RPM in disturbances ranging from 0% to 100% of the TC input speed are evaluated.

1.4 Dissertation Outline

This dissertation is organized into seven chapters as follows:

- Chapter 1 includes an introduction to the research problem, a literature review of the previous work on the topic, and discusses the control problem studied in this dissertation as related to the larger body of work.
- Chapter 2 presents the foundation of the TC and TCC nonlinear models, their linearization, and validation of the linear model used for controller design.
- Chapter 3 introduces a series of One Step Ahead (OSA) linear controllers to solve the TCC slip mode control problem.
- Chapter 4 introduces a D-DOBC controller with an in-depth analysis of how they are created, how it is implemented on the TCC control problem and the results of this author's research on them.
- Chapter 5 presents an I-DOBC controller. This chapter explains the difference between D-DOBC and I-DOBC along with a discussion of how it is implemented and the results of applying it to the control problem.
- Chapter 6 presents the results of a comparative study of the disturbance accommodating controllers introduced in Chapters 3 through 6.
- Chapter 7 Conclusions and suggestions for future work are presented.

CHAPTER TWO

A SIMPLIFIED TORQUE CONVERTER MODEL & MODEL VALIDATION

2.1 Introduction

To begin with, this chapter introduces a set of nonlinear mathematical equations that form the basis of the automotive automatic transmission TC fluid coupling model researched in this dissertation. The author expands these equations to include the TCC to model the full TC system during slip mode operation . A series of steps are presented here to demonstrate how to reduce the original nonlinear plant to a linear model of state equations. This model is then discretized for use with the DOPC controllers. Finally, the linear and discreate models are validated against the aforementioned nonlinear TC plant, including the TCC equations, to demonstrate that they exhibit similar steady state and dynamic performance characteristics with sufficient fidelity.

The foundation of the mathematical model of this TC research has its roots in the work of Ishihara and Emori [1], Kotwicki [2], and Hrovat [3]. This work is continued in a series of papers by Adibi Asl [4]-[6]. They use a four-state nonlinear ordinary differential system of equations (ODE) in the mass-acceleration format. These equations were modified in this dissertation to include the additional torque input from the TCC by including a friction clutch model derived from Rong [7] and Bai, Maguire, and Peng [8] creating a nonlinear multiple-input-multiple-output (MIMO) system of equations (SoE).

This system has:

- Four state variables
- Five time-varying inputs
- Three system outputs.

The states are the pump speed (directly connected to the engine), the stator speed (internal to the TC), the turbine speed (directly connected to the gear box), and the internal TC fluid flow rate. The five inputs to the system are the pump torque, turbine torque, stator torque, TCC torque acting on the pump, and TCC torque acting on the turbine. The outputs are the pump, stator, and turbine speeds.

2.2 A Nonlinear Model of the Torque Converter System and Model Parameters:

This dissertation's research of a TC is based on a nonlinear TC system model presented in [54] summarized in equation (2.1) – (2.4) below:

$$\mathrm{I_p}\dot{\omega}_\mathrm{p}(\mathrm{t}) + \rho \mathrm{S_p}\dot{\mathrm{Q}}(\mathrm{t}) = -\rho\left(\omega_\mathrm{p}(\mathrm{t})\mathrm{R_p^2} + \frac{\mathrm{R_p Q(t)}}{\mathrm{FlowArea}}\tan\left(\mathrm{a_p}\right) - \omega_\mathrm{s}(\mathrm{t})\mathrm{R_s^2} - \frac{\mathrm{R_s Q(t)}}{\mathrm{FlowArea}}\tan(\mathrm{a_s})\right)\mathrm{Q(t)} + \mathrm{T_p(t)} \tag{2.1}$$

$$\mathrm{I_t}\dot{\omega}_\mathrm{t}(\mathrm{t}) + \rho \mathrm{S_t}\dot{\mathrm{Q}}(\mathrm{t}) = -\rho\left(\omega_\mathrm{t}(\mathrm{t})\mathrm{R_t^2} + \frac{\mathrm{R_t Q(t)}}{\mathrm{FlowArea}}\tan(\mathrm{a_t}) - \omega_\mathrm{p}(\mathrm{t})\mathrm{R_p^2} - \frac{\mathrm{R_p Q(t)}}{\mathrm{FlowArea}}\tan\left(\mathrm{a_p}\right)\right)\mathrm{Q(t)} - \mathrm{T_t(t)} \tag{2.2}$$

$$\mathrm{I_s}\dot{\omega}_\mathrm{s}(\mathrm{t}) + \rho \mathrm{S_s}\dot{\mathrm{Q}}(\mathrm{t}) = -\rho\left(\omega_\mathrm{s}(\mathrm{t})\mathrm{R_s^2} + \frac{\mathrm{R_s Q(t)}}{\mathrm{FlowArea}}\tan(\mathrm{a_s}) - \omega_\mathrm{t}(\mathrm{t})\mathrm{R_t^2} - \frac{\mathrm{R_t Q(t)}}{\mathrm{FlowArea}}\tan(\mathrm{a_t})\right)\mathrm{Q(t)} + \mathrm{T_s(t)} \tag{2.3}$$

$$\rho\left(S_p\dot{\omega}_p(t) + S_t\dot{\omega}_t(t) + S_s\dot{\omega}_s(t)\right) + \frac{\rho L_f}{\mathrm{FlowArea}}\dot{Q}(t) = \rho\left(R_p^2\left(\omega_p^2(t) - \omega_t(t)\omega_p(t)\right) + R_t^2\left(\omega_t^2(t) - \omega_s(t)\omega_t(t)\right) + R_s^2\left(\omega_s^2(t) - \omega_p(t)\omega_s(t)\right)\right) + \frac{\omega_p(t)Q(t)}{\mathrm{FlowArea}}\rho\left(R_p\tan(a_p) - R_s\tan(a_s)\right) + \frac{\omega_t(t)Q(t)}{\mathrm{FlowArea}}\rho\left(R_t\tan(a_t) - R_p\tan(a_p)\right) + \frac{\omega_s(t)Q(t)}{\mathrm{FlowArea}}\rho\left(R_s\tan(a_s) - R_t\tan(a_t)\right) - P_L \tag{2.4}$$

Although the above model is applicable to any TC system and the TCC controllers introduced in Chapters 3 – 5 of this dissertation are applicable to any TC system in general, a Honda CRV TV system was chosen for the purpose of all illustrations and simulation studies presented in this dissertation. The model parameters pertaining to a Honda CRV TV system are summarized in Table 2.1.

The effects of the TCC acting on the plant is captured by the clutch capacity of the multidisc frictional clutch acting between the pump and turbine as presented by Bai and Aguire [8]. This nonlinear clutch application has a single input, pressure, and two states, the clutch friction coefficient and slip speed, as shown in equation (2.5):

$$T_{CAP} = \mu(t)nr(Ap(t) - F_s) * \tanh\left(\frac{\Delta\omega(t)}{\alpha}\right) \tag{2.5}$$

Table 2.1 - System States, Inputs/Outputs, and Parameters for a Honda CRV TC [54]

Pump Speed (ω_p)	RPM
Turbine Speed (ω_t)	RPM
Stator Speed (ω_s)	RPM
Fluid Flow (Q)	m^3/sec
Fluid density (ρ)	840 kg/m^3
Flow Area (A)	0.0097 m^2
Pump Radius (R_p)	0.11 m
Turbine Radius (R_t)	0.066 m
Stator Radius (R_s)	0.066 m
Pump Exit Angle (a_p)	18.01 deg
Stator Exit Angle (a_t)	-59.04 deg
Stator Exit Angle (a_s)	59.54 deg
Pump Torque (T_P)	Lb-ft
Turbine Torque (T_T)	Lb-ft
Stator Torque (T_S)	Lb-ft
TCC Torque (T_{TCC})	Lb-ft
Pump Inertia (I_P)	0.092 kg m^2
Turbine Inertia (I_T)	0.026 kg m^2
Stator Inertia (I_S)	0.012 kg m^2
Fluid Inertia Length (L_f)	0.28 m
Shock Loss Coefficient (C_{sh})	1
Frictional Loss Coefficient (C_f)	0.25
Pump Design Constant (S_P)	-0.001 m^2
Turbine Design Constant (S_T)	-0.00002 m^2
Stator Design Constant (S_S)	0.002 m^2

The T_{CAP} is the torque carrying capacity of the TCC [20] and its parameters are defined in Table 2.2.

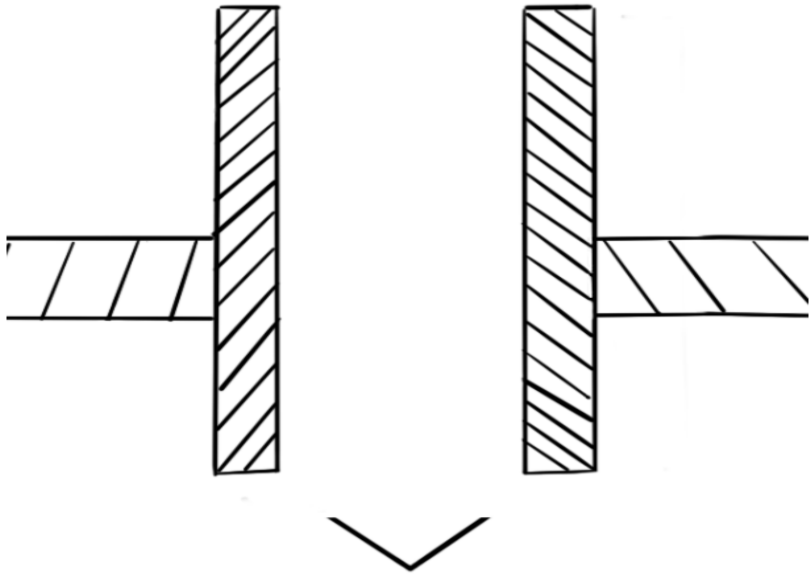

Figure 2.1 - Cross Section of Frictional Clutches [8]

To modify the TC SoE, T_{CAP} is added to the pump torque, T_P, in (2.1) to act as an additional load on the ICE, thus decreasing its speed when applied, and subtracted from the turbine torque, thus reducing the vehicle load and increasing its speed when applied to (2.2). The stator is not connected to the TCC and is free to rotate in slip mode, so it transmits no torque and is not effected by the application of T_{CAP}. Adding the TCC model (2.5) to the TC system of equations (2.1) – (2.2) create a new model of the TC shown in equations (2.6) – (2.9) below, with the system input $p(t)$ for the TCC apply pressure.

Table 2.2 - Parameters of the Torque Converter Clutch

Torque Capacity of the Clutch	$\mathrm{T_{CAP}(t)}$
Friction Coefficient	$\mu(t)$
Number of Friction Surfaces	n
Radius of the Clutch Plate	r
Hydraulic Pressure	p(t)
Slip Delta Speed of the Clutch	$\Delta\omega$
Scaling Factor	α

$$I_p\dot{\omega}_p(t) + \rho S_p\dot{Q}(t) = -\rho\left(\omega_p(t)R_p^2 + \frac{R_pQ(t)}{A}\tan(a_p) - \omega_s(t)R_s^2 - \frac{R_sQ(t)}{A}\tan(a_s)\right)Q(t) + T_p(t) + \mu nr(Ap(t) - F_s)\tanh\left(\frac{\Delta\omega}{\alpha}\right) \tag{2.6}$$

$$I_t\dot{\omega}_t(t) + \rho S_t\dot{Q}(t) = -\rho\left(\omega_t(t)R_t^2 + \frac{R_tQ(t)}{A}\tan(a_t) - \omega_p(t)R_p^2 - \frac{R_pQ(t)}{A}\tan(a_p)\right)Q(t) - T_t(t) + \mu nr(Ap(t) - F_s)\tanh\left(\frac{\Delta\omega}{\alpha}\right) \tag{2.7}$$

$$I_s\dot{\omega}_s(t) + \rho S_s\dot{Q}(t) = -\rho\left(\omega_s(t)R_s^2 + \frac{R_sQ(t)}{A}\tan(a_s) - \omega_t(t)R_t^2 - \frac{R_tQ(t)}{A}\tan(a_t)\right)Q(t) - T_s(t) \tag{2.8}$$

$$\rho\left(S_p\dot{\omega}_p(t) + S_t\dot{\omega}_t(t) + S_s\dot{\omega}_s(t)\right) + \frac{\rho L_f}{A}\dot{Q}(t) = \rho\left(R_p^2\left(\omega_p^2(t) - \omega_t(t)\omega_p(t)\right) + R_t^2(\omega_t^2(t) - \omega_s(t)\omega_t(t)) + R_s^2\left(\omega_s^2 - \omega_p\omega_s\right)\right) + \frac{\omega_pQ(t)}{A}\rho\left(R_p\tan(a_p) - R_s\tan(a_s)\right) + \frac{\omega_t(t)Q(t)}{A}\rho\left(R_t\tan(a_t) - R_p\tan(a_p)\right) + \frac{\omega_s(t)Q(t)}{A}\rho\left(R_s\tan(a_s) - R_t\tan(a_t)\right) - P_L(t) \tag{2.9}$$

2.3 A Simplified Linear Model of the Torque Converter System

Since the above TC system equations are highly nonlinear and too complicated for controller design, this section describes how to reduce the complexity of the above equations and develop a linear model that incorporates a disturbance term to account for the nonlinearities and modeling uncertainties. This is a five-step simplification process of applying some constraints and mathematical manipulations to reduce the model complexity, while retaining the basic characteristics of the original nonlinear model. These steps are:

1. Limit the TC mode
2. Fixing the fluid flow to a steady state value
3. Simplifying the TCC applied torque
4. Replacing the pump and turbine torque input with fixed values
5. Grouping non time-varying parameters

The first step to reduce the complexity of the four-state nonlinear plant model of a TC system involves limiting the operating conditions of the TCC. TCs operate in four modes:

i. Torque multiplication mode $(\omega_t \ll \omega_p)$

ii. Coupled mode $\left(\omega_t > 90\% * \omega_p\right)$

iii. TCC locked mode $(\omega_t = \omega_p)$ and

iv. TCC slip controlled mode $(\omega_p > \omega_t > (\omega_p - 100\text{ RPM}))$.

During coupled and slip modes, the TC's fluid coupling maintains system equilibrium keeping the pump and turbine speed nearly equal. It accomplishes this by using the one-way clutch to disconnect the stator from the TC housing allowing it to rotate with the pump and turbine and enabling the pump, stator, and turbine to turn together. The effect of this is the $T_s = 0$, $\omega_p > \omega_s > \omega_t$, and $T_p = -T_t$. By limiting the TCC controller application to only slip controlled mode, the system's inputs are reduced by setting $T_S = 0$ in equation (2.8).

The second step of the reduction involves replacing the time-varying fluid flow state Q(t) in (2.6) to (2.9) with a fixed value. It has been shown that during this coupled operating mode, and by definition, slip mode, the rate of fluid flow is almost constant at steady state speeds and only varies slightly with pump and turbine speed. These changes in fluid flow are so small when compared to other states that they can be replaced during the slip mode with a constant value This is well documented in [18] and the experimental results in [14]. By fixing the flow rate during TCC slip mode in this dissertation, Q(t) in equations (2.6) – (2.9) is replaced by the constant 0.032 meter^3/sec flow rate and $\dot{Q}(t)$ is replaced with 0. The new SoE presented with these substitutions are presented in (2.10) – (2.13).

$$I_p\dot{\omega}_p(t) = -0.032\rho\left(\omega_p(t)R_p^2 + 0.032\frac{R_p}{A}\tan(a_p) - \omega_s(t)R_s^2 - 0.032\frac{R_s}{A}\tan(a_s)\right) + T_p(t) + \mu nr(Ap(t) - F_s)\tanh\left(\frac{\Delta\omega}{\alpha}\right) \tag{2.10}$$

$$I_t\dot{\omega}_t(t) = -0.032\rho\left(\omega_t(t)R_t^2 + 0.032\frac{R_t}{A}\tan(a_t) - \omega_p(t)R_p^2 - 0.032\frac{R_p}{A}\tan(a_p)\right) - T_t(t) + \mu nr(Ap(t) - F_s)\tanh\left(\frac{\Delta\omega}{\alpha}\right) \tag{2.11}$$

$$I_s\dot{\omega}_s(t) = -0.032\rho\left(\omega_s(t)R_s^2 + 0.032\frac{R_s}{A}\tan(a_s) - \omega_t(t)R_t^2 - 0.032\frac{R_t}{A}\tan(a_t)\right) \tag{2.12}$$

$$\rho\left(S_p\dot{\omega}_p(t) + S_t\dot{\omega}_t(t) + S_s\dot{\omega}_s(t)\right) = \rho\left(R_p^2\left(\omega_p^2(t) - \omega_t(t)\omega_p(t)\right) + R_t^2(\omega_t^2(t) - \omega_s(t)\omega_t(t)) + R_s^2\left(\omega_s^2 - \omega_p\omega_s\right)\right) + 0.032\frac{\omega_p}{A}\rho\left(R_p\tan\left(a_p\right) - R_s\tan(a_s)\right) + 0.032\frac{\omega_t(t)}{A}\rho\left(R_t\tan(a_t) - R_p\tan\left(a_p\right)\right) + 0.032\frac{\omega_s(t)}{A}\rho\left(R_s\tan(a_s) - R_t\tan(a_t)\right) - P_L(t) \tag{2.13}$$

Further discussion of these replacements is continued in the model validation section below. With the flow state replaced with a constant, we are left with three states and four equations in the TC SoE. Requiring only three equations to solve the system, (2.13) is eliminated from the model. This equation was selected because, with $\dot{Q}(t) = 0$, the acceleration constants on the left side, S_p, S_t, and S_s, make their contribution less than 1/1000th of the other states making this equation not as effective as the other three.

The third step in model simplification concerns reducing the TCC torque capacity model complexity. The torque capacity equations introduced in (2.5) are based on well-known wet multidisc friction clutch models that require in-depth knowledge of their mechanical and hydraulic properties along with experimental results to develop accurate models. Such experimentation and parameter validation are outside the scope of this dissertation and will be left to other researcher by replacing the complicated and nonlinear clutch carrying capacity model equations with a simplified clutch torque input parameters throughout the rest of this dissertation.

$$T_{TCC-p}(t) = \frac{\mu n r(Ap(t) - F_s)\tanh(\frac{\Delta\omega}{\alpha})}{I_P} \tag{2.14}$$

$$T_{TCC-t}(t) = -\frac{\mu n r(Ap(t) - F_s)\tanh(\frac{\Delta\omega}{\alpha})}{I_t} \tag{2.15}$$

The new SoE with these substitutions are presented in (2.16) – (2.18).

$$\mathrm{I_p}\dot{\omega}_\mathrm{p}(\mathrm{t}) = -0.032\rho\left(\omega_\mathrm{p}(\mathrm{t})\mathrm{R_p^2} + 0.032\frac{\mathrm{R_p}}{\mathrm{A}}\tan\left(\mathrm{a_p}\right) - \omega_\mathrm{s}(\mathrm{t})\mathrm{R_s^2} - 0.032\frac{\mathrm{R_s}}{\mathrm{A}}\tan(\mathrm{a_s})\right) + \mathrm{T_p}(\mathrm{t}) + \mathrm{T_{TCC-p}}(\mathrm{t}) \tag{2.16}$$

$$\mathrm{I_t}\dot{\omega}_\mathrm{t}(\mathrm{t}) = -0.032\rho\left(\omega_\mathrm{t}(\mathrm{t})\mathrm{R_t^2} + 0.032\frac{\mathrm{R_t}}{\mathrm{A}}\tan(\mathrm{a_t}) - \omega_\mathrm{p}(\mathrm{t})\mathrm{R_p^2} - 0.032\frac{\mathrm{R_p}}{\mathrm{A}}\tan\left(\mathrm{a_p}\right)\right) - \mathrm{T_t}(\mathrm{t}) - \mathrm{T_{TCC-t}}(\mathrm{t}) \tag{2.17}$$

$$\mathrm{I_s}\dot{\omega}_\mathrm{s}(\mathrm{t}) = -0.032\rho\left(\omega_\mathrm{s}(\mathrm{t})\mathrm{R_s^2} + 0.032\frac{\mathrm{R_s}}{\mathrm{A}}\tan(\mathrm{a_s}) - \omega_\mathrm{t}(\mathrm{t})\mathrm{R_t^2} - 0.032\frac{\mathrm{R_t}}{\mathrm{A}}\tan(\mathrm{a_t})\right) \tag{2.18}$$

The fourth step in simplifying the TC model is constraining the vehicle to steady engine power output and steady road load. This is accomplished by fixing the pump torque and the turbine torque input parameters to time-invariant constants. This is desirable because this dissertation's focus is on extending the application of TCC slip mode control to lower speed vehicle cruising application under constant conditions. In contrast, when the vehicle is under increasing load, like when going up a hill or under acceleration, torque multiplication mode over slip mode is preferred to increase the torque output of the TC to overcome the increased vehicle loading. Similarly, when the torque demands are reducing, such as when the vehicle is slowing down or coasting, coupled mode is preferred because it improves efficiency by reducing the engine braking load on the vehicle. By limiting the reduced linear model application to slip mode, the changes in engine (pump) speed and vehicle (turbine) speed, are held steady and by conservation of power their torques, have almost no acceleration. These acceleration changes are governed by Newton's 2nd Law as applied to rotating forces, i.e.

Torque = $mr^2\alpha$ where m (mass) and r (radius) are constants, and torque changes are proportional to α (acceleration). When the vehicle is cruising and the TCC is in slip mode, these minor changes in speed produce insignificant changes in acceleration, α, thus making the torque input changes negligible. This reduction allows the pump torque and turbine torque time-invariant parameters to be replaced with constant valued parameters as shown in (2.19) – (2.23).

$$\mathrm{T_p}(\mathrm{t}) = \mathrm{T_p} \tag{2.19}$$

$$\mathrm{T_t}(\mathrm{t}) = \mathrm{T_t} \tag{2.20}$$

The replacements are shown in the SoE (2.21) – (2.11).

$$\mathrm{I_p}\dot{\omega}_\mathrm{p}(\mathrm{t}) = -0.032\rho\left(\omega_\mathrm{p}(\mathrm{t})\mathrm{R_p^2} + 0.032\frac{\mathrm{R_p}}{\mathrm{A}}\tan(\mathrm{a_p}) - \omega_\mathrm{s}(\mathrm{t})\mathrm{R_s^2} - 0.032\frac{\mathrm{R_s}}{\mathrm{A}}\tan(\mathrm{a_s})\right) + \mathrm{T_p} + \mathrm{T_{TCC-p}}(\mathrm{t}) \tag{2.21}$$

$$\mathrm{I_t}\dot{\omega}_\mathrm{t}(\mathrm{t}) = -0.032\rho\left(\omega_\mathrm{t}(\mathrm{t})\mathrm{R_t^2} + 0.032\frac{\mathrm{R_t}}{\mathrm{A}}\tan(\mathrm{a_t}) - \omega_\mathrm{p}(\mathrm{t})\mathrm{R_p^2} - 0.032\frac{\mathrm{R_p}}{\mathrm{A}}\tan(\mathrm{a_p})\right) - \mathrm{T_t} - \mathrm{T_{TCC-t}}(\mathrm{t}) \tag{2.22}$$

$$\mathrm{I_s}\dot{\omega}_\mathrm{s}(\mathrm{t}) = -0.032\rho\left(\omega_\mathrm{s}(\mathrm{t})\mathrm{R_s^2} + 0.032\frac{\mathrm{R_s}}{\mathrm{A}}\tan(\mathrm{a_s}) - \omega_\mathrm{t}(\mathrm{t})\mathrm{R_t^2} - 0.032\frac{\mathrm{R_t}}{\mathrm{A}}\tan(\mathrm{a_t})\right) \tag{2.23}$$

The fifth and final reduction step is algebraic manipulation and grouping the time-invariant terms together. These force|mass|acceleration formatted equations are shown with the derivative of the state, its acceleration (α), multiplied by the inertia (I) on the left and the states' torques (τ) on the right. The are converted to the more common ODE format of $\dot{\mathrm{a}} = \tau/\mathrm{I}$ by dividing both sides by their inertias presented, which give rise to equations (2.24) to (2.26):

$$\dot{\omega}_p(t) = \Big(-0.032\rho\Big(\omega_p(t)R_p^2 + 0.032\frac{R_p}{A}\tan(a_p) - \omega_s(t)R_s^2 - 0.032\frac{R_s}{A}\tan(a_s)\Big) + T_p + T_{TCC-p}(t)\Big)/I_P \tag{2.24}$$

$$\dot{\omega}_t(t) = \Big(-0.032\rho\Big(\omega_t(t)R_t^2 + 0.032\frac{R_t}{A}\tan(a_t) - \omega_p(t)R_p^2 - 0.032\frac{R_p}{A}\tan(a_p)\Big) - T_t - T_{TCC-t}(t)\Big)/I_T \tag{2.25}$$

$$\dot{\omega}_s(t) = \Big(-0.032\rho\Big(\omega_s(t)R_s^2 + 0.032\frac{R_s}{A}\tan(a_s) - \omega_t(t)R_t^2 - 0.032\frac{R_t}{A}\tan(a_t)\Big)\Big)/I_S \tag{2.26}$$

Combining the time-invariant parameters from (2.24) - (2.26) with the constants torques creates the following constant terms defined by (2.27a) – (2.27l)

$$E_{11} = -0.032\frac{\rho R_p^2}{I_P} \tag{2.27a}$$

$$E_{12} = 0 \tag{2.27b}$$

$$E_{13} = 0.032\frac{\rho R_s^2}{I_P} \tag{2.27c}$$

$$E_{14} = \frac{\frac{0.032^2}{A}\big(R_s\tan(a_s) - R_P\tan(a_p)\big) + T_P}{I_P} \tag{2.27d}$$

$$E_{21} = 0.032\frac{\rho R_p^2}{I_T} \tag{2.27e}$$

$$E_{22} = -0.032\frac{\rho R_t^2}{I_T} \tag{2.27f}$$

$$E_{23} = 0 \tag{2.27g}$$

$$E_{24} = \frac{\frac{0.032^2}{A}\big(R_p\tan(a_p) - R_t\tan(a_t)\big) + T_t}{I_t} \tag{2.27h}$$

$$E_{31} = 0 \tag{2.27i}$$

$$E_{32} = 0.032\frac{\rho R_t^2}{I_S} \tag{2.27j}$$

$$E_{33} = -0.032\frac{\rho R_s^2}{I_s} \tag{2.27k}$$

$$E_{44} = \frac{\frac{0.032^2}{A}(R_t \tan(a_t) - R_s \tan(a_s))}{I_s} \tag{2.27l}$$

Substituting the constants from (2.27) into (2.24) - (2.26) gives the new system of linear equations (2.28) – (2.30):

$$\dot{\omega}_p(t) = E_{11}\omega_p(t) + E_{12}\omega_t(t) + E_{13}\omega_s(t) + E_{14} + T_{TCC-p}(t) \tag{2.28}$$

$$\dot{\omega}_t(t) = E_{21}\omega_p(t) + E_{22}\omega_t(t) + E_{23}\omega_s(t) + E_{24} + T_{TCC-t}(t) \tag{2.29}$$

$$\dot{\omega}_s(t) = E_{31}\omega_p(t) + E_{32}\omega_t(t) + E_{33}\omega_s(t) + E_{34} \tag{2.30}$$

The TC model equations given by (2.28) - (2.30) can be represented in the following state space format:

$$\dot{x}(t) = Ax(t) + Bu(t) + E \tag{2.31}$$

$$y(t) = Cx(t) \tag{2.32}$$

where

$$x(t) = \begin{bmatrix} \omega_p \\ \omega_t \\ \omega_s \end{bmatrix} \tag{2.33}$$

$$A = \begin{bmatrix} E_{11} & E_{12} & E_{13} \\ E_{21} & E_{22} & E_{23} \\ E_{31} & E_{32} & E_{33} \end{bmatrix} \tag{2.34}$$

$$B = \begin{bmatrix} 1 & 0 & 0 \\ 0 & 1 & 0 \\ 0 & 0 & 1 \end{bmatrix} \tag{2.35}$$

$$u(t) = \begin{bmatrix} T_{TCC-p}/I_P \\ T_{TCC-t}/I_T \\ 0 \end{bmatrix} \tag{2.36}$$

$$C = \begin{bmatrix} 1 & 0 & 0 \\ 0 & 1 & 0 \\ 0 & 0 & 1 \end{bmatrix} \tag{2.37}$$

$$E = \begin{bmatrix} E_{14} \\ E_{24} \\ E_{34} \end{bmatrix} \tag{2.38}$$

and y(t) denotes the TC's outputs.

2.4 Validation of Linear Torque Converter Model

To confirm the accuracy of the three-state linear model given in equations (2.31) and (2.32), closed-loop simulations of both the nonlinear model and the reduced linear model were evaluated. We conducted ten second simulations by subjecting both systems to the same reference tracking inputs, including the application of the TCC at four second to drive the TC into slip mode. Figure (2.2) shows the TC fluid flow rate of the nonlinear model plotted against the constant, 0.032, used in the linear model. The small changes in the nonlinear plant track very well with the expected results from [14] confirming the assertion that replacing the nonlinear fluid flow with a linear constant maintains the model's steady state tracking.

The simulation also generated plots of both models' output speeds. The results for the nonlinear model is presented in Figure 2.3a and that of the linear model is presented in Figure 2.3b. Both are plotted against the tracking reference inputs that drive the TCC actuation. These results show that they both track the reference points, and each other, within a few RPM except during the abrupt transition into slip mode at four seconds. Further review shows that the linear model tracks the nonlinear plant during the TCC application however, with a less aggressive gradient and without the overshoot seen in the nonlinear model. This less aggressive gradient without the overshoot shows a more damped response to the setpoint transients. This can be attributed to the flow rate of the linear model being lower than the nonlinear model at 4 seconds. , As shown in Figure (2.2), the nonlinear model shows a sharp but brief increase in flow during the initial application of slip mode. An examination of equations (2.6) – (2.9) shows that the fluid flow is a major contributor to the TC’s dynamic response and is overly sensitive to the change in speed states. By removing this characteristic, the linear model is underdamped and not able to respond to changes as quickly as the linear model.

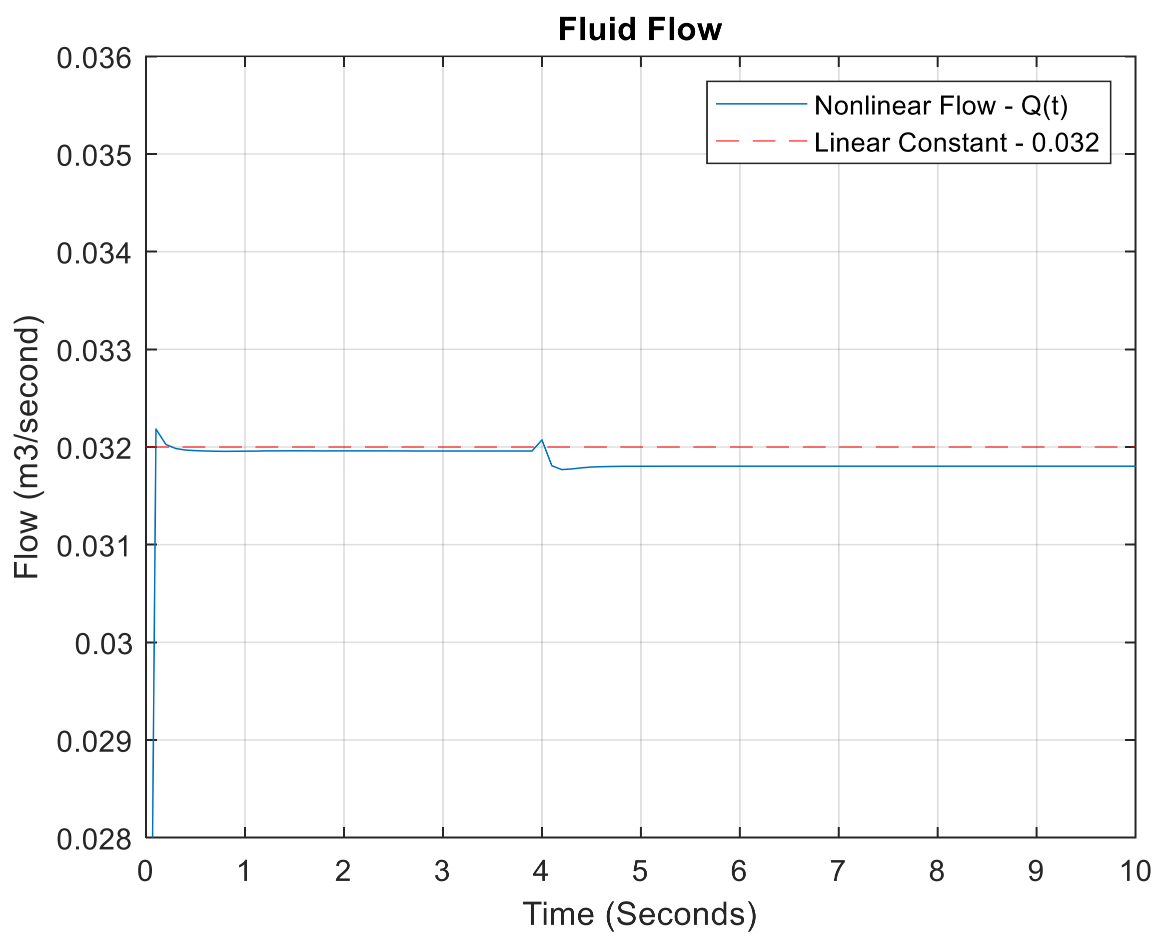

Figure 2.2 - Nonlinear Fluid Flow Rate vs. Constant Flow Rate

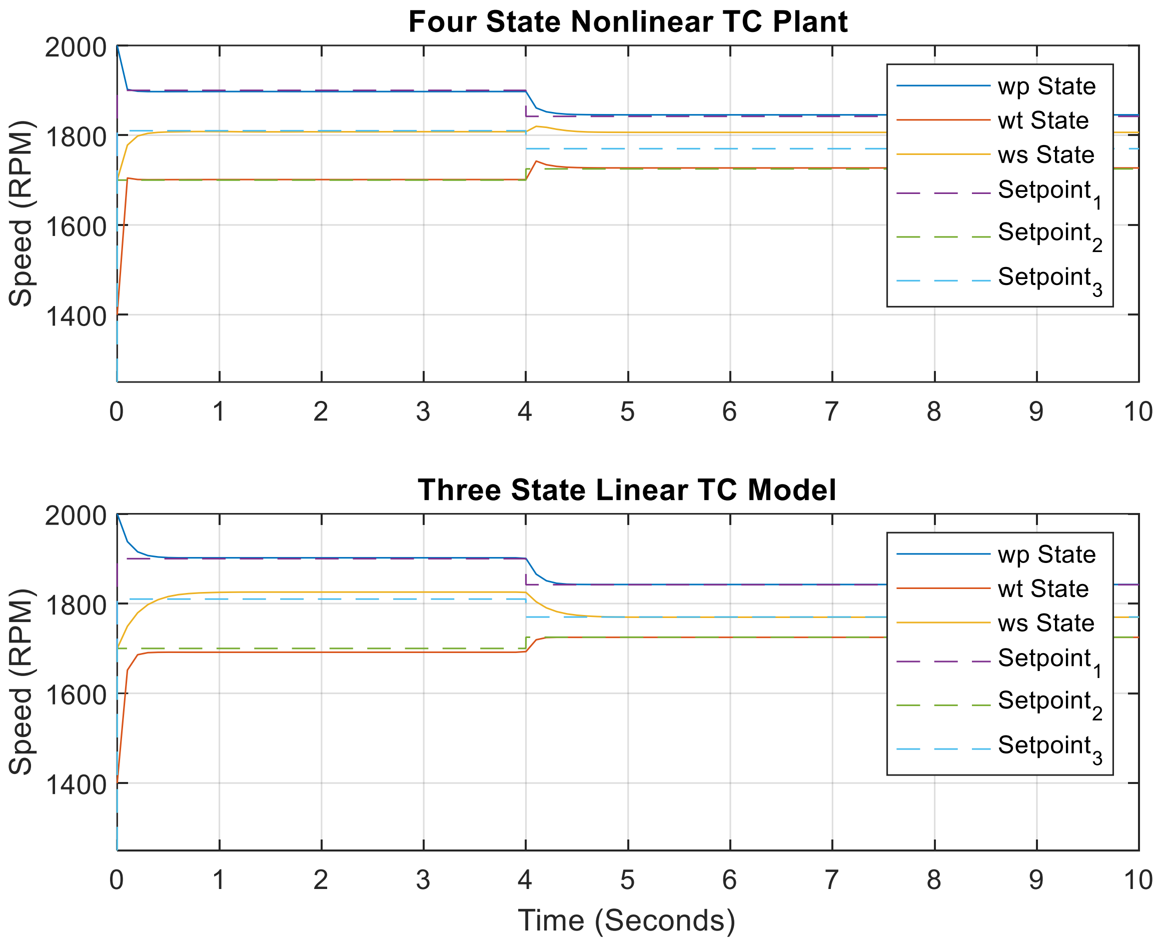

Figure 2.3 - TC Plant and Linear Model Simulation

2.5 Discretization of the Linear Torque Converter Model

Using the validated continuous linear TC model as a base, this dissertation discretizes it for use in Chapter 3. The Euler Method was chosen to calculate discrete approximations of derivatives because of its simplicity and small tracking and step error when using small discrete steps. Automotive applications typically use small 10 to 100 nanosecond calculations for millisecond actuations, making these small set sizes ideal for this application.

Forward Euler Method is a discrete approximation of a differential equation of the form $\dot{x} = f(t, x, u)$ by

$$x(k+1) = x(k) + \Delta t f\big(x(k), u(k)\big) \tag{2.39}$$

where Δt is the step size, k is the sample number, $x(k) = x(k\Delta t)$, and $f\big(x(k), u(k)\big)$ denotes the function to be discretized. Applying forward Euler Method to (2.31) yields:

$$x(k+1) = x(k) + \Delta t(Ax(k) + Bu(k) + E) \tag{2.40}$$

Grouping the terms from (2.40) given by:

$$x(k+1) = (I + \Delta tA)x(k) + \Delta tBu(k) + \Delta tE. \tag{2.41}$$

By defining

$$\bar{A} = (I + \Delta tA), \tag{2.42}$$

$$\bar{B} = \Delta tB, \tag{2.43}$$

and

$$\bar{E} = \Delta tE \tag{2.44}$$

the discretized system can be rewritten as

$$x(k+1) = \bar{A}x(k) + \bar{B}u(k) + \bar{E} \tag{2.45}$$

The above discretized model is used later in this dissertation.

2.7 Modeling of Random State Disturbance

This dissertation considers three independent random signals as the disturbance expected in the TCC control environment. The formation of these disturbances relies on an understanding of what they represent. In this TC application, these disturbances are primarily from the pump speed fluctuations that come from the ICE's combustion cycle torque and speed impulses. These function impulses correspond to the combustion cycles of a 4-cylinder 4-stroke ICE. At speeds above 2000 RPM, these impulses can be ignored because they are mechanically dampened by the physical lowpass filter of the rotating mass of the ICE's flywheel making their effect on the rotating speed negligible. At lower speeds these impulses can be dramatic and can vary the pump speed by several hundred RPMs of the pump and turbine speeds. These disturbances, to a lesser degree, also include modeling errors of the TC and TCC system parameters. These tend to be small in amplitude and slowly changing as presented by Asl [17]. With a basic understanding of the physical characteristics of the TC fluid coupling, this disturbance will account for parameter uncertainties when creating the model. A final contributor to these disturbances considered in this dissertation are measurement errors. These are truly random speed fluctuations and typically come from the miss calculation of the speed states. These measurement errors have both physical measurement errors and observer estimating errors. This dissertation combines these three sources into a single disturbance for each system state.

MATLAB was used to create these disturbance signals by generating three random valued impulses. These impulses were then processed through a state lowpass filter to generate the three disturbances. The impulse period of 20 Hz with a period is 5 millisecond is used thought this research. These parameters are used because they correspond to the combustion cycles of an ICE operating in the TCC slip range around 1,500 RPM. The lowpass state filter used to process the impulses is presented in (2.46)

$$\dot{\mathrm{d}}(\mathrm{t}) = \mathrm{Md}(\mathrm{t}) + \mathrm{Nx}(\mathrm{t}) + \mathrm{R}(\mathrm{t}) \tag{2.46}$$

where M being the disturbance feedback gain, N is the state feedback gain, and R are the random impulses. A typical simulation of 25% disturbance used to evaluate the robustness of the TCC controllers is shown in Figure (2.4).

Modifying equation (2.31) to include these disturbances gives the following model:

$$\dot{x}(t) = \overline{A}x(t) + \overline{B}u(t) + d(t) \tag{2.47}$$

with

$$d(t) = \begin{bmatrix} d_1(t) \\ d_2(t) \\ d_3(t) \end{bmatrix}, \tag{2.48}$$

where d(t) includes both constant and time-varying disturbances arising due to pump speed fluctuation, system nonlinearities and modeling errors.

Also, using the discretization method discussed in Section 2.5, we can obtain a discretized version of equation (2.47) as:

$$x(k+1) = \widetilde{A}x(k) + \widetilde{B}u(k) + d(k) \tag{2.49}$$

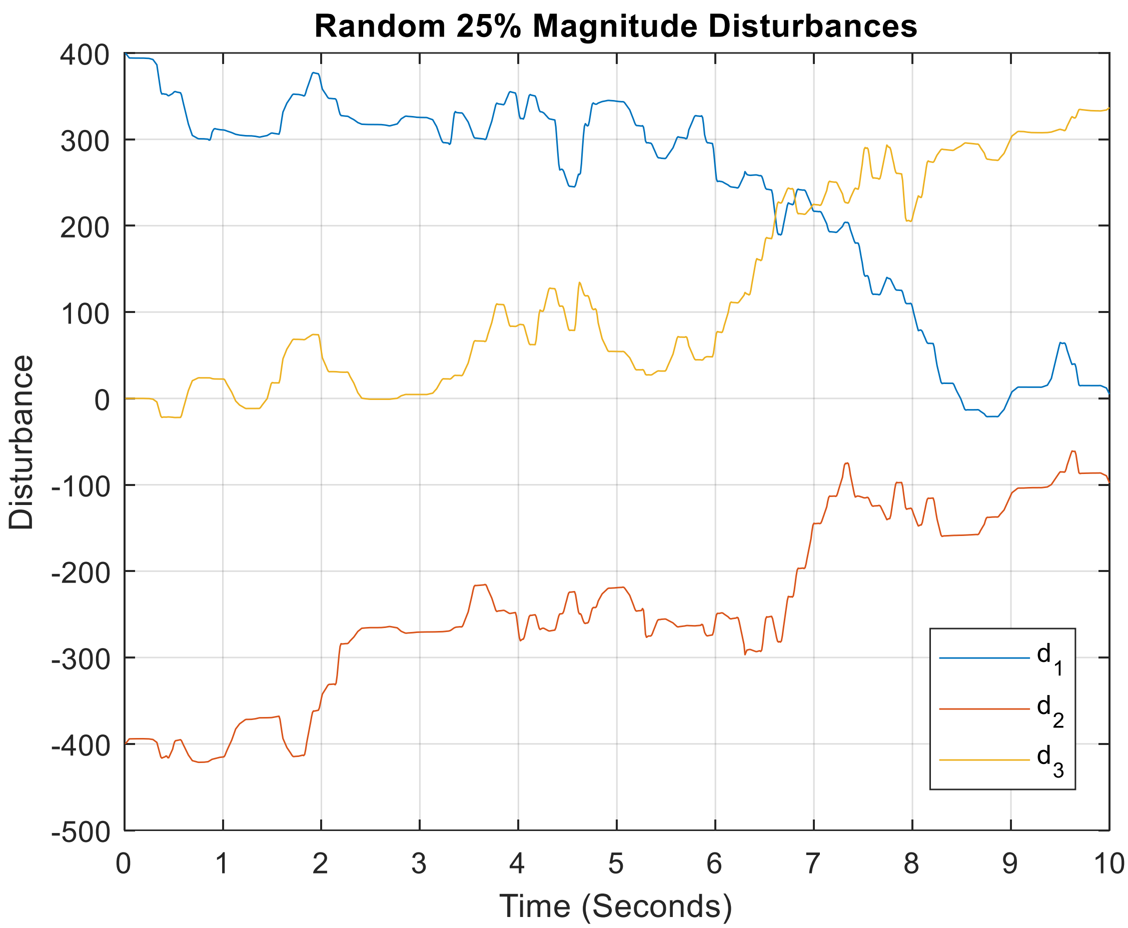

Figure 2.4 - Random 25% of State RPM Disturbances

CHAPTER THREE

A DISTURBANCE ACCOMMODATING DISCRETE ONE STEP AHEAD CONTROLLER

3.1 Introduction

This chapter introduces One Step Ahead (OSA) control of the linear model of the TC system in slip mode. These types of controllers utilize a closed-loop control method that algebraically calculates the necessary input to drive the system to a future output reference value. They can control discreate time systems with only the requirements of a discrete output function be able to be calculated at a future time. This simple requirement and their low computational requirements make them extremely easy to implement. OSA controllers are also known for their strong tracking ability, however, it comes at the expense of the high control efforts often required to drive the output to the reference

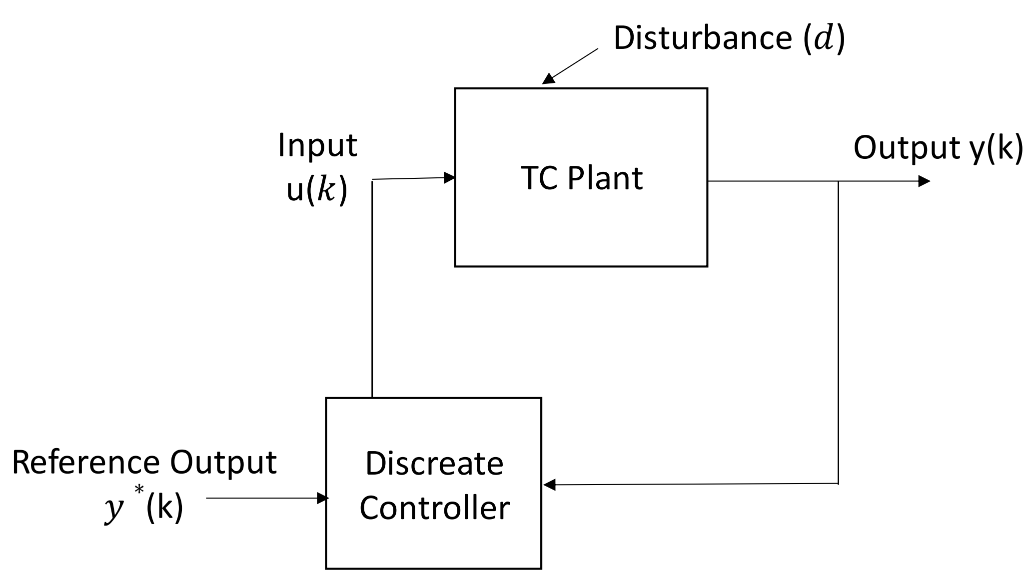

Figure 3.1 - One Step Ahead Controller Flowchart

value in one time step. This chapter presents discrete one step ahead predictive controllers with noise cancellation to exploit their tracking abilities while mitigating some of the high control efforts required.

3.2 Discrete One Step Ahead Predictive Control

The OSA based controller investigated in this dissertation is a modified version of the linear Disturbance Accommodating Discrete One-Step-Ahead Predictive Control (DA-DOPC) scheme presented in [55]. This control method implements a straightforward design procedure that incorporates direct tuning of the response characteristics of tracking and control effort of an OSA system by implementing the Q and R weighting matrices respectively. In addition to its straightforward design, the DA-DOPC scheme incorporates some robustness to disturbances without any additional computations or control inputs.

Starting with a linear discretized TC model with the state disturbance $d(k)$ presented in (2.49), consider a TC system modeled by:

$$x(k+1) = \overline{A}x(k) + \overline{B}u(k) + d(k) \tag{3.1a}$$

$$y(k) = Cx(k) \tag{3.1b}$$

We begin to design a DA-DOPC controller by creating a cost function. To minimize the cost function, we find its derivative and set it to zero to locate the optimum control law. Starting with

$$J = [y^*(k+1) - y(k)]^T Q [y^*(k+1) - y(k+1)] + u(k)^T R u(k) \tag{3.2}$$

where Q weighs the tracking error and R weighs the control effort, equation (3.2) becomes

$$J = e(k+1)^T Q e(k+1) + u(k)^T R u(k) \tag{3.3}$$

by making the error substitution

$$e(k+1) = y^*(k+1) - y(k+1) \tag{3.4}$$

into (3.2). By replacing $y(k+1)$ in (3.4) with (3.1) we get

$$e(k+1) = y^*(k+1) - (C\overline{A}x(k) + C\overline{B}u(k) + Cd(k)) \tag{3.5}$$

To solve for the cost function when the derivative is zero, $\frac{\partial j}{\partial u(k)} = 0$, we can use the chain rule to solve the equation. Starting with

$$\frac{\partial j}{\partial u(k)} = 2\frac{\partial e(k+1)^T}{\partial u(k)} Q e(k+1) + 2Ru(k) \tag{3.6}$$

where

$$\frac{\partial e(k+1)^T}{\partial u(k)} = \frac{\partial}{\partial u(k)}(y^*(k+1)^T - y(k+1)^T) \tag{3.7}$$

$$\frac{\partial e(k+1)^T}{\partial u(k)} = \frac{-\partial}{\partial u(k)} y(k+1)^T \tag{3.8}$$

and substituting back in for $y(k+1)$

$$\frac{\partial e(k+1)^T}{\partial u(k)} = \frac{-\partial}{\partial u(k)}(C^T\overline{A}^T x^T(k) + \overline{B}^T C^T u^T(k) + C^T d^T(k)) \tag{3.9}$$

Differentiation by $\partial u(k)$ removes the terms that are not functions of $u(k)$ and reduces to

$$\frac{\partial e(k+1)^T}{\partial u(k)} = -\overline{B}^T C^T. \tag{3.10}$$

Substituting (3.10) into (3.6) gives:

$$\frac{\partial j}{\partial u(k)} = -2\overline{B}^T C^T Q e(k+1) + 2Ru(k) \tag{3.11}$$

and substituting for $e(k+1)$ given by:

$$\frac{\partial j}{\partial u(k)} = -2\bar{B}^T C^T Q\left(y^*(k+1) - \left((C\bar{A}x(k) + C\bar{B}u(k) + Cd(k))\right)\right) + 2Ru(k) \tag{3.12}$$

When the $u(k)$ terms are grouped together, (3.12) simplifies to

$$\frac{\partial j}{\partial u(k)} = -2\bar{B}^T C^T Q\left(y^*(k+1) - \left((C\bar{A}x(k) + Cd(k))\right)\right) + 2(R - \bar{B}^T C^T QC\bar{B})u(k) \tag{3.13}$$

When $\frac{\partial j}{\partial u(k)} = 0$, to find the minimum, and (3.13) is solved for $u(k)$, the control law is

$$u(k) = (R - \bar{B}^T C^T QC\bar{B})^{-1}\bar{B}^T C^T Q\left(y^*(k+1) - \left((C\bar{A}x(k) + Cd(k))\right)\right) \tag{3.14}$$

The control law (3.14) includes the weighting parameters Q and R, which can be tuned to adjust the controls balance between tracking, high Q/R ratio, and controller effort, low Q/R ratio. Although not directly present in (3.14), the step size, Δt, also plays a role in system tuning, however this thesis exclusively used a fix step size of one millisecond commonly used in the automotive industry.

To achieve noise cancellation, a second control input is created to cancel the unknown disturbances. This is done by replacing the control input $u(k)$ with the new disturbance canceling input

$$\bar{u}(k) = u(k) - B^+\hat{d}(k) \tag{3.15}$$

where B^+ is the right pseudoinverse of B, $\hat{d}(k)$ is an estimate of $d(k)$.

Substituting (3.15) into (3.1) gives the new state equations

$$x(k+1) = \bar{A}x(k) + \bar{B}\left(u(k) - B^+\hat{d}(k)\right) + d(k) \tag{3.16}$$

Simplifying using the property $\bar{B}B^+ = I$ gives:

$$x(k+1) = \bar{A}x(k) + \bar{B}u(k) + \left(d(k) - \hat{d}(k)\right) \tag{3.17}$$

To obtain the disturbance estimate, this research utilizes the Least Mean Square (LMS) method. This method implements a fixed weighting factor used to update the disturbance estimate of the error between the reference output $y^*(k)$ and the actual output $y(k)$. This method has proven to be more computationally efficient than other methods. However, this method comes with disadvantages of providing slower reference tracking. The LMS algorithm is shown as follows

$$e(k) = y^*(k) - \left(C\bar{A}x(k) + C\bar{B}u(k) + C\left(d(k) - \hat{d}(k)\right)\right) \tag{3.18}$$

with

$$\hat{d}(k+1) = \hat{d}(k) + \mu e(k) \tag{3.19}$$

where

$e(k)$ is the current error of the disturbance estimate, $\hat{d}(k)$ is the current estimate of the disturbance, and μ is a constant step size, $0 < \mu < 1$.

3.3 Simulation Results and Discussion

As with most methods of reference tracking control, it requires the system designer to predefine the target output values for the system to track. This system was subjected to three slip target values with both ramp and step transitions between them to evaluate the controller's robustness. The simulation started with the TC in controlled mode and a rather large slip speed of 300 RPM. Four seconds into the simulation, the TCC controller attempted to reduce the slip speed between the pump speed (the first state) and the turbine speed (the second state), thus modeling the application of the TCC at lower speeds to improve system efficiency. It should be noted that that the objective is to keep the pump and turbine within 50 RPM for efficiency without allowing the slip speed to become zero RPM, because this would transmit the engine's vibrations to the vehicle drivetrain.

Figure 3.2a shows the controller performance with no disturbance applied. Figure 3.2b shows the controller performance in the presence of 10% of the state RPM values of disturbance added, without application of disturbance cancelation. Figure 3.2c shows the performance of the disturbance canceling controller, with a low Q/R ratio, whereas Figure 3.2d shows the same with a high Q/R ratio.

Figure 3.3 presents these same disturbances, dashed lines, along with their estimates, theta in the sold lines, of this three-state system's estimates of the disturbances. Figure 3.3a are the results of the OSA estimate, Figure 3.3b are the DA-DOPC with a low Q/R weighting, and Figure 3.3c is a DA-DOPC with a high Q/R weighting. In general, DA-DOPC controller does an excellent job in estimating the disturbances and canceling their effects. The one exception is the DA-DOPC with a low Q/R tuning. This estimate exhibits some ringing overshoot after substantial changes in the reference input that takes about a second to stabilize.

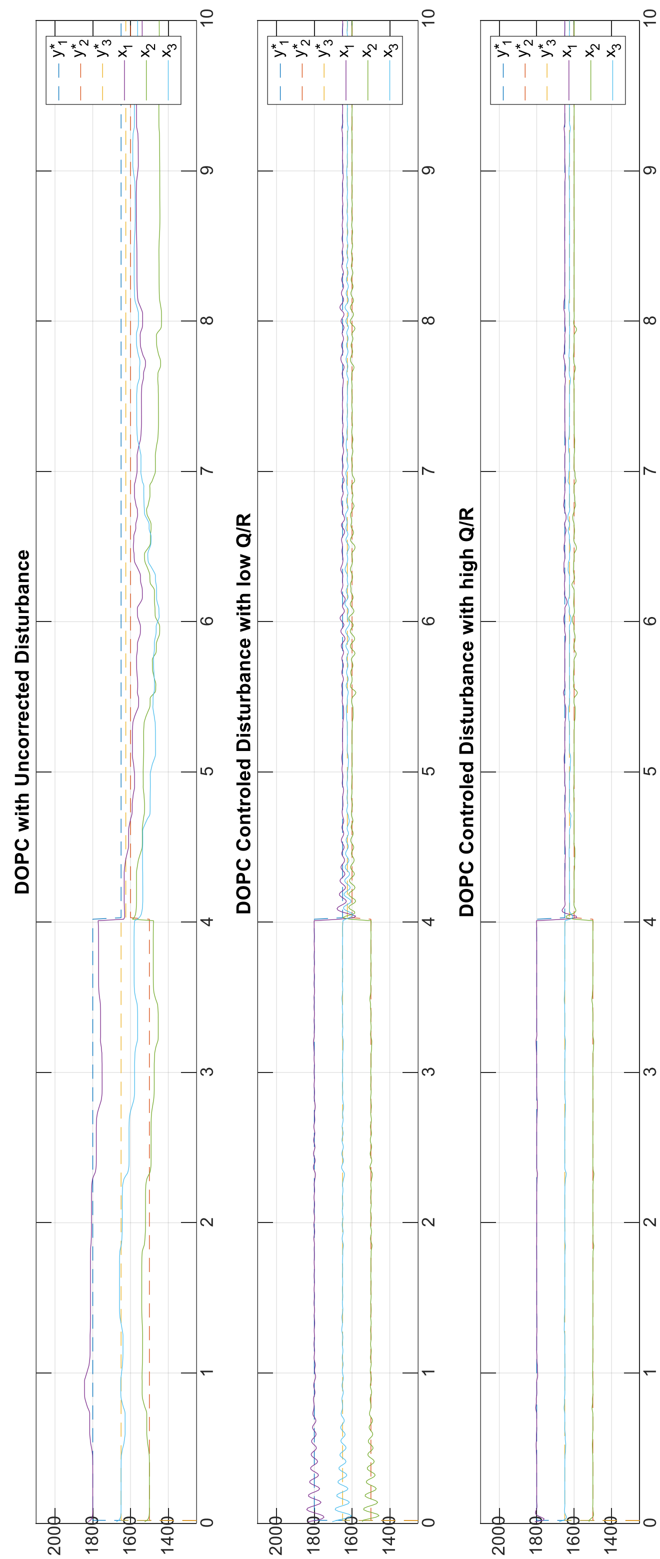

Figure 3.2 – Performance of DA-DOPC with 10% of State RPM Disturbance

By observing the simulation results presented in these Figures, several conclusions can be made about the robustness and tracking ability of DA-DOPC discreate controllers.

- With as little as 10% disturbance and no disturbance canceling control input, DA-DOPC (without a disturbance canceler) loses the ability to track the reference signal and is not suitable for implementation in a TC system.
- Up to about 25% to 50% of the state speed disturbance, the DA-DOPC remains in slip mode.
- At levels of 25% of state RPM of disturbance and above, the DA-DOPC Q/R ratio must remain large to prevent the ringing overshoots caused by the larger values of μ required for disturbance estimate tracking.
- With good choices of Q, R, and μ, 50% is the maximum disturbance the DA-DOPC controller is robust to and able to remain in slip mode.
- Figures 3.5 - 3.6 show the results of similar simulations as Figure 3.2 except with 25%, 50%, and 100% of the state speed disturbance added to evaluate their robustness to noise.

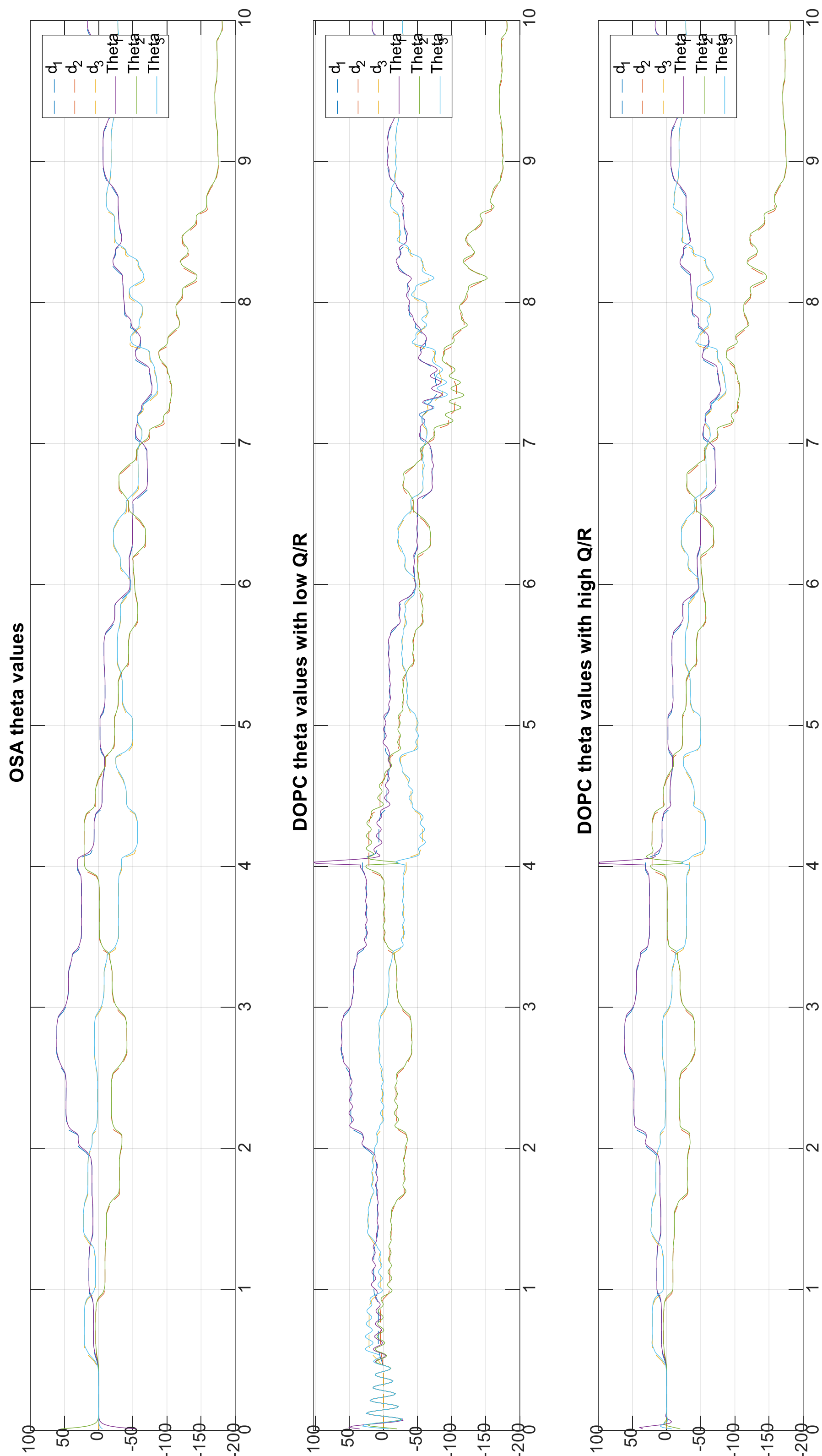

Figure 3.3 - Disturbances and their Estimates (denoted by Theta)

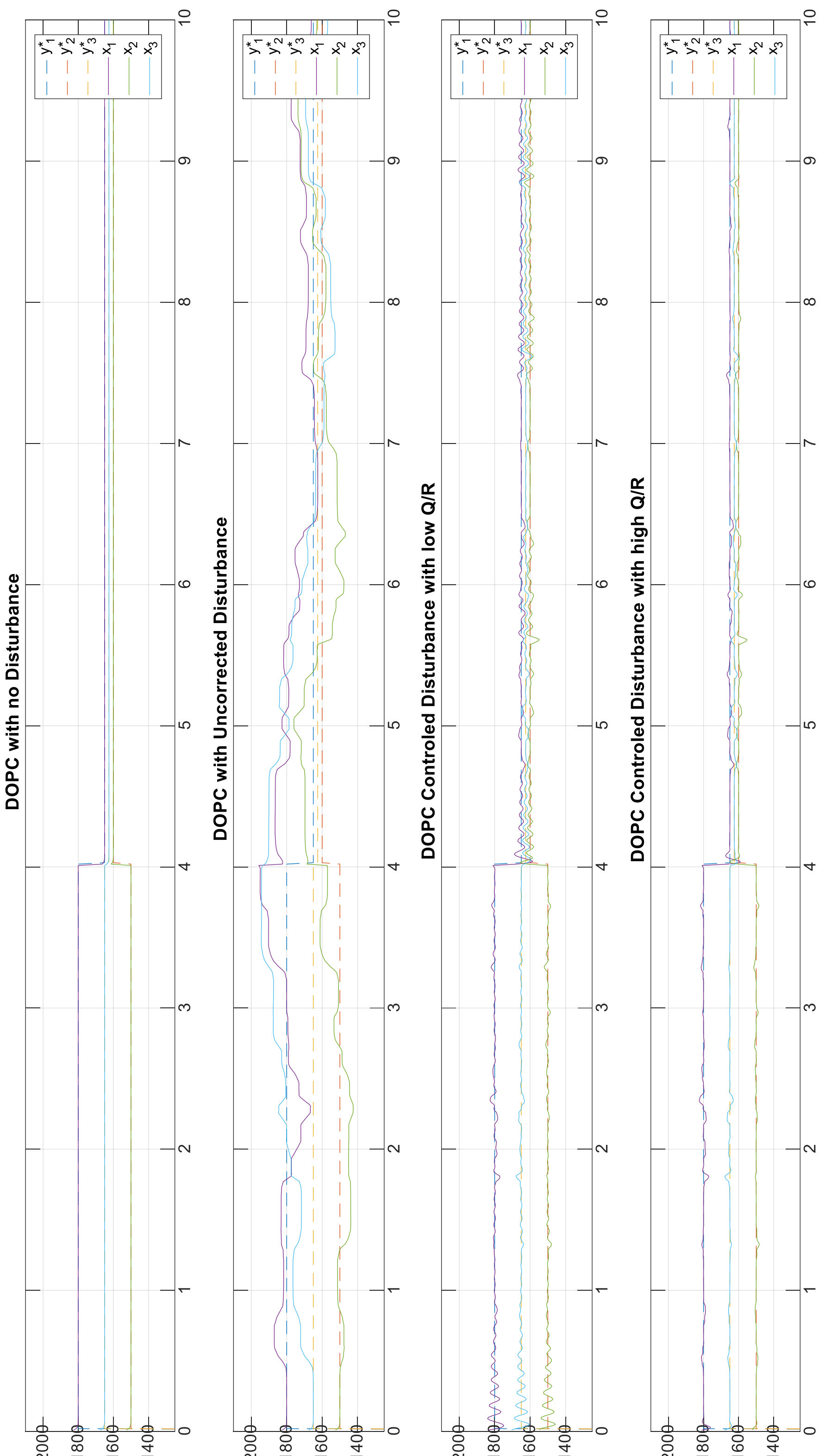

Figure 3.4 – Performance of DA-DOPC with 25% of State RPM Disturbance

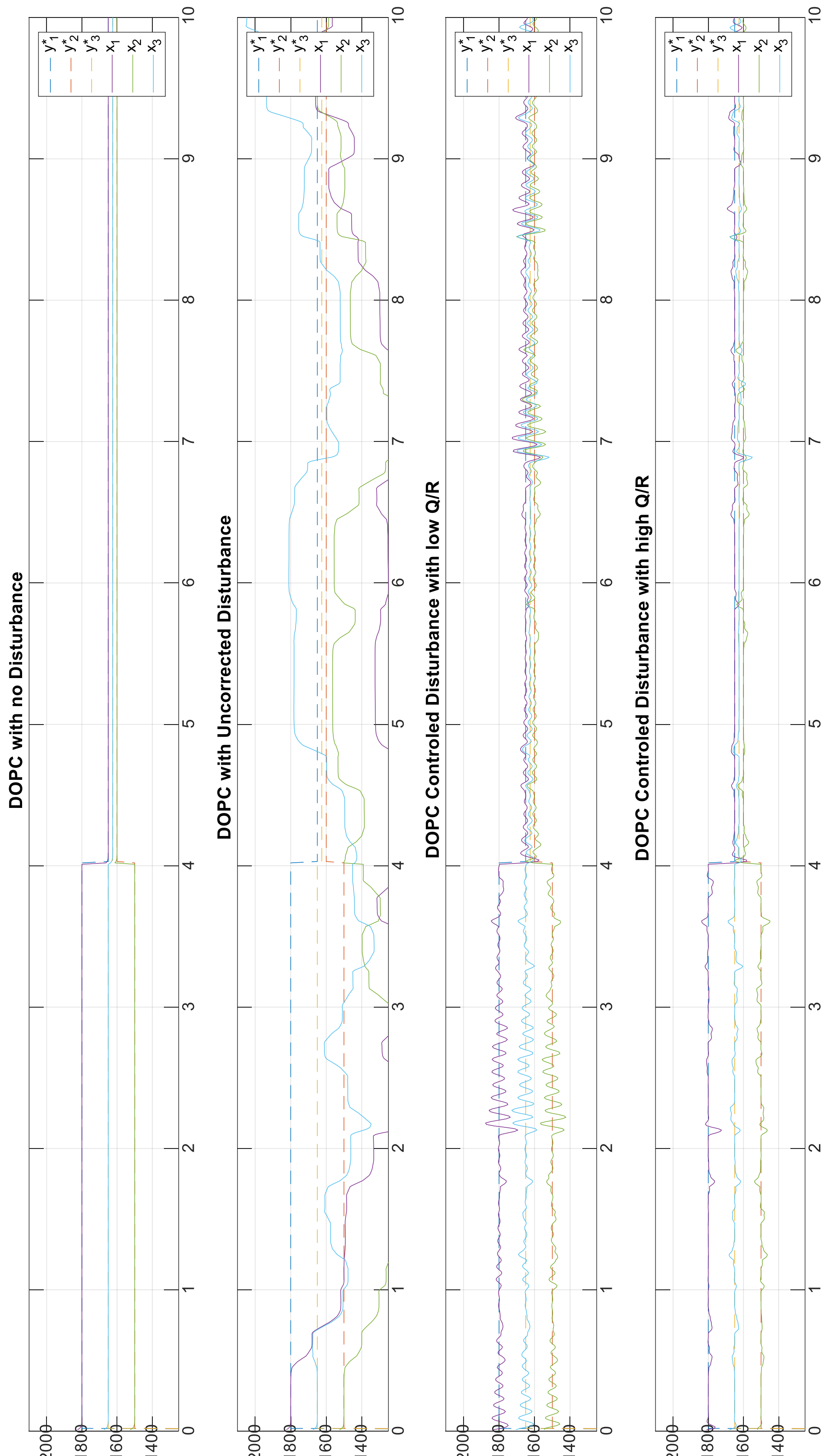

Figure 3. 5 – Performance of DA-DOPC with 50% of State RPM Disturbance

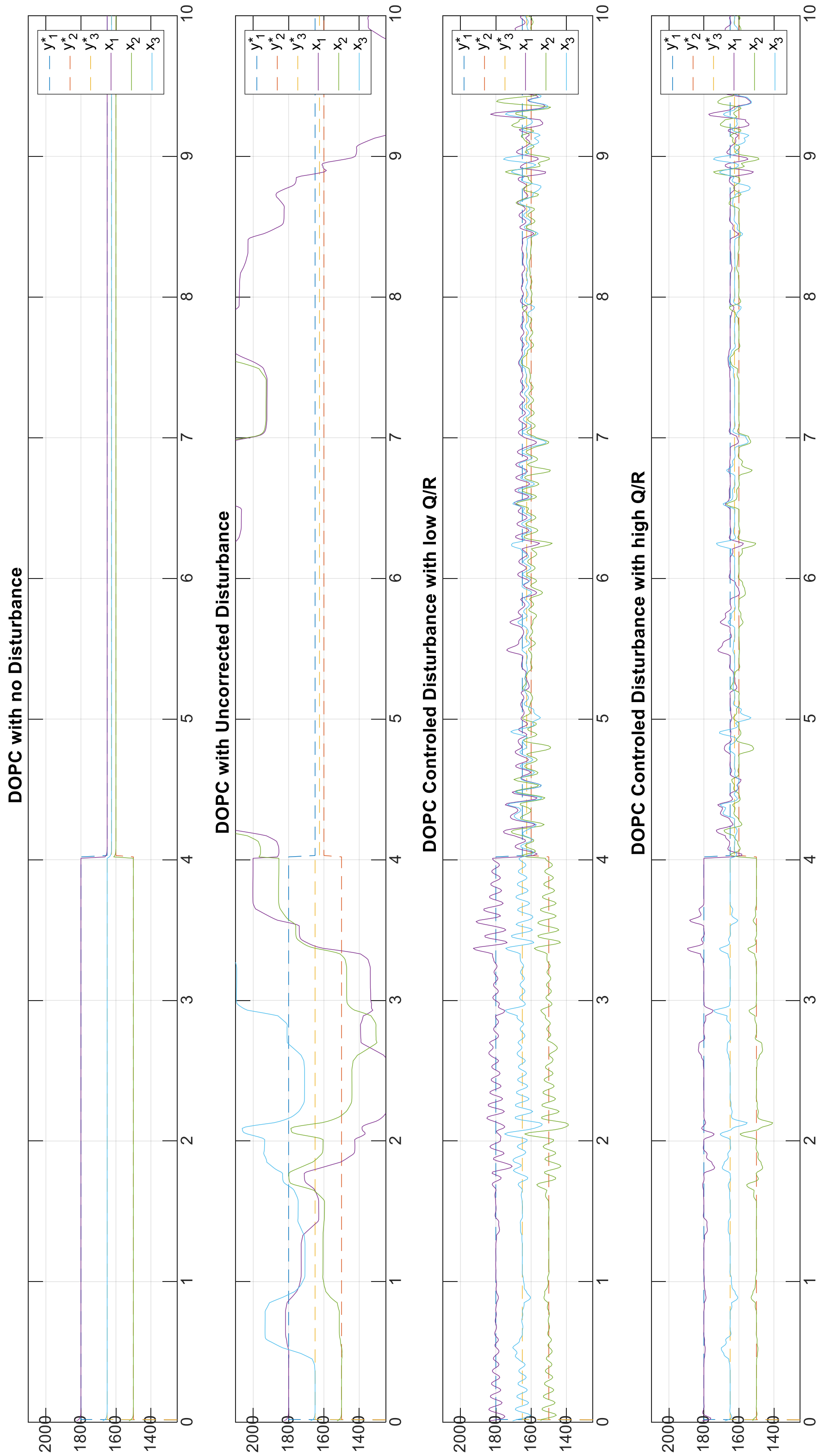

Figure 3.6 – Performance of DA-DOPC with 100% of State RPM Disturbance

CHAPTER FOUR

A DIRECT DISTURBANCE OBSERVER BASED CONTROLLER

4.1 Introduction

A Direct Disturbance Observer Based Control (D-DOBC) scheme is one that uses separate Unknown Input Observers (UIO) to model the states and the disturbances of the system separately. These UIO are for state feedback control to stabilize the plant and to dynamically cancel the state disturbances respectively [38], [56]. In TCC control, a third control input is used for reference point tracking of the system's output to state values. These types of controllers are advantageous when the type of disturbances expected are well understood and the necessary knowledge exists on how to model them.

This chapter considers applying the D-DOBC scheme to an automotive TCC in slip mode. The controller applies a targeted slip speed between the pump and turbine states where the disturbances represent speed measurement errors, ICE speed and torque fluctuations acting on the pump speed and modeling parameter uncertainties. Operating the TC and TCC in this way will allow the system to absorb the ICE torque impulses in the fluid coupling without transmitting them to the vehicle driveline.

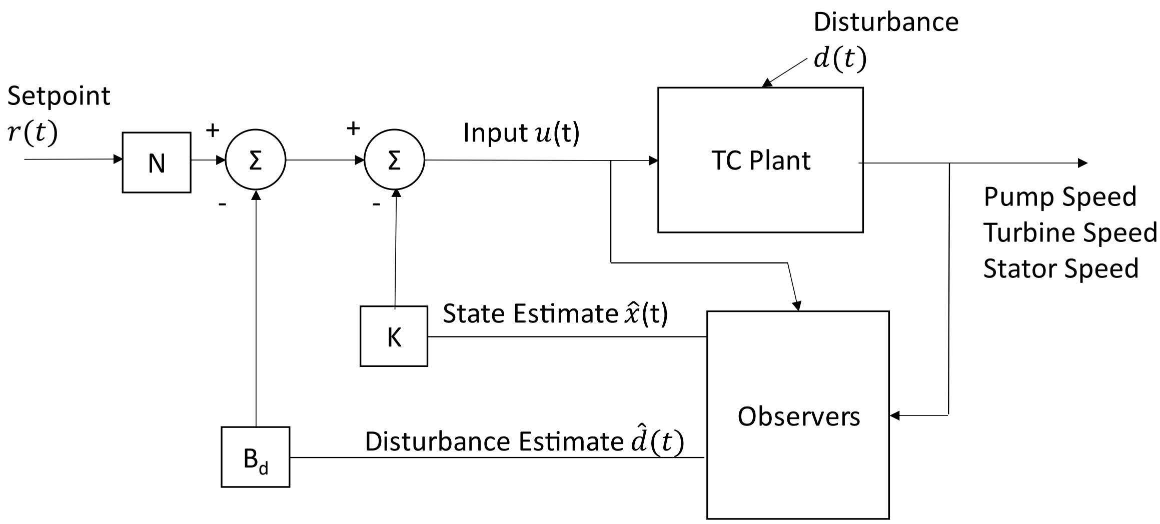

Figure 4.1 - D-DOBC Flow Chart

4.2 The Design of a D-DOBC TCC Control

The D-DOBC control scheme combines three separate inputs to control the TCC. They utilize the state feedback observer controller to stabilize and tune the TC's response to inputs, state noise elimination to reduce the impact of disturbances on the system, and setpoint regulator tracking to drive system's outputs to follow predefined speed profiles. The goals of this scheme are to control the TCC in such a way as the TC remains in slip mode in the presence of large random state disturbances. If the TC enters locked mode, when the turbine and pump speed are the same, the TC system will transmit the ICE's speed and torque impulses to the vehicle driveline creating a harsh vehicle ride. If the TC enters coupled mode, when the turbine speed is less than 90% of the pump speed, the TC system's efficiency decreases rapidly.

4.3 Design of a D-DOBC Observers for TCC Control

Starting with a linear TC model (2.14), this section describes the process to design a state observer and disturbance observer using the Luenberger method [57]. Starting with the TC state system

$$\dot{x} = Ax(t) + Bu + d(t) \tag{4.1}$$

$$\mathrm{y(t) = Cx(t)} \tag{4.2}$$

where the disturbance is large enough in magnitude that it includes the torque inputs, linearization constants, and reasonable model parameter uncertainties into the single parameter $\mathrm{d(t)}$.

The state observer of (4.1) is shown in (4.3) and a disturbance observer is shown in (4.4).

$$\mathrm{\dot{\hat{x}}(t) = A\hat{x}(t) + Bu(t) + B_d d(t) + L(y(t) - C\dot{x}(t))} \tag{4.3}$$

$$\mathrm{\dot{\hat{d}}(t) = -F\hat{d}(t)} \tag{4.4}$$

where $\mathrm{\hat{x}(t)}$ is noise state estimate and $\mathrm{\hat{d}(t)}$ is just the disturbance estimate, $\mathrm{B_d}$ is the disturbance gain matrix, F is the disturbance estimator matrix, and L is the observer gain matrix.

The disturbance gain matrix $\mathrm{B_d}$ is selected such that $\mathrm{B_d\dot{\hat{d}}(t)}$ can be fed into the plant input $\mathrm{u(t)}$ to cancel out $\mathrm{d(t)}$. The disturbance estimator matrix F sets the gain of disturbance feedback of the disturbance model and is typically set to be the identity matrix for a unity gain. This allows cancelation of piecewise constant disturbance. The observer gain matrix controls the weight of the error correction acting on the observer estimate of the state. This research uses the pole placement method to design this matrix to ensure the observer was not only stable, but also faster than the state feedback. Care should be taken that the observer poles are not too large, or the system will be subjected to noise and not be robust. To tune the controller's response characteristics the pole placement method is used. Pole placement is when the systems closed-loop pole locations are selected in such a way that the controller's rise time, oscillation responses, settling time are the roots of the characteristic equation that connects the inputs to the outputs. For closed-loop stability, these pole(s) must be in the negative, left, planes of the Cartesian coordinate system.

Many methods can be used for pole placement, however this thesis uses Ackermann's formula to calculate the observer gain L [57], as implemented in the MATLAB.

Combining (4.3) and (4.4) into a single UIO gives (4.5).

$$\begin{bmatrix} \dot{\hat{x}}(t) \\ \dot{\hat{d}}(t) \end{bmatrix} = \begin{bmatrix} A & B_d \\ 0 & F \end{bmatrix} \begin{bmatrix} \hat{x}(t) \\ \hat{d}(t) \end{bmatrix} + \begin{bmatrix} B \\ 0 \end{bmatrix} u(t) + L_0(y(t) - C\hat{x}(t)) \tag{4.5}$$

where $L_0 = \begin{bmatrix} L \\ 0 \end{bmatrix}$ and the zero matrix 0 is a square matrix of size compatible with the size of the disturbance state(s).

This state observer $\hat{x}(t)$ incorporates a disturbance less model of the TC's pump, turbine, and stator speeds. It is used in the state feedback controller to stabilize and tune the transient response of the TC system. The three state disturbances in this dissertation are modeled separately by $\dot{\hat{d}}(t)$ which represent the TC's speed variations, parameter uncertainties, and linearization constants. This observer is used in the disturbance canceling controller to apply the TCC in such a way that energy of the ICE torque impulses are stored in and released from the TC fluid coupling to provide a constant turbine speed and torque to the drive line [38], [39].

4.5 State Feedback, Disturbance Canceling, and Setpoint Tracking Controllers

The TC control problem is to actuate the TCC in such a way that the TC system is able to isolate the pump speed disturbances from the turbine speed while simultaneously improving system efficiency. The DOBC utilizes three control signals to stabilize and tune the TC response to dynamic changes, eliminate disturbances from the states to keep the TCC in slip mode, and provide tracking of the system speeds to the desired references. These methods are called state feedback control, state disturbance canceling control, and setpoint tracking control.

The state feedback controller uses the observer estimate of x to stabilize and control the TC system's response to TCC applications. The observer estimate is acted upon by the feedback gain to generate the continuous time system input u_c:

$$u_c(t) = -K\hat{x}(t) \tag{4.6}$$

where K is the feedback gain and is chosen by the Ackermann's formula to place closed-loop system poles at desired locations.

The disturbance canceling controller uses the disturbance estimate to cancel the effects of them on the system. Because this input is added to the other system inputs that are acted upon by the input gain, a disturbance gain must be used to cancel the effects of the input gain in this controller. The control law is:

$$u_d(t) = -B_d\hat{d}(t) \tag{4.7}$$

where $u_d(t)$ is the disturbance canceling control input, B_d is chosen to be the left pseudoinverse of B, and $\hat{d}(t)$ is the continuous disturbance estimate from the observer.

The setpoint tracking controller drives the TCC in such a way that the pump and turbine speeds follow a set profile to ensure slip mode operation of the TC. For this study, slip mode [4], [8] is defined as when the pump and turbine speed are within 25 to 100 RPM of each other, allowing the fluid coupling to dampen the pump speeds, giving a constant turbine speed to smooth operation. The regulator operates by adding a tracking reference signal to the system for feedforward control and a feedback signal to drive the states to predetermined values as shown in Figure 4.2 below.

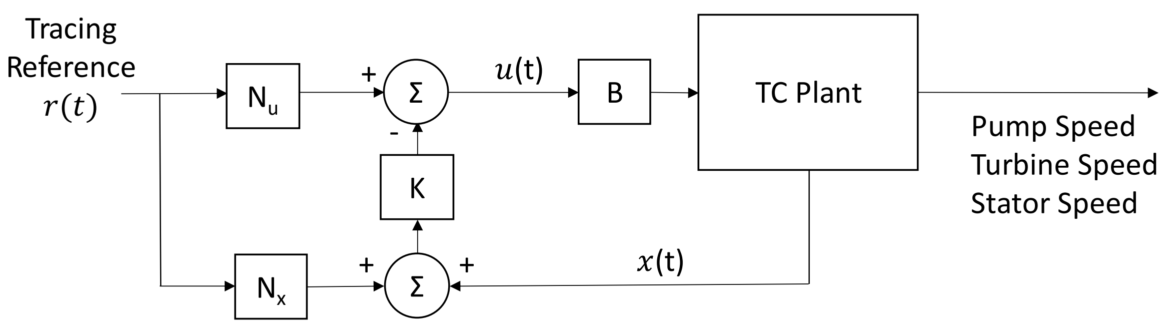

Figure 4.2 - Setpoint Tracking Control with Dual Inputs

The overall control law for this method is given by:

$$u_r(t) = N_u * r(t) + N_x * K * r(t) \tag{4.8}$$

where N_u is the feedforward gain, and N_x is the feedback gain and r are the continuous state tracking values. To solve for N_u and N_x, the steady state conditions for (4.8) values were found when $y(t) \approx r(t)$ for $t > 0$. Starting with the steady state $\dot{x}_{ss}$ without the disturbance the system becomes

$$\dot{x}_{ss} = AN_x x_{ss} + BN_u u_{ss} = (AN_x + BN_u) r_{ss} \tag{4.9}$$

$$y_{ss} = r_{ss} = Cx_{ss} + Du_{ss} = (CN_x + DN_u) r_{ss} \tag{4.10}$$

where the subscript "ss" denotes the time invariant steady state values of x, u, and r respectively.

For simplicity, the feedback signal can be routed through feedforward input if the feedback gain is included as shown in Figure 4.3.

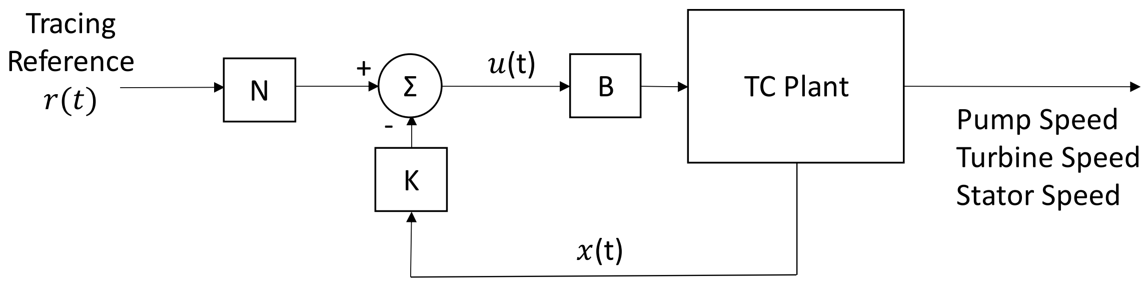

Figure 4.3 - Setpoint Tracking Control

where $N = \begin{bmatrix} N_x \\ KN_u \end{bmatrix}$. Using the simplified feedforward scheme, the control law for the set point regulator becomes

$$u_r(t) = Nr(t) \ . \tag{4.11}$$

The three control elements from (4.6), (4.7) ,and (4.11) give the D-DOBC control law:

$$u(t) = -K\hat{x}(t) - B_d\hat{d}(t) + Nr(t) \tag{4.12}$$

Substituting (4.12) into (4.1) gives the closed-loop system:

$$\dot{x} = Ax(t) + B(-K\hat{x}(t) - B_d\hat{d}(t) + Nr(t)) + d(t) \tag{4.13}$$

Distributing the input matrix throughout (4.13) given by:

$$\dot{x} = Ax(t) - BK\hat{x}(t) - BB_d\hat{d}(t) + BNr(t) + d(t) \tag{4.14}$$

When combined with the system of equations (SoE) in (4.5), a combined SoE for the TC, including both observers and the combined control laws, is:

$$\begin{bmatrix} \dot{x}(t) \\ \dot{\hat{x}}(t) \\ \dot{\hat{d}}(t) \end{bmatrix} = \begin{bmatrix} A & -BK & 1 \\ LC & A - BK - LC & B_d \\ 0 & 0 & F \end{bmatrix} \begin{bmatrix} x(t) \\ \hat{x}(t) \\ \hat{d}(t) \end{bmatrix} + \begin{bmatrix} BN \\ BN \\ 0 \end{bmatrix} r(t) + \begin{bmatrix} d(t) \\ 0 \\ 0 \end{bmatrix}$$

should this be

$$\begin{bmatrix} \dot{x}(t) \\ \dot{\hat{x}}(t) \\ \dot{\hat{d}}(t) \end{bmatrix} = \begin{bmatrix} A & -BK & -B_d \\ LC & A - BK - LC & 0 \\ 0 & 0 & F \end{bmatrix} \begin{bmatrix} x(t) \\ \hat{x}(t) \\ \hat{d}(t) \end{bmatrix} + \begin{bmatrix} BN \\ BN \\ 0 \end{bmatrix} r(t) \begin{bmatrix} F \\ 0 \\ 0 \end{bmatrix} + \begin{bmatrix} d(t) \\ 0 \\ 0 \end{bmatrix}$$

and

$$\begin{bmatrix} \dot{x}(t) \\ \dot{\hat{x}}(t) \\ \dot{\hat{d}}(t) \end{bmatrix} = \begin{bmatrix} A & -BK & 1 \\ LC & A - BK - LC & B_d \\ 0 & 0 & F \end{bmatrix} \begin{bmatrix} x(t) \\ \hat{x}(t) \\ \hat{d}(t) \end{bmatrix} + \begin{bmatrix} BN \\ BN \\ 0 \end{bmatrix} r(t) + \begin{bmatrix} d(t) \\ 0 \\ 0 \end{bmatrix} \tag{4.15}$$

This D-DOBC control method is applied to the three-state linear TC model described in Chapter Two to drive the TCC input in such a way that the pump and turbine speeds track the reference speeds forcing the TC to remain in slip mode.

4.6 Simulation Results and Discussion

The goal of this section is to simulate and evaluate the effectiveness of the D-DOBC control method on a TC system using the same parameters used in the model creation as presented Chapter Two. The simulations are preformed using MATLAB and the SoE are solved using the MATLAB ODE solvers. The simulation period is for 10 seconds with the TCC applied at 4 seconds. The analysis of these results focuses on the quality of the state observer, the estimation of random disturbance, and the system's robustness to track the reference input with large state disturbances.

The TC pump, turbine, and stator speeds are quickly stabilized within the first few milliseconds of simulation. The state observer acts even quicker to track the TC plant speed almost instantaneously during this simulation. Its robustness continues throughout the simulation as is shown during the abrupt application of the TCC control at 4 seconds when it enters slip mode. The excellent tracking of the observer is the result of the choice of the poles in (4.3), creating an observer that is fast enough to follow the abrupt speed changes without noticeable overshoot system ringing. The three linearized TC states and their corresponding observer estimate states are shown in Figure 4.4.

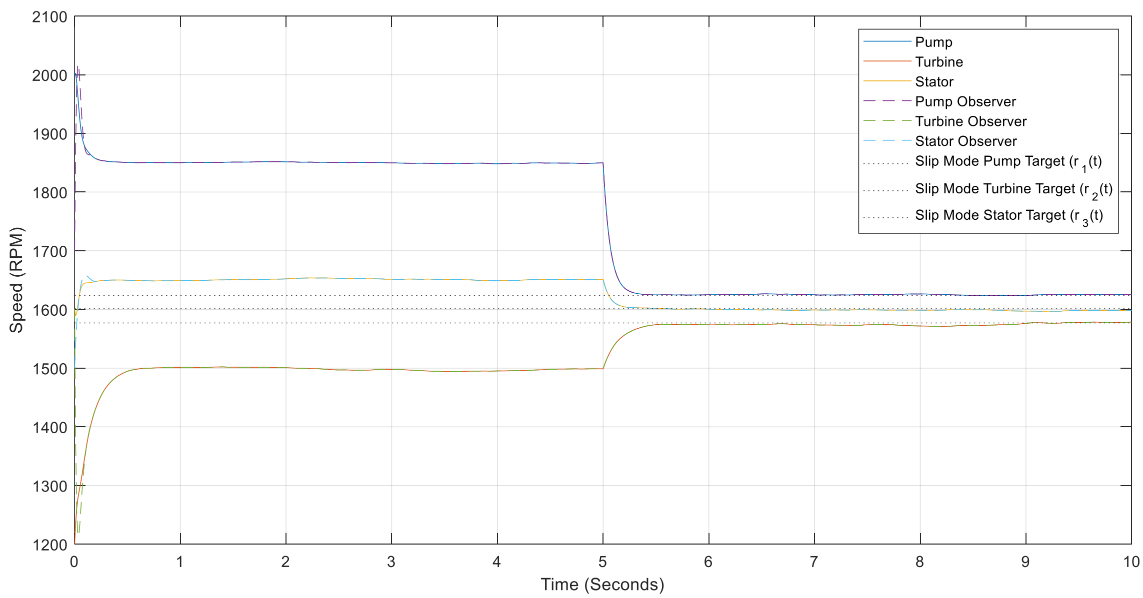

Figure 4.4 - Torque Converter Outputs, Observers and Tracking Reference

The magnitude of the disturbance, about ±10% of the state values, are shown, along with their estimates, in Figure 4.5. Figure 4.6 shows the instantaneous errors of the estimates during the simulation.

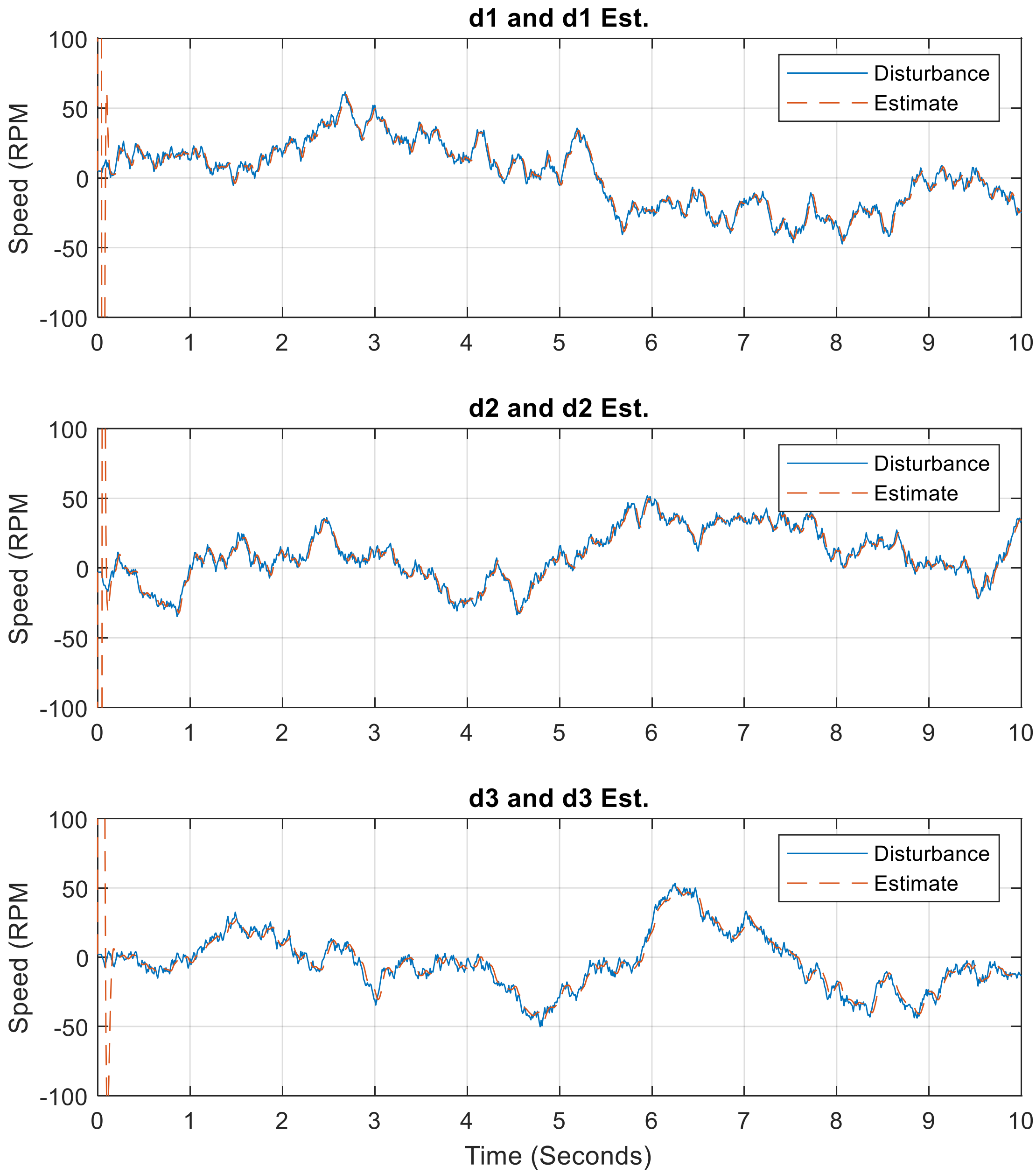

Figure 4.5 - Disturbance with their Estimates Using High R Observer L Matrix

Noting objective of this research is to design a controller with reference output tracking and disturbance rejection, the LQR Observer matrix is selected to have a faster, larger value for the parameter R, ensuring good output by weighting tracking of the observer states over plant states. Additionally, the state and disturbance observers give good estimates for state feedback control and disturbance rejection controllers respectively. Figure 4.6 demonstrates the estimate not only tracks the magnitude of disturbance very well, but there is very little delay resulting in an error of ± 10 RPM.

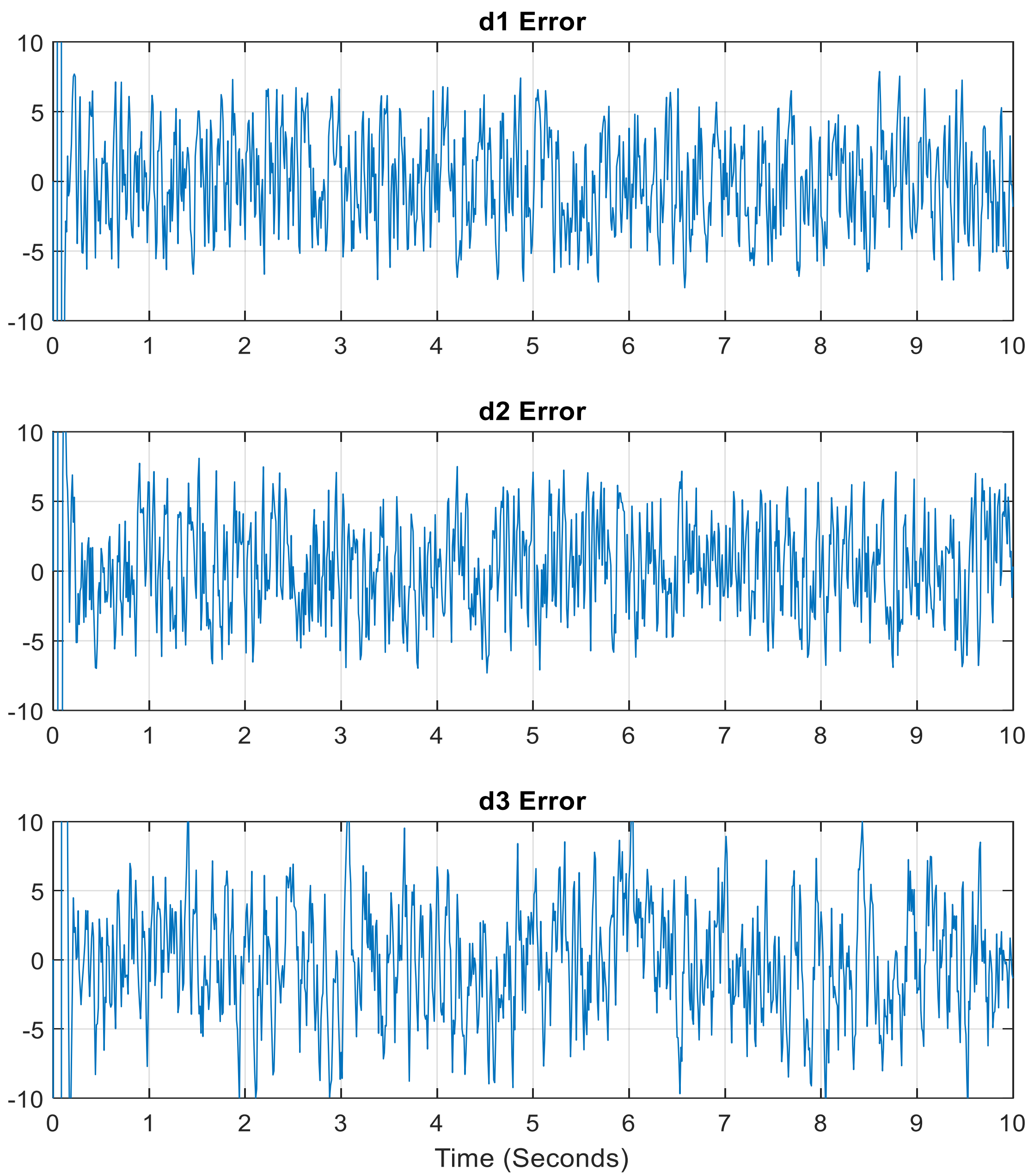

Figure 4.6 - Disturbance Errors Using High R Observer L Matrix

For comparison, the results of the disturbance estimates with a weaker observer, less negative poles, are presented in Figure 4.7. The magnitude of the disturbance is similar but, because of the slower observer, the error caused by this delay is ±100 RPM and the system takes several seconds to stabilize.

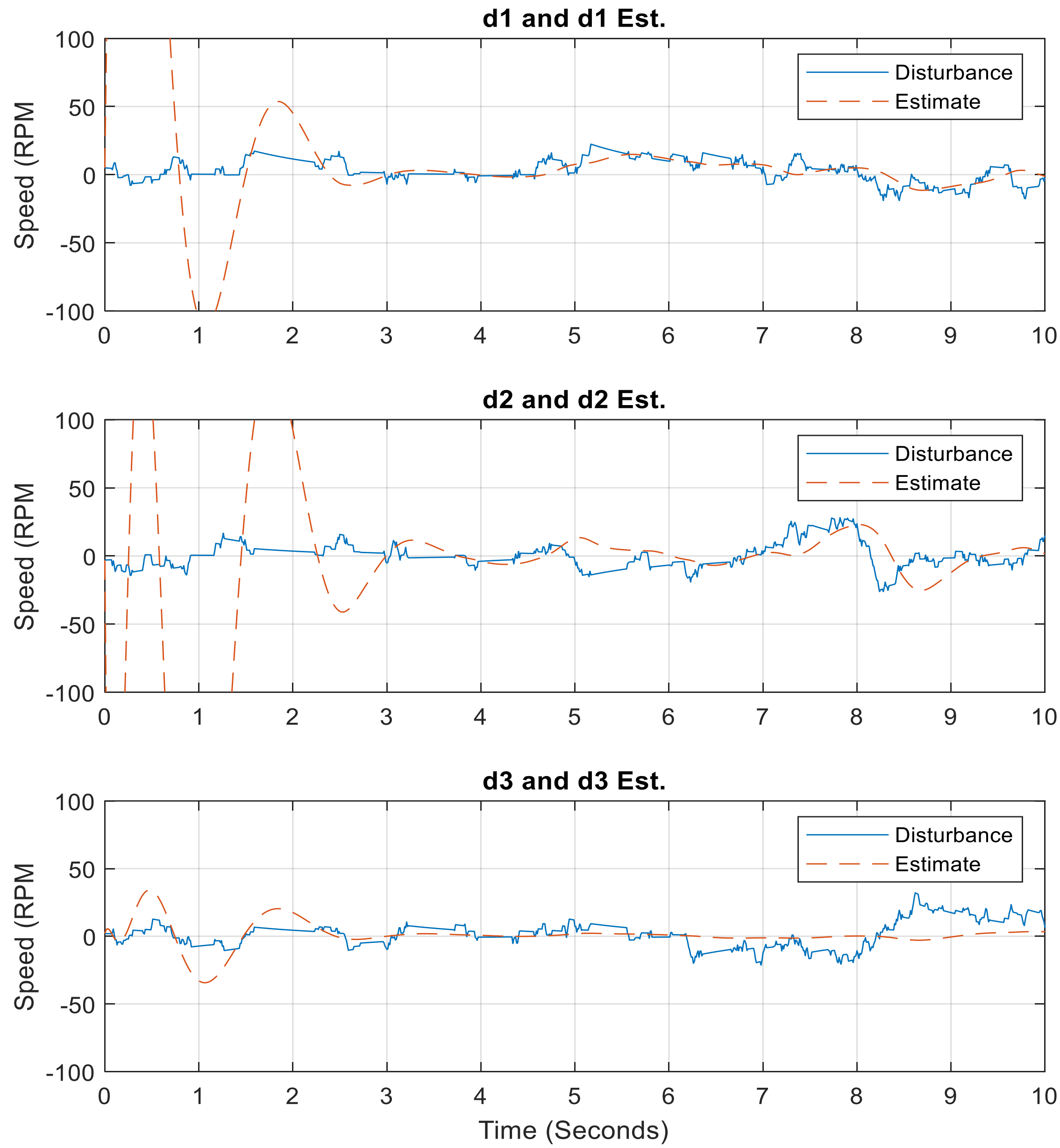

Figure 4.7 - Disturbance Estimates with Weaker Observer Matrix

The results of the errors with the slower observer are shown in Figure (4.8).

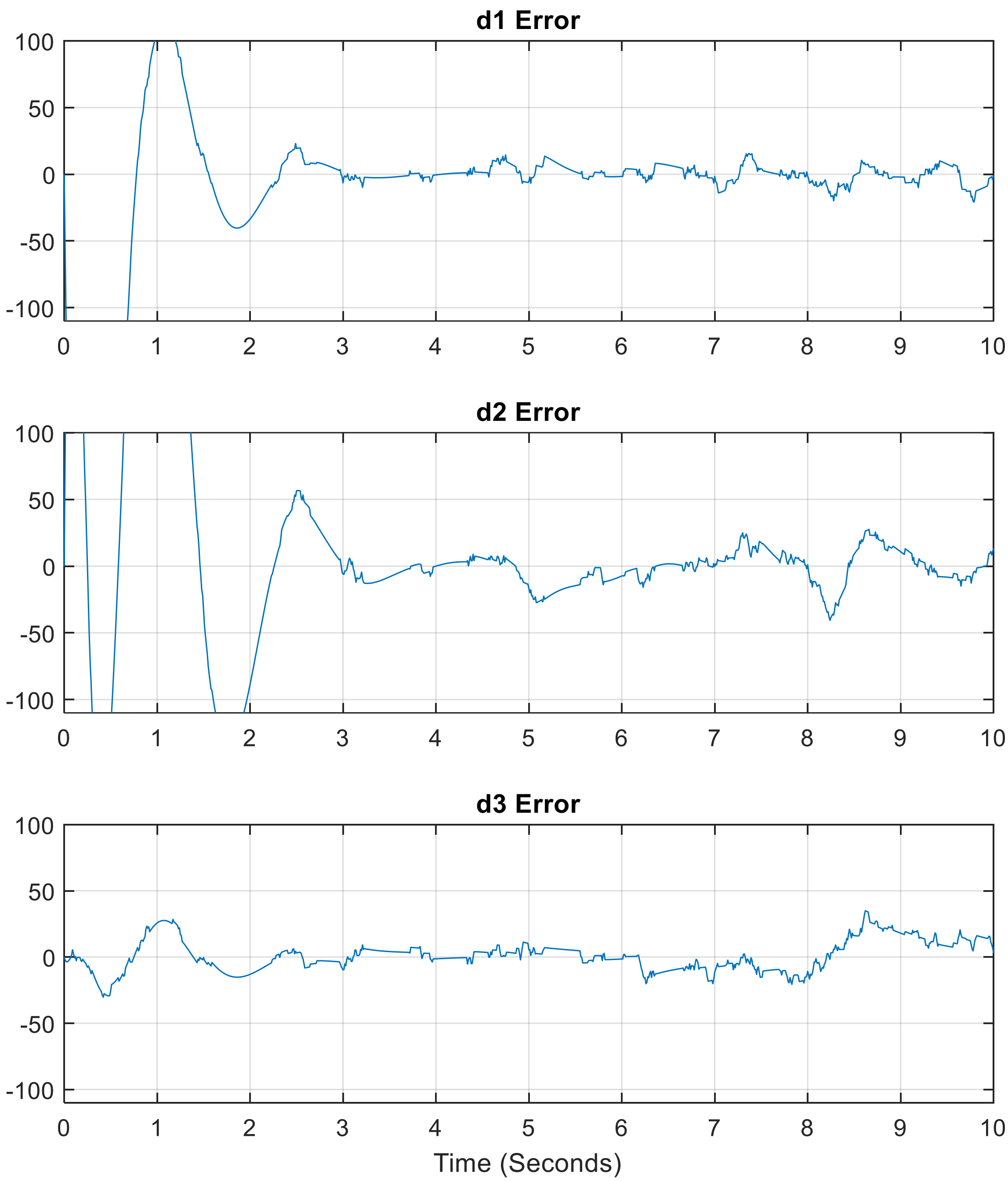

Figure 4.8 - Disturbance Errors Using Weaker Observer Matrix

As expected, the use of a slower observer matrix caused the observer to take longer to track the target reference speeds. Because the observers are used for state feedback, this also delayed the pump, turbine and stator tracking. These results are presented in Figure 4.9.

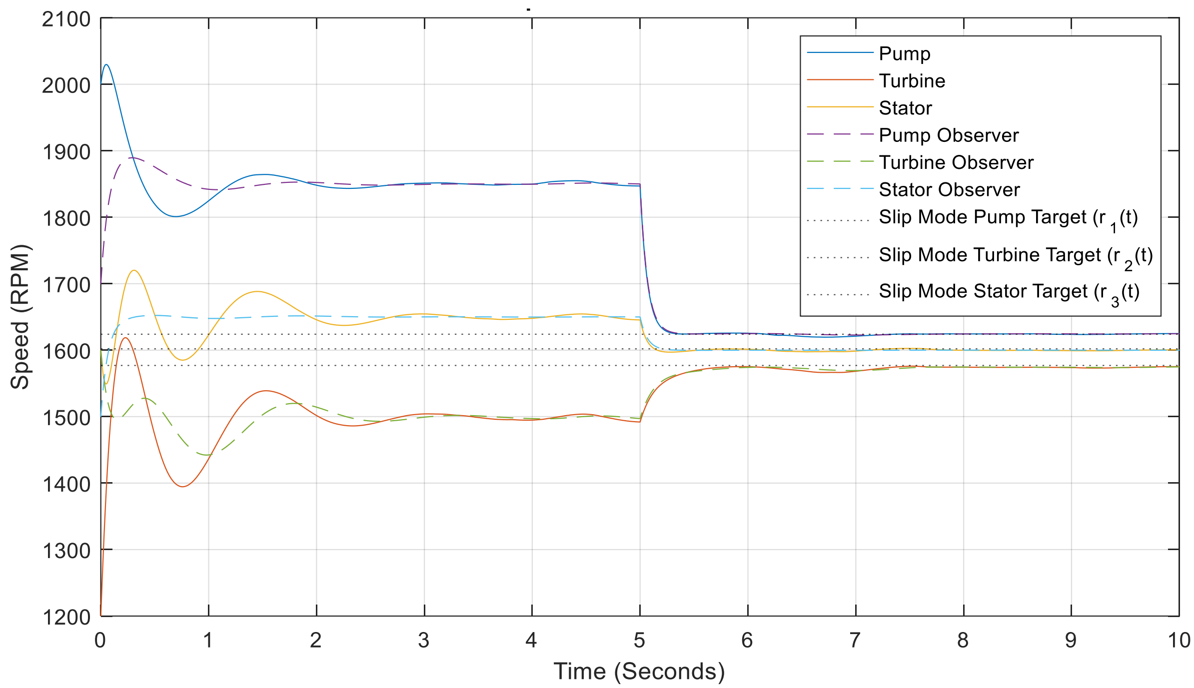

Figure 4.9 - Plant Output with Weaker Observer

To evaluate the robustness to distrubance rejection of D-DOBC control with a fast observer, disturbances of 25% and 50% of the state RPMs were intoduced. These disturbances and their estimates are shown in Figures 4.10 and 4.11 respectively.

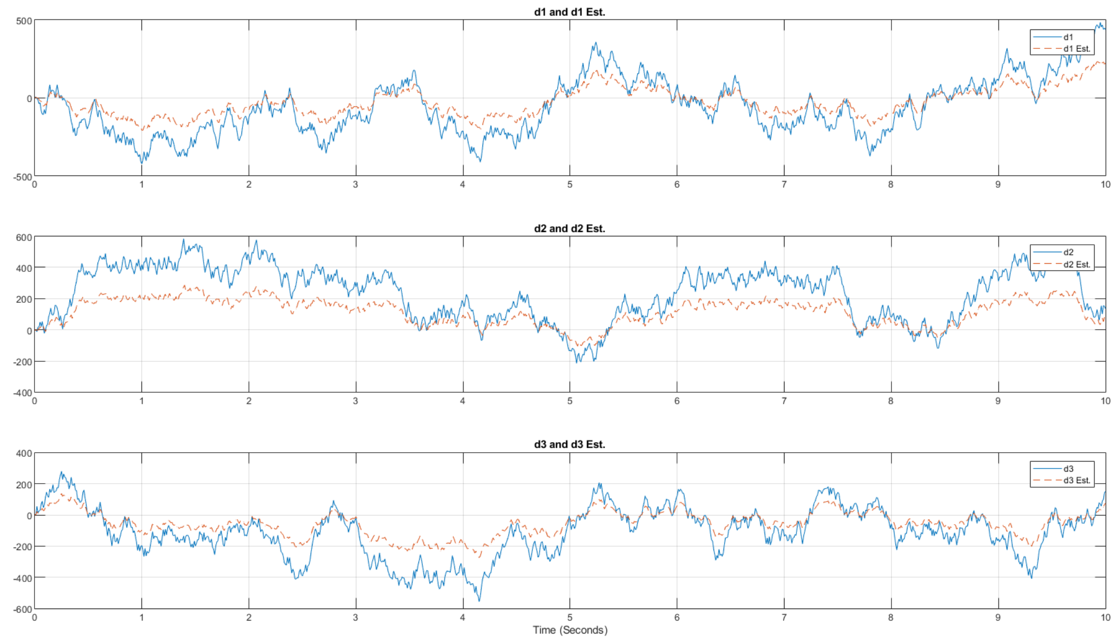

Figure 4.10 - TC State Disturbance of 25% of State RPM

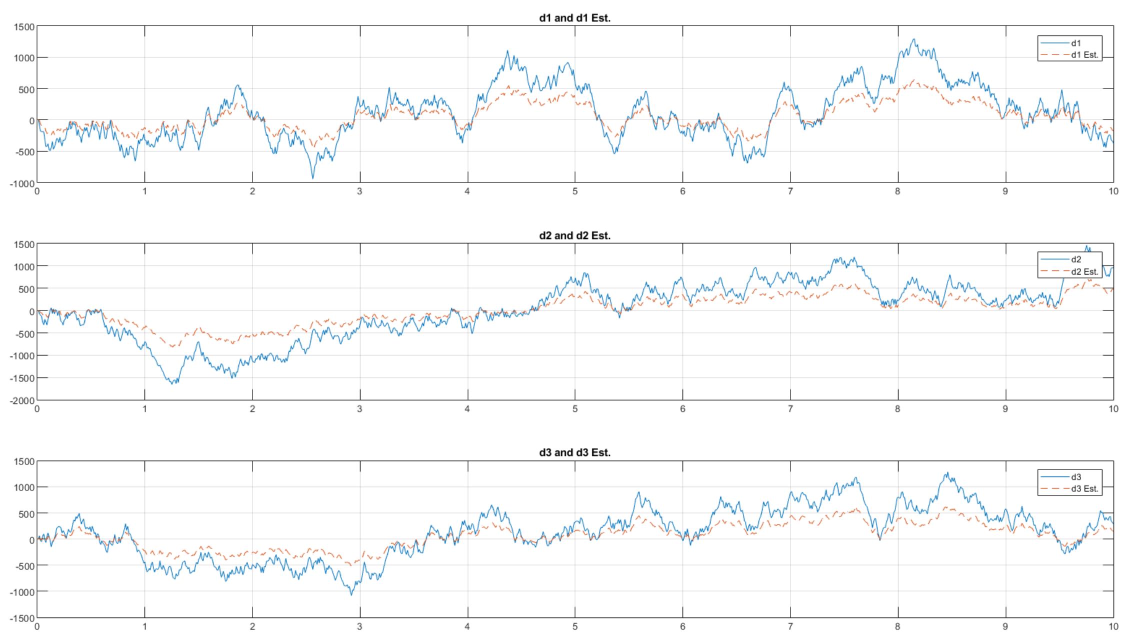

Figure 4.11 - TC State Disturbance of 50% of State RPM

The resulting effect on the TC model states of the introduction of 25% and 50% of the state RPM distrubances are shown in are shown in Figures 4.12 and 4.13 respectively.

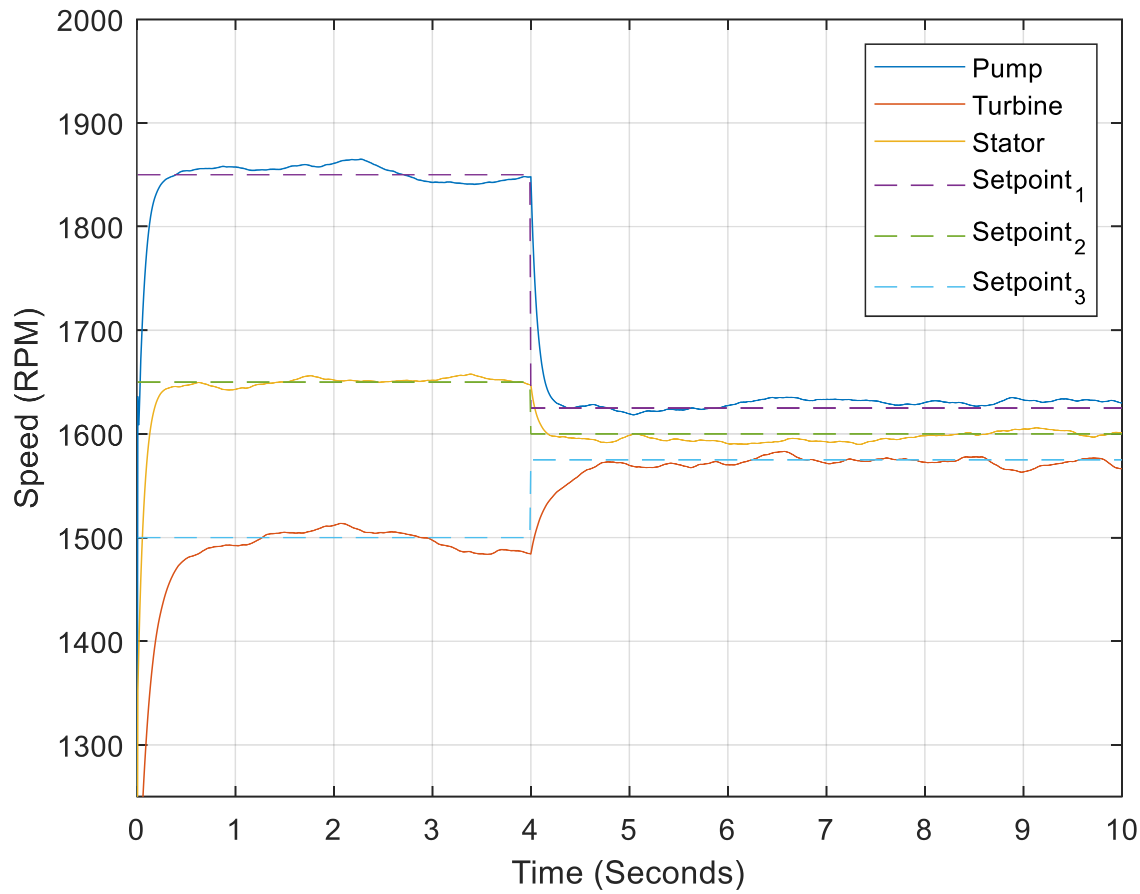

Figure 4.12 - TC States and Output with 25% State RPM Disturbance

The results of the 25% of the state RPM distrubance simulations shows the controller was able to maintain the slip between the pump and turbine thus the TCC remained in slip mode and dampen the ICE’s speed fluctionations. However the disturbance canceling controller allowed some of the disturbances to be transmitted to the TC turbine and vehicle driveline.

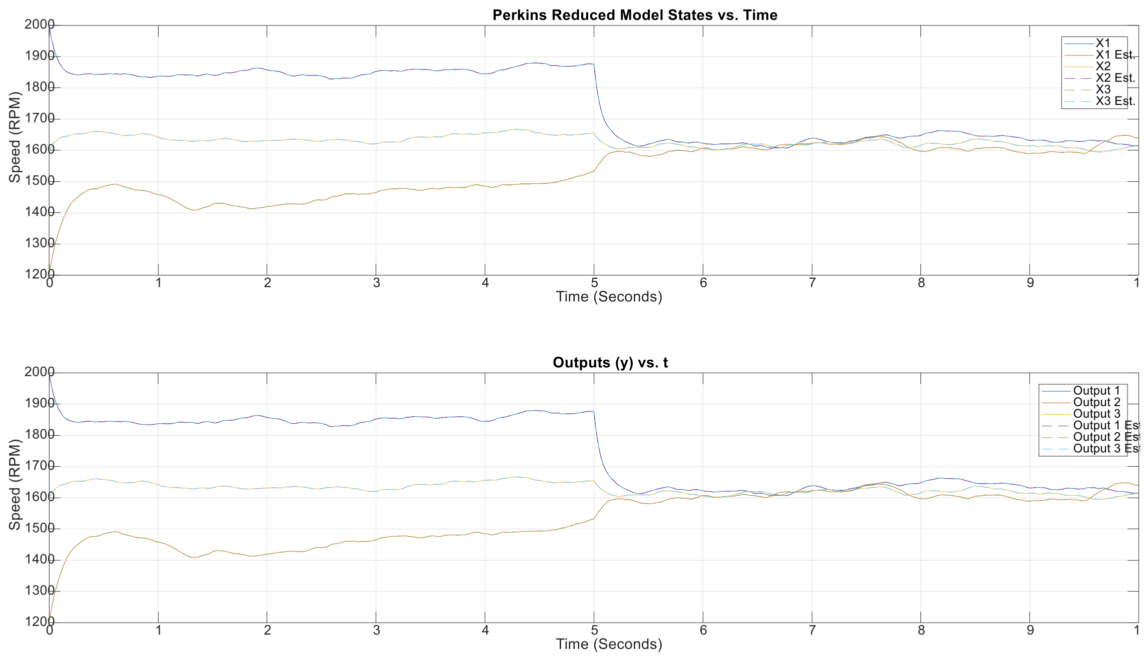

Figure 4.13 - TC States and Output with 50% of State RPM Disturbance

With 50% of the state RPM disturbances, the TC was not able to maintain a RPM difference between the pump and turbine several times closing the TCC. When the slip RPM is zero the TC enteres locked mode and the TC's fluid coupler does not dampen any of the engine's speed fluctations causing them to be transmitted to the vehicle's driveline causing harness.

In conclusion, the D-DOBC is able to drive the TC outputs to the setpoint using the control regulator very well. It is noteworthy that when the TC enters slip mode at 4 seconds into the simulation, it took the plant model about 1 second to stabilize and reestablish input tracking at the new reference values. The limiting factor here was not the controller but the plants' inertia, limiting the systems ability to respond to such an abrupt input change. The disturbance canceling element of the D-DOBC works very well to about 10 - 20% state disturbance. Figure 4.13a presents the TC speeds without disturbance canceling control and Figure 4.13b with the disturbance canceling control active. It is shown in the former that with as little as 10% of the state RPM as disturbance the TC is uncontrollable while with noise canceling the reference tracking is nearly 100%.

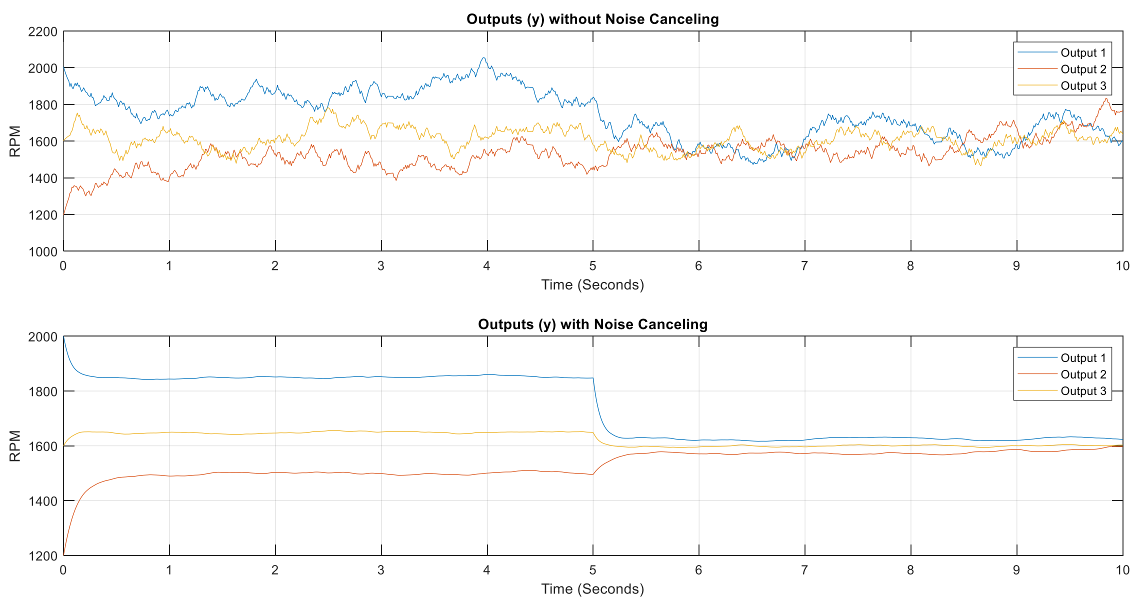

Figure 4.14 - Torque Converter States Without and With Noise Canceling

CHAPTER FIVE

DESIGN OF AN INDIRECT DISTURBANCE OBSERVERBASED CONTROLLER

5.1 Introduction

This chapter of the dissertation presents an Indirect Disturbance Observer Based Controller (I-DOBC) that uses multiple controllers to regulate the speeds of the TC system during slip mode. As in the previous chapter, this method combines three control signals. They are state feedback, setpoint reference tracking, and disturbance canceling controls. The difference between D-DOBC and I-DOBC is that the I-DOBC calculates a single estimate of a noisy observer that includes both the state and disturbance. The disturbance is then algebraically separated from the state signal. This dissertation presents two different methods to calculate this disturbance and the methods used to design the noise canceling controller later in this chapter.

The I-DOBC TCC controller is useful when an independent estimate of the disturbance is not available or practical because of the nature or quality of state measurements. We have chosen to implement an I-DOBC control scheme on our Torque Converter system to evaluate it under extremely noisy conditions with exceptionally low Signal-to-Noise Ratios.

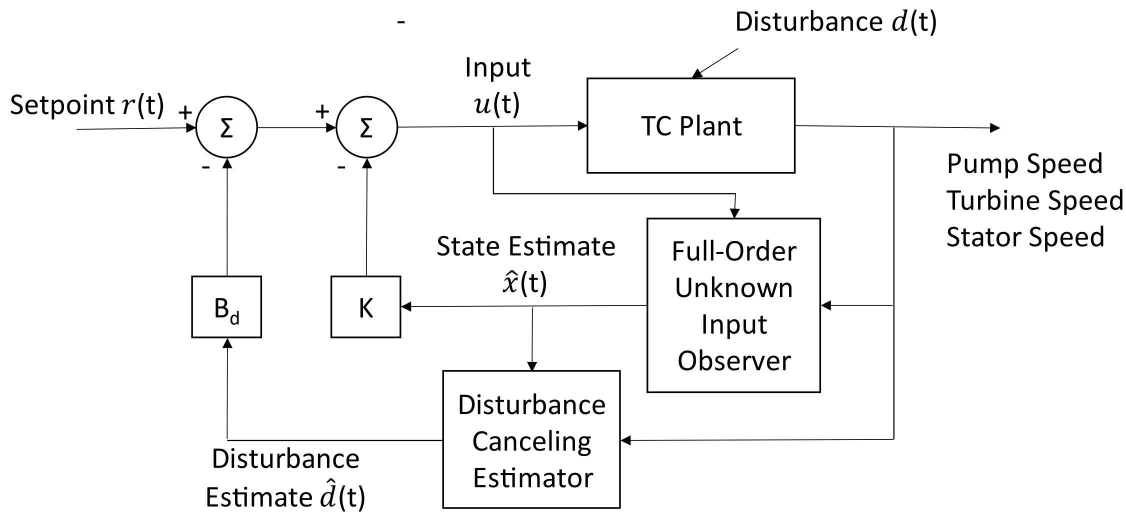

Figure 5.1 - Flow Chart of an Indirect DOBC (I-DOBC) Control Scheme

The I-DOBC TCC control scheme consists of three separate controllers: full state feedback, input reference tracking, and disturbance canceling. The main difference between the direct and indirect DOBC controllers has to do with how the disturbance estimate $\hat{d}(t)$ is obtained. The I-DOBC controller utilizes a noisy observer estimate of states $\bar{x}(t)$, which consists of a joint state and disturbance estimates, as shown in equation (5.1). This noisy observer estimate $\bar{x}(t)$ is obtained by using an unknown input observer (UIO) [41], which is discussed in the following subsection. The disturbance estimate $\hat{d}(t)$ is then separated from the state estimate $\hat{x}(t)$ and used by the disturbance canceling controller and combined with the feedback and reference controllers into a single plant control signal.

$$\bar{x}(t) = \hat{x}(t) + \hat{d}(t) \tag{5.1}$$

5.2 The Design of an Indirect Noisy State Observer for TCC control

The I-DOBC method uses an unknow input observer (UIO) to estimate the plant states [51]. This estimate is a noisy, it includes the plant states and the disturbances, and is used for both feedback control and disturbance estimation. These types of observers are especially useful when the plant model is understood, however measurement data is not available because it is either impractical or expensive to obtain.

This thesis implements the UIO as shown in Figure 5.2.

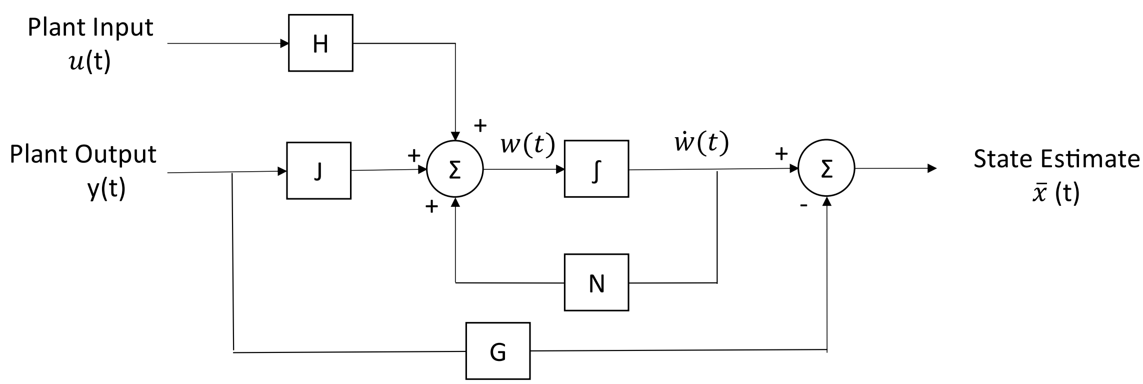

Figure 5.2 - Unknown Input Observer Flow Chart

where

$$\bar{x}(t) = w + Gy \tag{5.2}$$

$$w(t) = Nw + Jy + Hu. \tag{5.3}$$

With $\dot{x}(t)$ already known, $\dot{\bar{x}}(t)$ from (5.2) and (5.3) is restated in terms of $x(t)$, $u(t)$, and $d(t)$ as

$$\dot{\bar{x}}(t) = (N - NGC + JC + GCA)x(t) + (H + GCB)u(t) + (GCW)d(t) \tag{5.4}$$

For the estimate to be useful, the error should be minimized as $\mathrm{e(t)} \rightarrow 0$ as $\mathrm{t(t)} \rightarrow \infty$ with $\mathrm{e(t)}$ defined as

$$\dot{\mathrm{e}}(\mathrm{t}) = \dot{\hat{\mathrm{x}}}(\mathrm{t}) - \dot{\mathrm{x}}(\mathrm{t}). \tag{5.5}$$

Substituting (5.4) into (5.5) given by:

$$\dot{\mathrm{e}}(\mathrm{t}) = \mathrm{Ne(t)} + (\mathrm{N} - \mathrm{NGC} + \mathrm{JC} - \mathrm{A} + \mathrm{GCA})\mathrm{x(t)} + (\mathrm{H} - \mathrm{B} + \mathrm{GCB})\mathrm{u(t)} + (\mathrm{GCW} - \mathrm{W})\mathrm{d(t)} \tag{5.6}$$

For asymptotically stable convergence to be guaranteed, the coefficients of $\mathrm{x(t)}$, $\mathrm{u(t)}$, and $\mathrm{d(t)}$ must equal zero, as shown in (5.7), (5.8), and (5.9):

$$0 = \mathrm{N} - \mathrm{NGC} + \mathrm{JC} - \mathrm{A} + \mathrm{GCA} \tag{5.7}$$

$$0 = \mathrm{H} - \mathrm{B} + \mathrm{GCB} \tag{5.8}$$

$$0 = \mathrm{GCW} - \mathrm{W} \tag{5.9}$$

Solving (5.9) for the G matrix given by:

$$\mathrm{G} = \mathrm{W(CW)}^{+} \tag{5.10}$$

where $\mathrm{(CW)}^{+}$ is the pseudo inverse of (CW) and solving (5.8) for H

$$\mathrm{H} = \mathrm{YB} \tag{5.11}$$

with

$$\mathrm{Y} = (\mathrm{I} - \mathrm{GC}). \tag{5.12}$$

Using Y to restate (5.7) given by:

$$N = YA - SC \tag{5.13}$$

with

$$S = (J - NG) \tag{5.14}$$

With the above relationships of the UIO established, the following four steps are used to design the observer.

- Step One: Calculate the G and Y matrix for the TC observer using (5.10) and (5.12).
- Step Two: Select an S matrix such that (5.14) is stable. In this step, the eigenvalues of $(YA - SC)$ are placed on the complex s-plant such that the pair (C, YA) are observable.
- Step Three: Calculate the H matrix from (5.11)
- Step Four: Calculate J from

$$J = L + NE \tag{5.15}$$

With the UIO designed, the work of estimation the disturbance using $\bar{x}(t)$ is described in the next section of this Chapter.

<u>5.3 Estimation of Noise $\hat{d}(t)$ from Noisy State Estimate $\bar{x}(t)$</u>

The UIO discussed above provides a noisy observer estimate of states $\bar{x}(t)$, which consists of a joint state and disturbance estimates, as shown in equation (5.1). This section presents a method of extracting the disturbance estimate $\hat{d}(t)$ from $\bar{x}(t)$. It is based on the principle of state variable filtering, as explained below.

A state variable filter (SVF) is typically used to estimate the parameters of a continuous time system without computing any derivatives of the input and output signals [58], [59]. In this case, however, we use it to separate out $\hat{d}(t)$ and $\hat{x}(t)$ from $\overline{x}(t)$, as follows.

To start with, consider the following state space equations of the TCC system:

$$\dot{x}(t) = Ax(t) + Bu(t) + d(t) \tag{5.16}$$

We can estimate d(t) from the above equation provided we know x(t), $\dot{x}(t)$ and u(t). The UIO discussed in section 5.2 above provides us $\overline{x}(t)$, which is a good estimate of x(t), and u(t) is known. However, since $\dot{x}(t)$ is not available directly, we can use a SVF to find a good estimate of it.

To simplify the computations, first let

$$A = \begin{bmatrix} A_1 \\ A_2 \\ A_3 \end{bmatrix} \tag{5.17}$$

$$B = \begin{bmatrix} B_1 \\ B_2 \\ B_3 \end{bmatrix} \tag{5.18}$$

where A_i, B_i, $1 \leq i \leq 3$, denote the i^{th} rows of the above matrices. Equation (5.16) can then be broken up into three separate state equations that correspond to the three state variables:

$$\dot{x}_i(t) = A_i x(t) + B_i u(t) + d_i(t), 1 \leq i \leq 3 \tag{5.19}$$

In view of above, since $\overline{x}(t)$ is a good estimate of x(t), it should obey the same equation as (5.19), i.e.

$$\dot{\overline{x_i}}(t) = A_i \overline{x_i}(t) + B_i u(t) + d_i(t), 1 \leq i \leq 3 \tag{5.20}$$

Next, in terms of differential operator, D = d/dt, we introduce a polynomial operator,

$$F(D) = (D + p), \tag{5.21}$$

and define the following filtered signals:

$$\overline{x_{if}}(t) = \frac{x_i(t)}{F(D)} \tag{5.22}$$

$$\dot{\overline{x_{if}}}(t) = \frac{D\dot{x}_i(t)}{F(D)} \tag{5.23}$$

$$u_f(t) = \frac{u(t)}{F(D)} \tag{5.24}$$

$$1_f(t) = \frac{1}{F(D)} \tag{5.25}$$

It should be pointed out that the choice of the filter's pole, p, depends on the desired trade-off between the filter's bandwidth and estimation accuracy [58], [59].

Dividing both sides of equation (5.19) by F(D) and utilizing equations (5.22) - (5.25), we get:

$$\dot{\overline{x_{if}}}(t) = A_i\overline{x_{if}}(t) + B_i u_f(t) + 1_f d_i(t), 1 \leq i \leq 3 \tag{5.26}$$

For notational convenience, let

$$z_i(t) = \dot{\overline{x_{if}}}(t) - A_i\overline{x_{if}}(t) - B_i u_f(t), 1 \leq i \leq 3 \tag{5.27}$$

and substitute in (5.11) to get

$$z_i(t) = 1_f d_i(t), 1 \leq i \leq 3 \tag{5.28}$$

Drawing analogy with the parameter estimation methods [34], each equation in (5.28) is seen to be of the form:

$$z(t) = \emptyset(t)^T\theta, \tag{5.29}$$

where $\phi(t)$ denotes a regression vector and θ denotes an unknown parameter. In this case, $\phi(t) = 1_f$ and $\theta = d_i$. Next, in order to use a discrete time parameter estimation method to estimate θ recursively, suppose z(k) and $\phi(k)$ denote the samples of z(t) and $\phi(t)$, respectively, at instances, $t_k = kT$, where k denotes the sampling index and T denotes the sampling interval. Then equation (5.18) can be written in a discretized form:

$$z(k) = \emptyset(k)^T\theta, \tag{5.30}$$

and the parameter, θ, can now be estimated using any recursive parameter estimation method [34]. Two such methods, recursive least squares (RLS) and least mean squares (LMS), have been investigated in this study. These are briefly summarized below.

<u>Recursive Least Squares (RLS) method</u>

Suppose $\widehat{\Theta}(k)$ denotes an estimate of θ at sampling time, k. In RLS method, the update equations for $\widehat{\Theta}(k)$ and the associated error covariance matrix, P(k), are given by:

Prediction error: $e(k) = z(k) - \Phi(k-1)^T\widehat{\Theta}(k-1)$ (5.31)

$$\widehat{\Theta}(k) = \widehat{\Theta}(k-1) + \frac{P(k-2)\Phi(k-1)}{1+\Phi(k-1)^T P(k-2)\Phi(k-1)}[e(k)] \tag{5.32}$$

$$P(k-1) = P(k-2) + \frac{P(k-2)\Phi(k-1)\Phi(k-1^T P(k-2)}{1+\Phi(k-1)^T P(k-2)\Phi(k-1)} \tag{5.33}$$

$$\widehat{\Theta}(0) = \Theta_0 \tag{5.34}$$

$$P(-1) = \sigma I \tag{5.35}$$

where Θ_0 denotes an initial estimate of Θ, and σ is chosen to be a large positive number [34].

<u>Least Mean Squares (LMS) method</u>

In LMS method, the update equation for $\widehat{\Theta}(k)$ is given by:

$$\widehat{\Theta}(k) = \widehat{\Theta}(k-1) + \mu e(k) \tag{5.36}$$

where μ is a constant step size, which is chosen to be a small number to prevent divergence of the parameter estimates.

In a TC system, the states are the turbine speed, the pump speed, and the stator speed. The TC pump is connected directly to the ICE and is often referred to as the input of the TC system. Its speed is measured by using the ICE's RPM and includes the speed fluctuations inherent to the four-cycle ICE combustions process. The second state is from the turbine which is connected to transmission gearbox and is often called the TC output. This speed is calculated from the time between teeth on a reluctor wheel or tone ring connected to the gearbox input. This method of speed calculation is subject to measurement errors induced during the reluctor time to RPM conversion. The final state is the stator's speed in RPM. The stator is the third moving object in the fluid coupling that is sandwiched between the pump and turbine. Because of its physical location, direct speed measurements are impractical, however, its speed is known to be bound between the pump and turbine speeds. In this dissertation, we rely on the accuracy of the mathematical models of the author derived from the work of Asi in [17], [18] to represent the stator speed. These three states, including the system disturbances, are presented as the parameter $x(t)$. The noise estimates, $\hat{d}(t)$, can be subtracted from the noisy observer estimates, $\bar{x}(t)$, to get clean state estimates, $\hat{x}(t)$.

5.4 Design of an I-DOBC TCC controller

The second component of the I-DOBC system is the state feedback controller. The state feedback controller is used to shape the response of the TC system to TCC signals triggered by setpoint changes. By making the closed-loop poles more negative, the system will increase the control effort making the TC respond faster at the cost of harness and overcorrection. This controller used the same Ackermann's Formula presented in Chapter 4 to create the feedback gain K [60]. This method sets the desired closed-loop poles of the TC system more negative than the open loop poles to ensure system stability by assuring the feedback is faster than the uncontrolled system. When the feedback gain matrix is applied, the control law becomes

$$u_c(t) = -Kx(t) \tag{5.37}$$

The set point tracking regulator operates by introducing a tracking reference signal into the input gain matrix B (feedforward control) and feedback gain matrix K (feedback control) to drive the states and thus the output to predetermined values as shown in Figure 5.3 below.

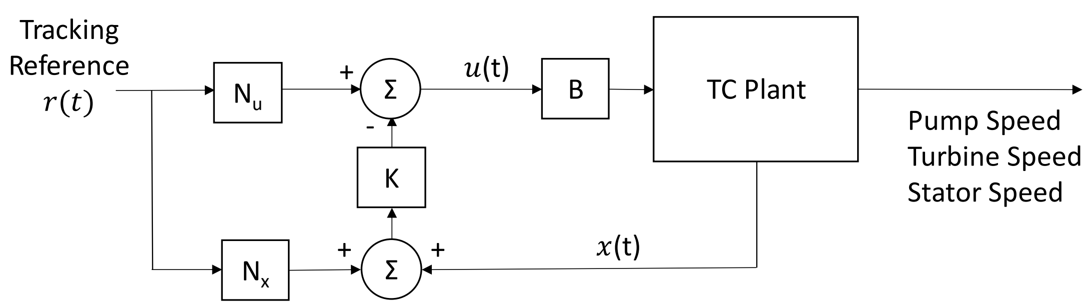

Figure 5.3 - Setpoint Tracking Control with Dual Inputs

The control law for this method is:

$$u_r(t) = N_u * r(t) + N_x * K * r(t) \tag{5.38}$$

where N_u is the feedforward gain and N_x is the feedback gain. The objective of this controller is to drive the steady state output to $y(t) \approx r(t)$ for $t > 0$. This dissertation solves these gains algebraically by noting that at steady state conditions, there are two equations and two unknowns, as presented in (5.39) and (5.40):

$$\dot{x}_{ss} = AN_x x_{ss} + BN_u u_{ss} = (AN_x + BN_u) r_{ss} \tag{5.39}$$

$$y_{ss} = r_{ss} = Cx_{ss} + Du_{ss} = (CN_x + DN_u) r_{ss} \tag{5.40}$$

where the subscript, ss, denotes the time invariant steady state values of x, u, and r, respectively.

For simplicity, the feedback signal can be routed through feedforward input if the feedback gain is included as shown in Figure 5.4 below.

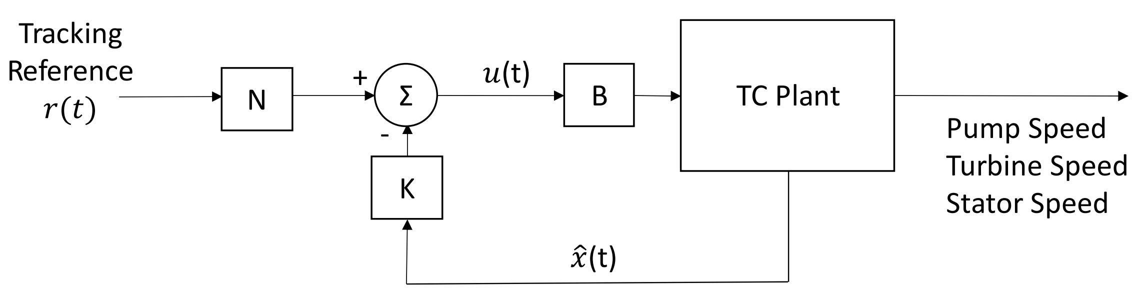

Figure 5.4 - Setpoint Tracking Control with Dual Input

where $N = \begin{bmatrix} N_x \\ KN_u \end{bmatrix}$. Using the reduced form, the control law for the set point regulator becomes:

$$u_r = Nr(t). \tag{5.41}$$

The second component of the I-DOBC system is the setpoint controller. This controller applies a signal to the TC system by using the TCC application as the system input to the pump speed, turbine speed, and stator speed, as the system outputs as shown in Figure 5.5.

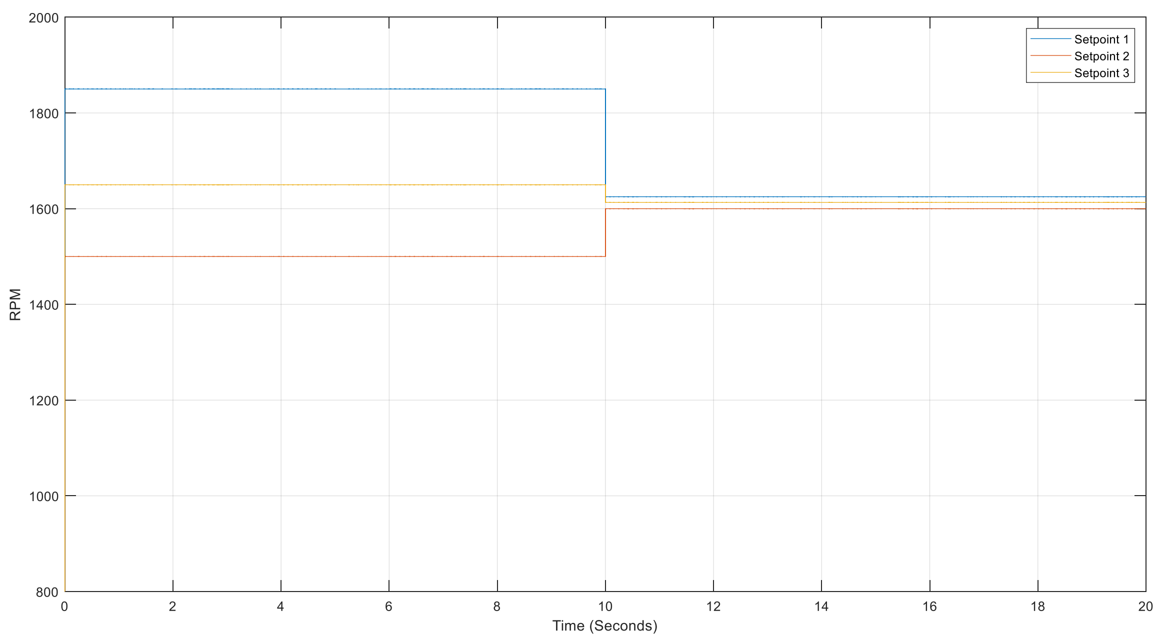

Figure 5.5 - TC Setpoint Tracking Inputs

The final controller in the I-DOBC scheme is the noise canceling controller. Its control law is shown in (5.42) and reflects the simplicity of how to cancel the unknown disturbance by subtracting the current disturbance estimate $\hat{d}(t)$.

$$u_d(t) = -B_d\hat{d}(t) \tag{5.42}$$

where $B_d = B'$ to cancel the effects of the Input Gain on the disturbance estimate.

Combining these three control laws in a single equation gives the new control law:

$$u(t) = -Kx(t) + Nr(t) - B_d\hat{d}(t) \tag{5.43}$$

The simulation of the disturbances to be estimated in the TC application relies on an understanding of what they represent. In this TC application, these disturbances are primarily from the pump speed fluctuations of the combustion cycle torque impulses. At higher speeds above 2000 RPM, these impulses are primarily filtered out by the physical low pass filter the rotating mass of the ICE and TC and are negligible. At lower speeds, they can be dramatic and, momentarily, can be as high as the actual engine RPM. The TC disturbances also includes modeling errors of the system parameters. These tend to be small in amplitude and slow changing as presented by Asl [17]. A final area of disturbance considered is measurement error. This would be a truly random miss calculation of the speed conversions outlined in the observer section.

5.5 Simulation Results and Discussion

Applying the same parameters used in the D-DOBC simulation presented in Table 2.2, this dissertation simulates a TC beginning in open-loop mode and entering slip mode at 10 seconds by applying the TCC. The reference speeds applied by the reference controller to pump, turbine, and stator speeds are 1625, 1575, and 1600, respectively. Three random state disturbances, a typical example of which is shown in Figure 5.6, are applied separately to each of the three plant states. The amplitude of these disturbances varies from 0% to 100% during different simulations to evaluate the controller's robustness to noise.

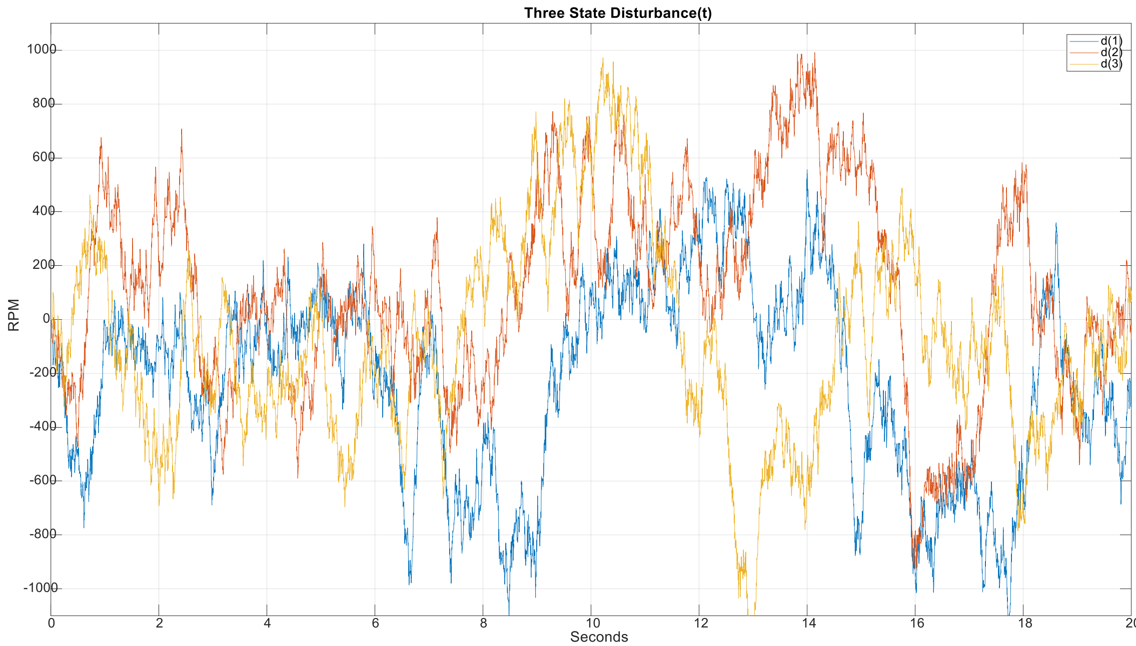

Figure 5.6 - State Disturbance

These disturbances are added separately to the TC's pump, turbine, and stator speed states to create a noisy plant including the disturbance, [x + d]. The results of a simulation of this noisy plant are presented in Figure 5.7.

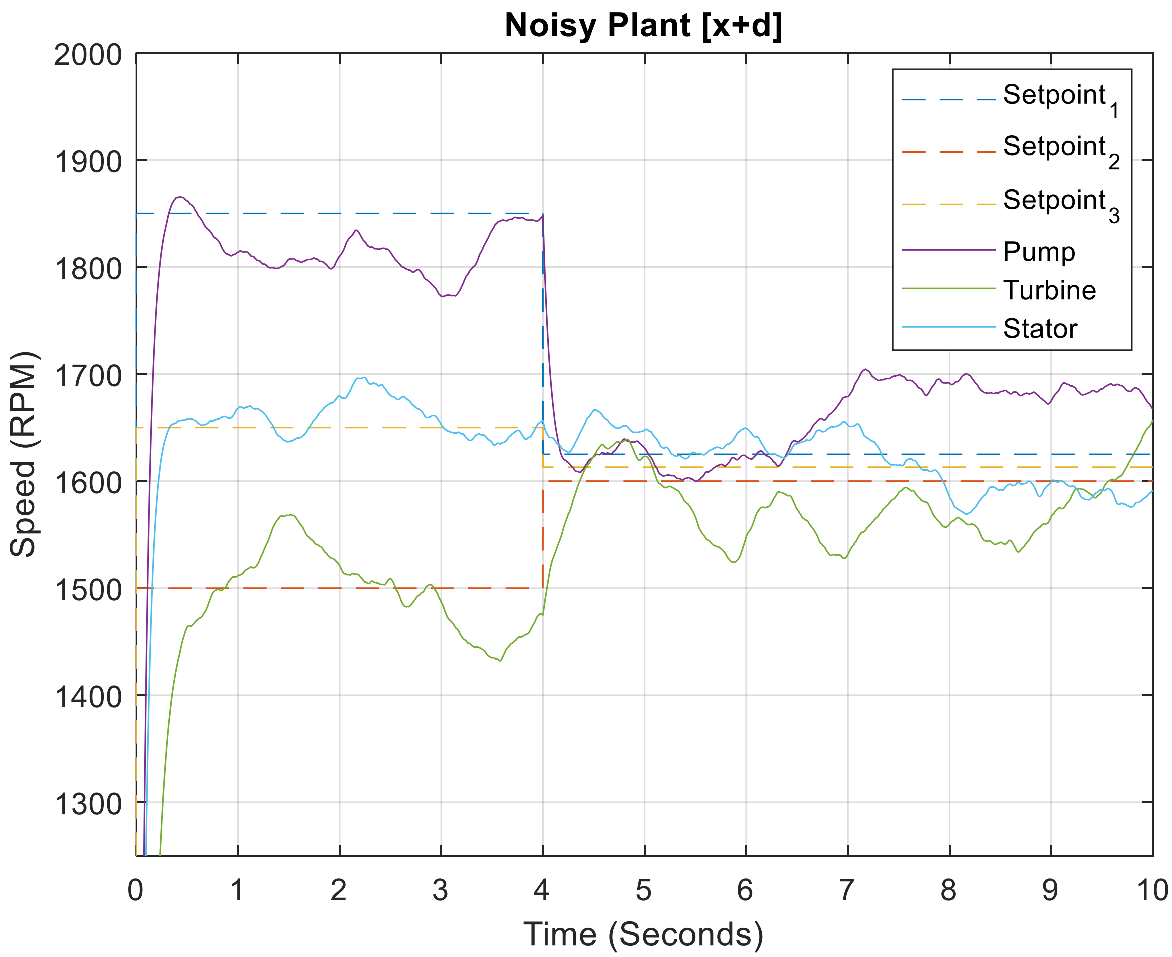

Figure 5.7 - Noisy TC with 25% State RPM Disturbance w/o Noise Rejection

As can be seen, after the TCC is applied at 4 seconds into the simulation, it is impossible to remain in slip mode, a controlled RPM difference between the pump and turbine speeds, because the speed fluctuations are often greater than 25 RPM slip delta set point of the reference controller. The I-DOBC method addresses this by applying a canceling estimate of the disturbance to the states in real time. The section discusses both the fixed and variable gain error correction methods, LMS and RLS, respectively.

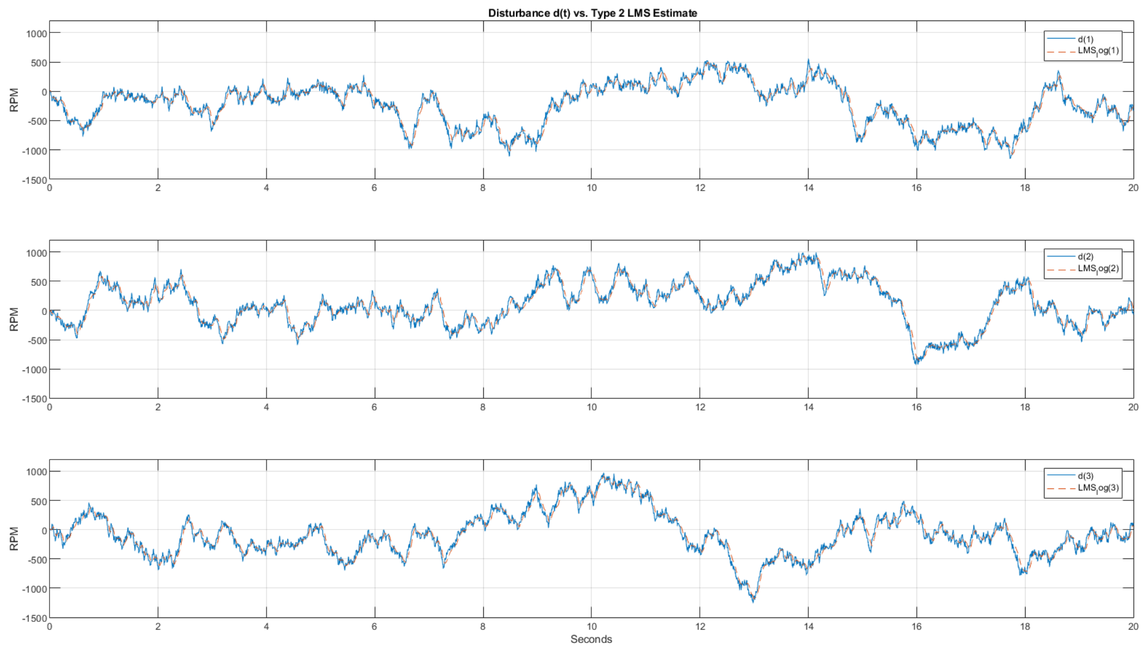

Figure 5.8 - Three State Disturbances and their LMS Estimates

Figure 5.8 shows the three independent random disturbances and their LMS estimates during the simulation. This figure shows the powerful robustness to noise and disturbance tracking ability of I-DOBC. To examine these changes more closely, the LMS estimate of the disturbances are magnified between 7.5 and 9.5 seconds and presented in Figure 5.9.

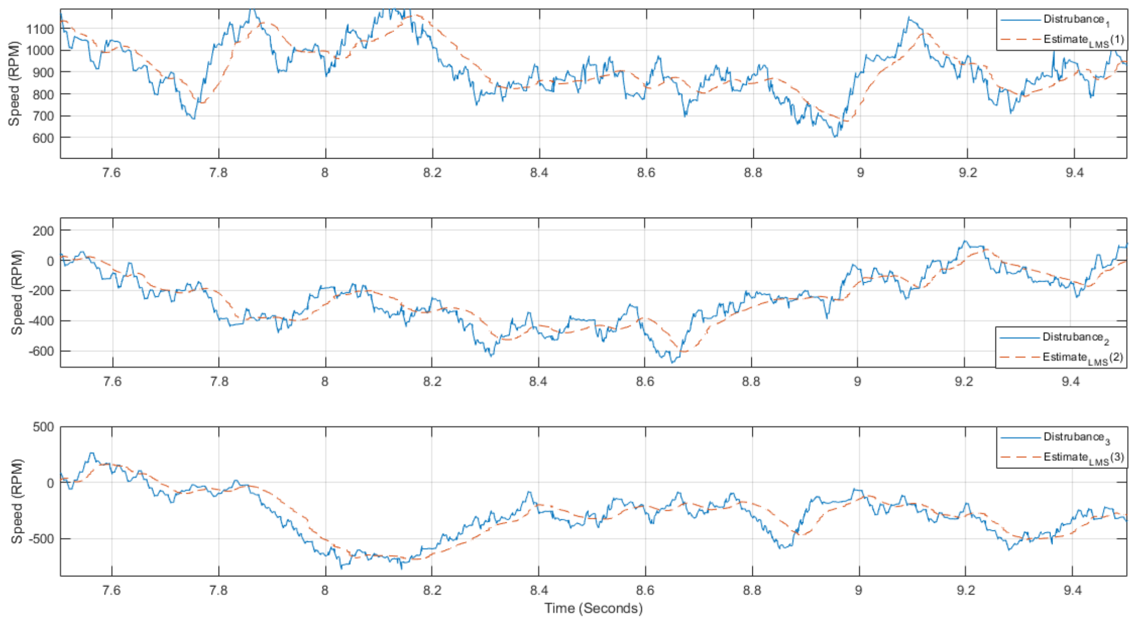

Figure 5.9 - Magnified LMS Disturbance Estimate

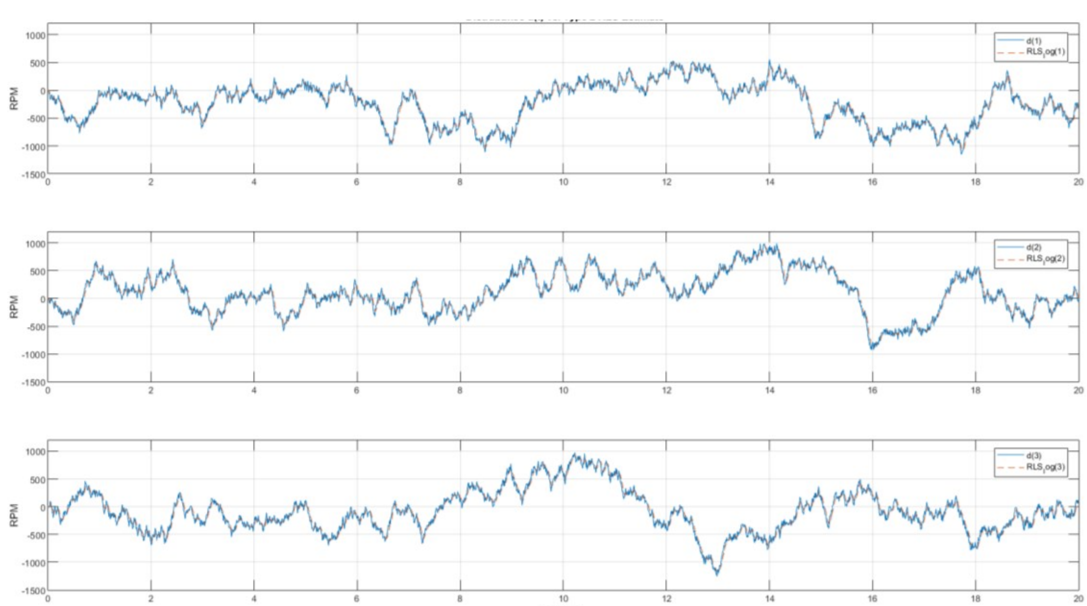

Figure 5.10 - Three State Disturbance and RLS Estimate

The results of the RLS simulation are shown in Figure 5.10. Although similar to the LMS, the RLS tracks slightly better. This can be attributed to the adaptive error correction gain of the RLS estimate, as opposed to LMS estimate's fixed gain error correction. This tracking is most notable on the higher frequency transient changes to the disturbance. To illustrate this improvement more closely, the magnified RLS estimates of this same disturbance are presented in Figure 5.11. Although the RLS improvements can be seen, this improved tracking will have negligible effects on the TC system because of its low-pass mechanical damping characteristics and inability to respond to them.

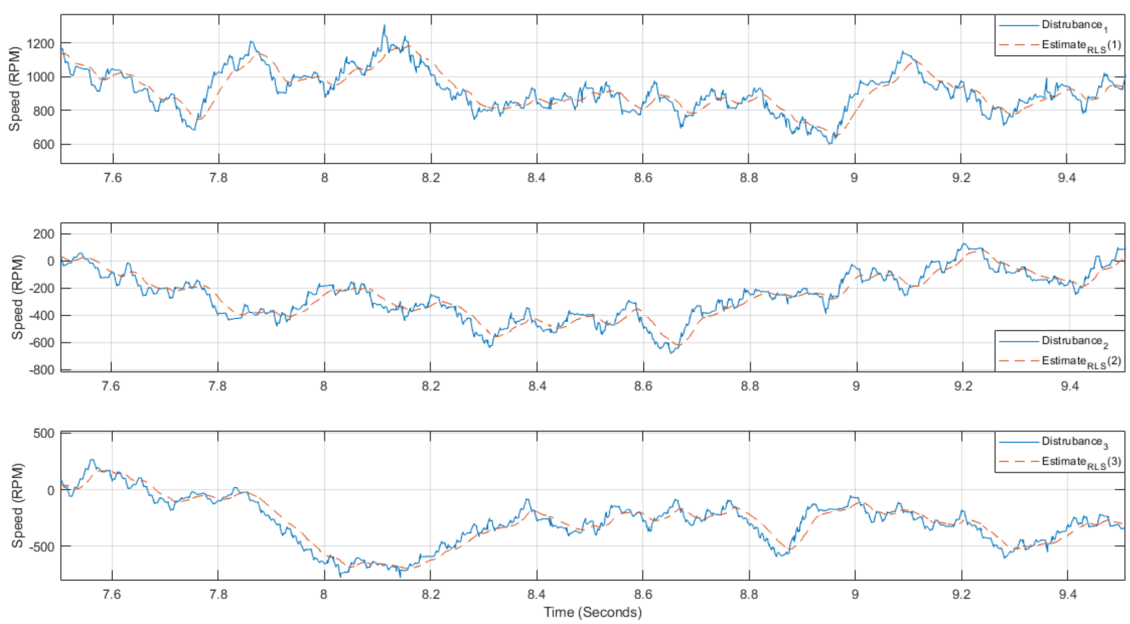

Figure 5.11 - Magnified RLS Disturbance Estimate

Figure - 5.12 presents the algebraic disturbance canceling controller, where the RLS estimated is subtracted from the true disturbance. It can be seen that this controller has rejected about 90% of the original disturbance signal acting on the TC plant and these results are presented in Figure 5.13.

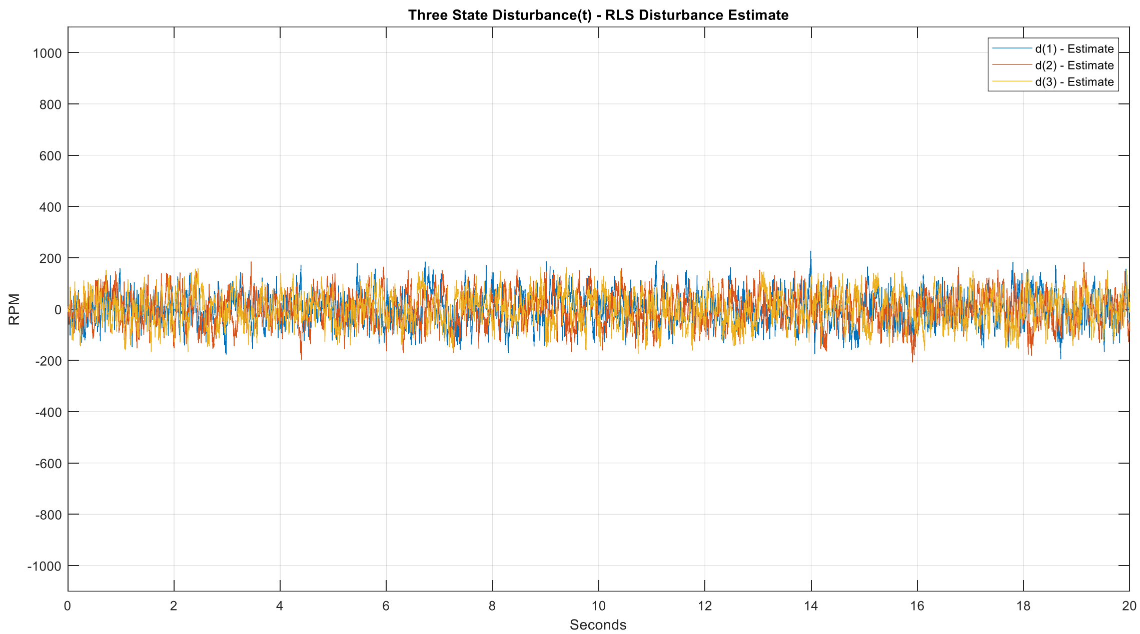

Figure 5.12 - Disturbance with RLS Estimate Cancelation

Applying the I-DOBC controller as presented in (5.42), the results of the simulation are shown in Figure 5.13. These results show almost none of the disturbances on the TC speed states. During the TCC Slip Mode, from 10 to 20 seconds of simulation, the regulator maintained 50 RPM of slip to allow the fluid coupling to isolate the ICE impulses giving the vehicle a smooth ride.

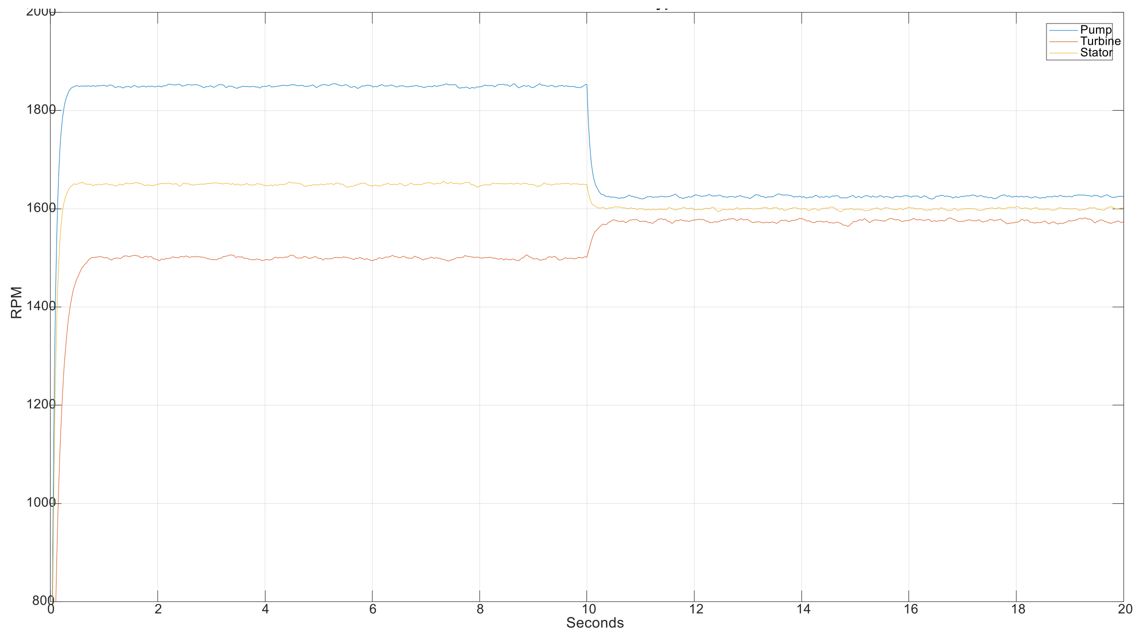

Figure 5.13 - DOBC Controller TC

In conclusion, the I-DOBC Torque Converter Clutch control method proved remarkably successful for the highly nonlinear TC system under extremely noisy state conditions that were unachievable using the D-DOBC control scheme. The robustness of this control scheme will allow the I-DOBC to be used during harsher operating conditions such as lower TCC engagement speeds as shown in Figure 5.14, larger model parameter uncertainties, and defective speed measurement equipment.

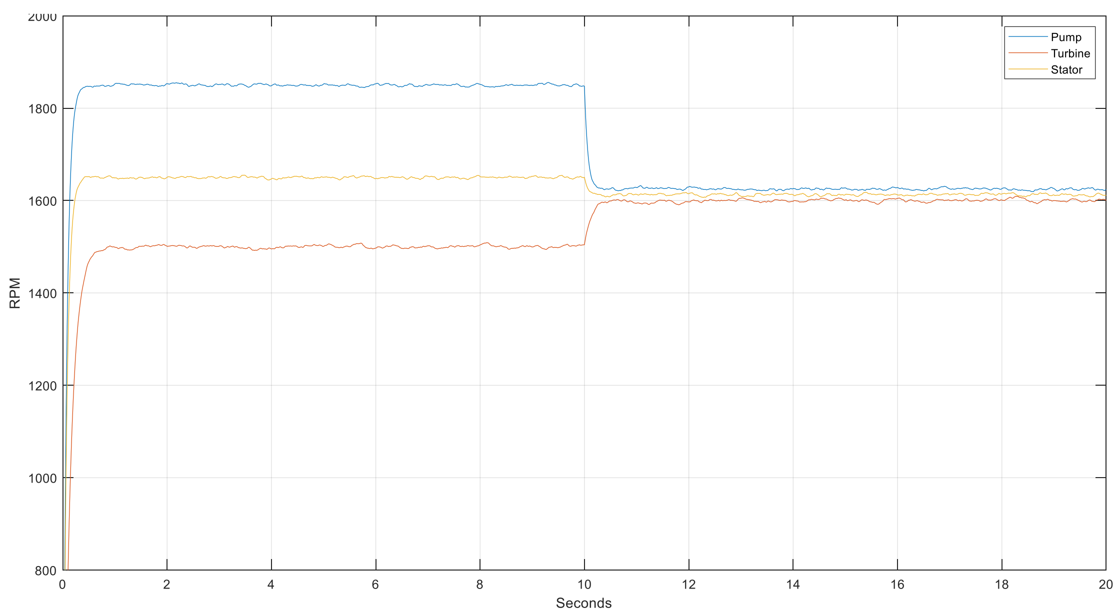

Figure 5.14 - TC State with 25 RPM of Slip Mode Control

CHAPTER SIX

A COMPARATIVE STUDY OF THE PROPOSED DISTURBANCE ACCOMMODATING CONTROLLERS

This chapter of the dissertation is an in-depth comparison of the DOPC, D-DOBC, and I-DOBC controllers presented in chapters 3, 4, and 5 respectively. In addition to a summary of their performance, a comparison of their performance including their suitability to the TC sip mode application control problem are discussed. The chapter concludes with a discussion about proposed future work.

6.1 Comparison of Complexity

This dissertation used three different strategies to control the Torque Converter Clutch engagement during slip mode operation. These methods include DA-DOPC, D-DOBC and I-DOBC.

The D-DOBC and I-DOBC DOBC are significantly more complex than the OSA controllers because of the requirement to create observers. These observers required complex matrix algebra dual systems using Ordinary Differential Equations (ODE) solvers to iterate their solutions at each time step. Setting up these simulations required complex systems of equations that required the processor to perform multiple calculations between each time step. In addition to the complexity of these calculations, both these methods require adaptation calculations to correct the observer errors.

For example, the D-DOBC method not only requires the solving the SoE

$$\begin{bmatrix} \dot{x}(t) \\ \dot{\hat{x}}(t) \\ \dot{\hat{d}}(t) \end{bmatrix} = \begin{bmatrix} A & -BK & 1 \\ LC & A - BK - LC & B_d \\ 0 & 0 & E \end{bmatrix} \begin{bmatrix} x(t) \\ \hat{x}(t) \\ \hat{d}(t) \end{bmatrix} + \begin{bmatrix} BN \\ BN \\ 0 \end{bmatrix} r(t) + \begin{bmatrix} d(t) \\ 0 \\ 0 \end{bmatrix} \tag{6.1}$$

it also requires the initial calculations of the observer matrix L and the feedback gain matrix K. The I-DOBC is even more complex in that in addition to the observers required in D-DOBC, the three-state disturbance must be calculated at each step.

6.2 Comparison of Tracking, Control Effort and Disturbance Rejection

The DA-DOPC steady state tracking with no disturbances is particularly good and is shown in Figure 6.1. Its dynamic disturbance rejection using and LMS method for 10%, 25%, 50% and 100% disturbance is shown in Figures 6.2 through 6.5, respectively. In these Figures, the “a” figures are the simulation results with a slow, $3x10^4$, Q/R weighting ratio. The “b” figures present the fast, $15x10^{15}$, Q/R weighting ratio. Throughout all these DA-DOPC simulations, the response to step inputs and steady state tracking was good. However, the robustness to disturbances varied with the weighting ratio. The low ratio interacted with the LMS disturbance rejection to cause various amounts of overshoot ringing with step inputs were introduced. In all cases this overshoot was dampened within about one second. The high weighting ratio controllers presented almost no overshot and stabilized within a few milliseconds. The LMS disturbance canceler rejects 10% (Figure 6.2) and 25% (Figure 6.3) of the disturbance inputs and maintain the slip speed between the pump, x_1, and turbine, x_3, speed of the TCC. However, when the disturbances rise to 50% (Figure 6.4) and 100% (Figure 6.5) the controller is not robust enough to reject them and has several uncontrolled spikes causing the TCC to enter locked mode.

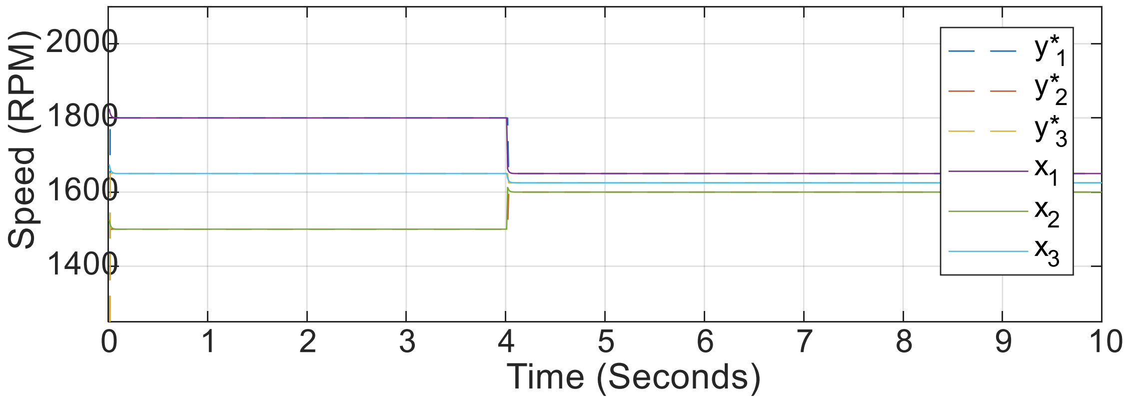

Figure 6.1 - DA-DOPC Controller without Disturbance

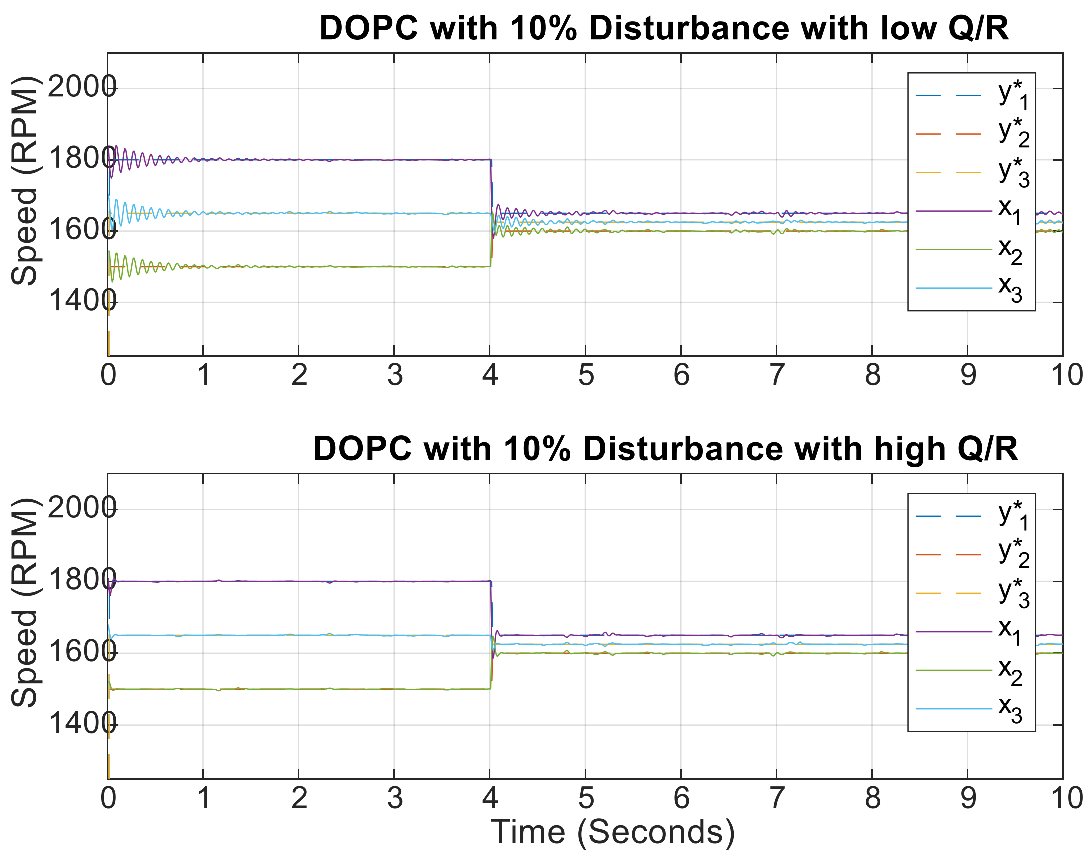

Figure 6.2 - DA-DOPC with 10% of State RPM Disturbance

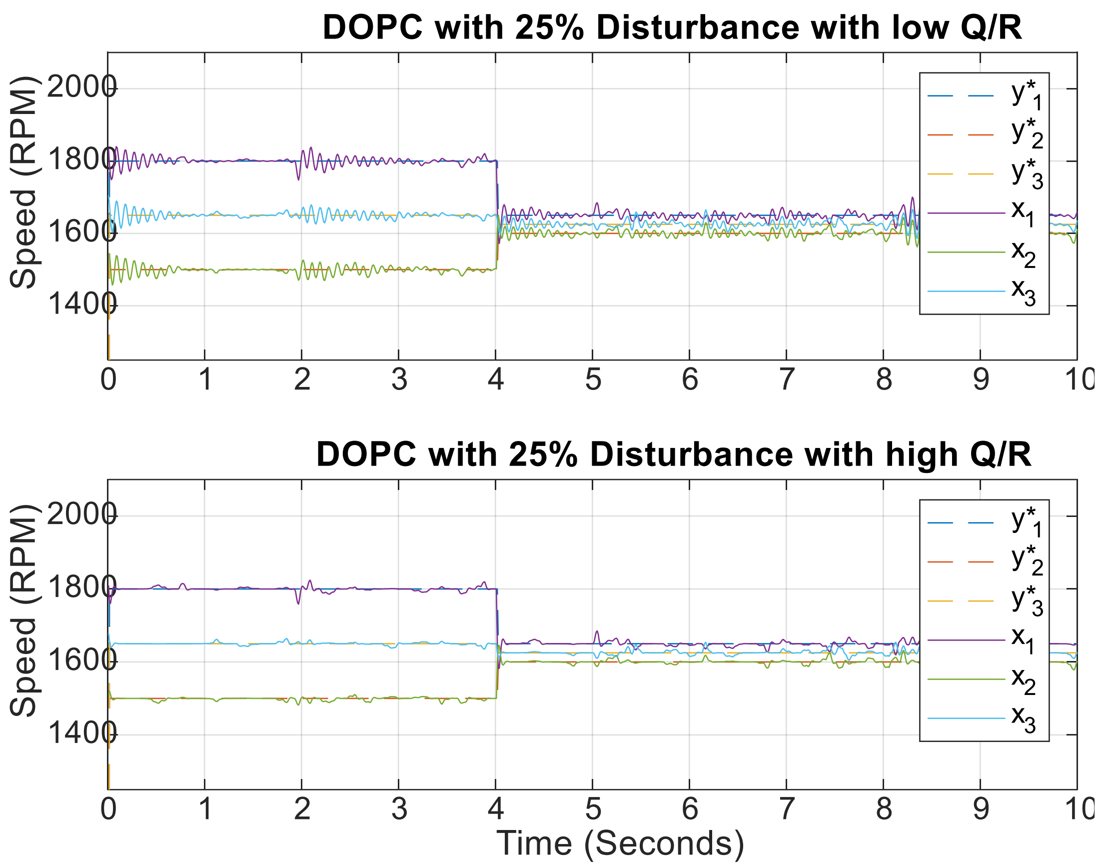

Figure 6.3 - DA-DOPC with 25% of State RPM Disturbance

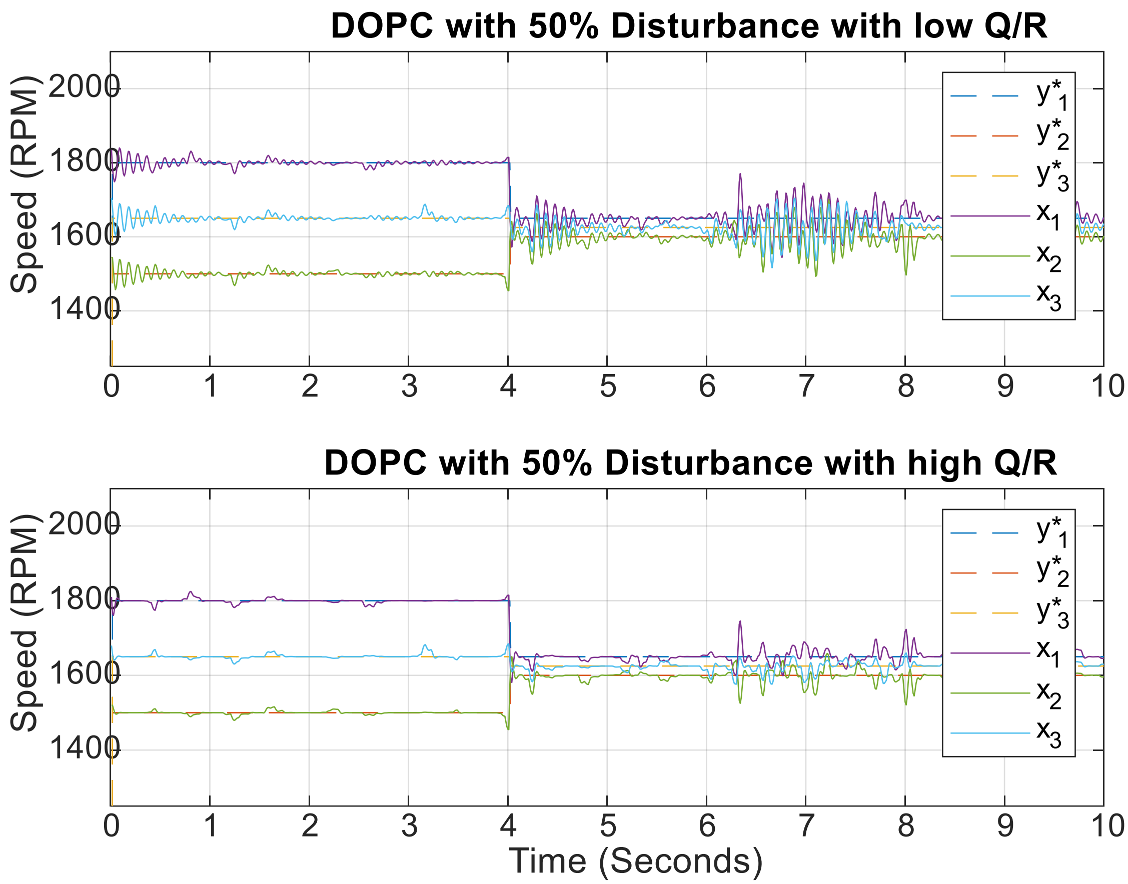

Figure 6.4 - DA-DOPC with 50% of State RPM Disturbance

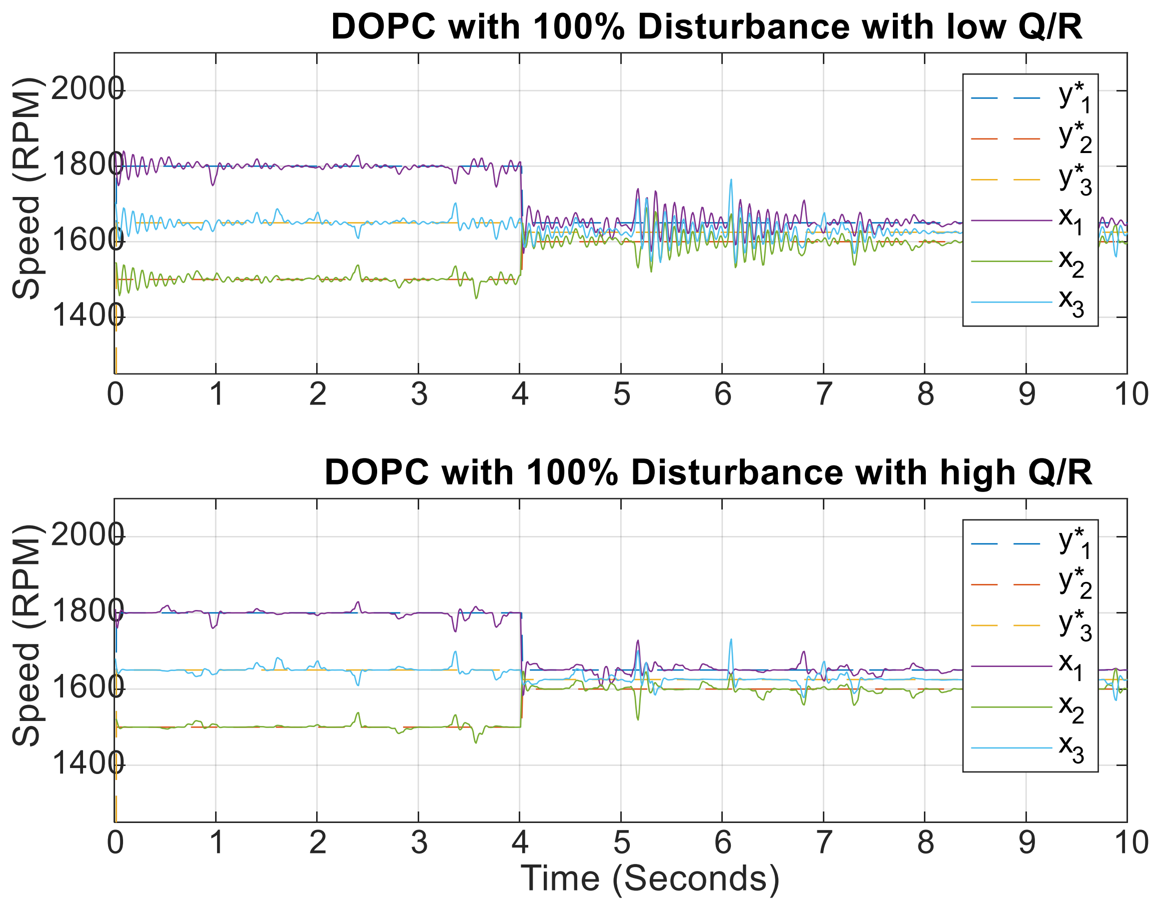

Figure 6.5 - DA-DOPC with 100% of State RPM Disturbance

The D-DOBC controller steady state tracking response is similar to DA-DOPC except during its steady state transitions. Because of the D-DOBC's lower control effort, it took about 500 milliseconds to respond to the step changes to the setpoint. This was primarily due to the time it took the D-DOBC's Unknown Input Observers (UIO) to respond. A factor in their slower response time is they have been tuned for smaller steady state errors. This tuning is also reflected in their lower control effort. This lower effort is similar to what is seen in the DA-DOPC systems.

The final controller simulated in this dissertation, I-DOBC, also did an excellent job of tracking the desired steady state reference inputs. However, the DOBC didn't respond as quickly to dramatic step inputs. This is evident in Figures 6.4 and 6.5 at 4.0 seconds into the simulation, when the reference input commands the system to 50 RPM of slip. The DA-DOPC algorithm dampens this transitional response for about 500 milliseconds. Tuning the controller to respond faster to the step input to the reference point faster is not practical because of the lowpass nature of the disturbance estimator. If it were fast enough to track this input, it would interfere with the disturbance estimator. This tuning gave more weight to steady state and disturbance robustness over quick response to setpoint changes. This tuning is preferred in this TC application because it reduces the shock transients of the TCC engagement being translated through the driveline to the vehicle thus providing a more comfortable experience to the vehicle driver. Figure 6.6 is a simulation with 10% disturbance present.

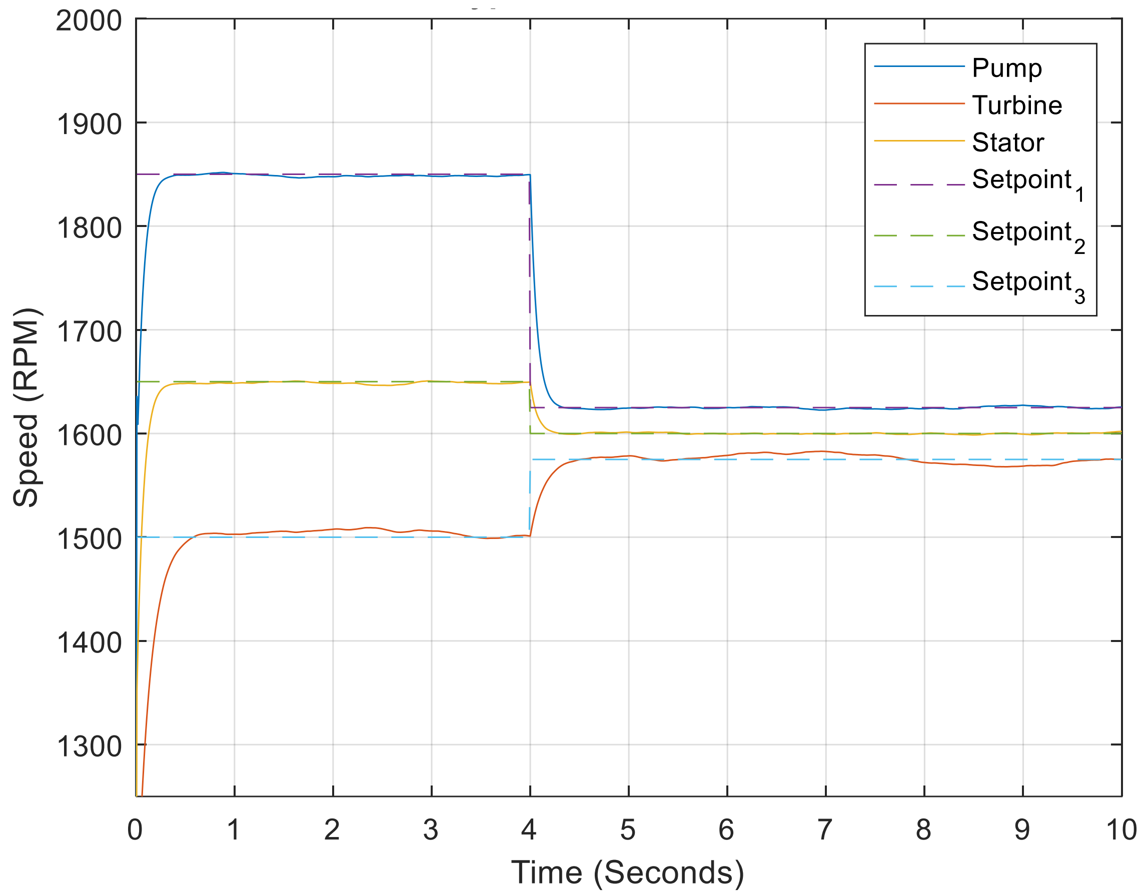

Figure 6.6 - D-DOBC with 10% of State RPM Disturbance

Figures 6.7, 6.8, and 6.9. show 25%, 50% and 100% disturbance respectively. This controller is robust to both the 10% and 25% disturbance inputs however it is marginally able to maintain TCC slip with 50% disturbance. Although not always able to prevent lockup, when it does briefly occur at 4.5 seconds in Figure 6.8, it is primarily from the over shooting of the step input opposed to the controller's inability to maintain steady state slip control. Figure 6.9 shows that the D-DOBC controller is unable to maintain steady state control of the TC and allows the TCC to move between coupled, slip controlled and locked operating modes.

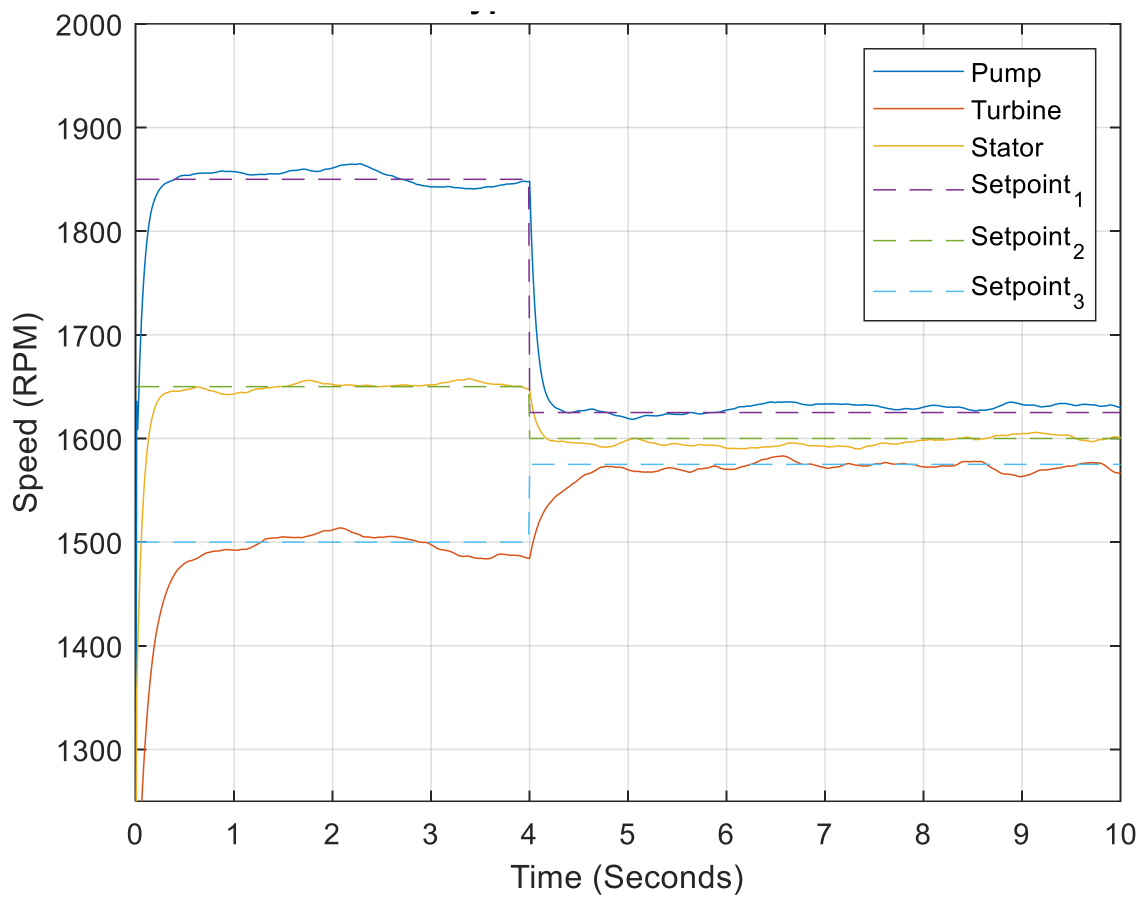

Figure 6.7 - D-DOBC with 25% of State RPM Disturbance

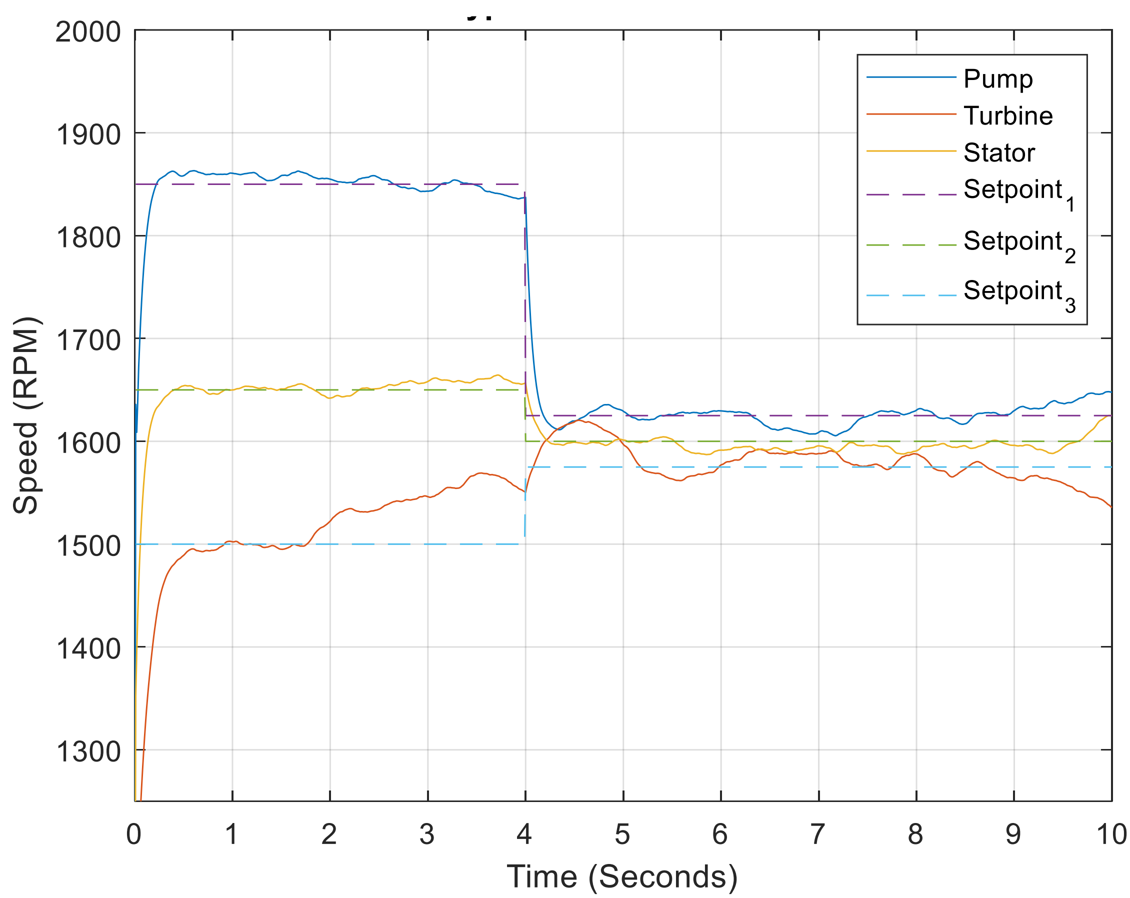

Figure 6.8 - D-DOBC with 50% Disturbance of State RPM

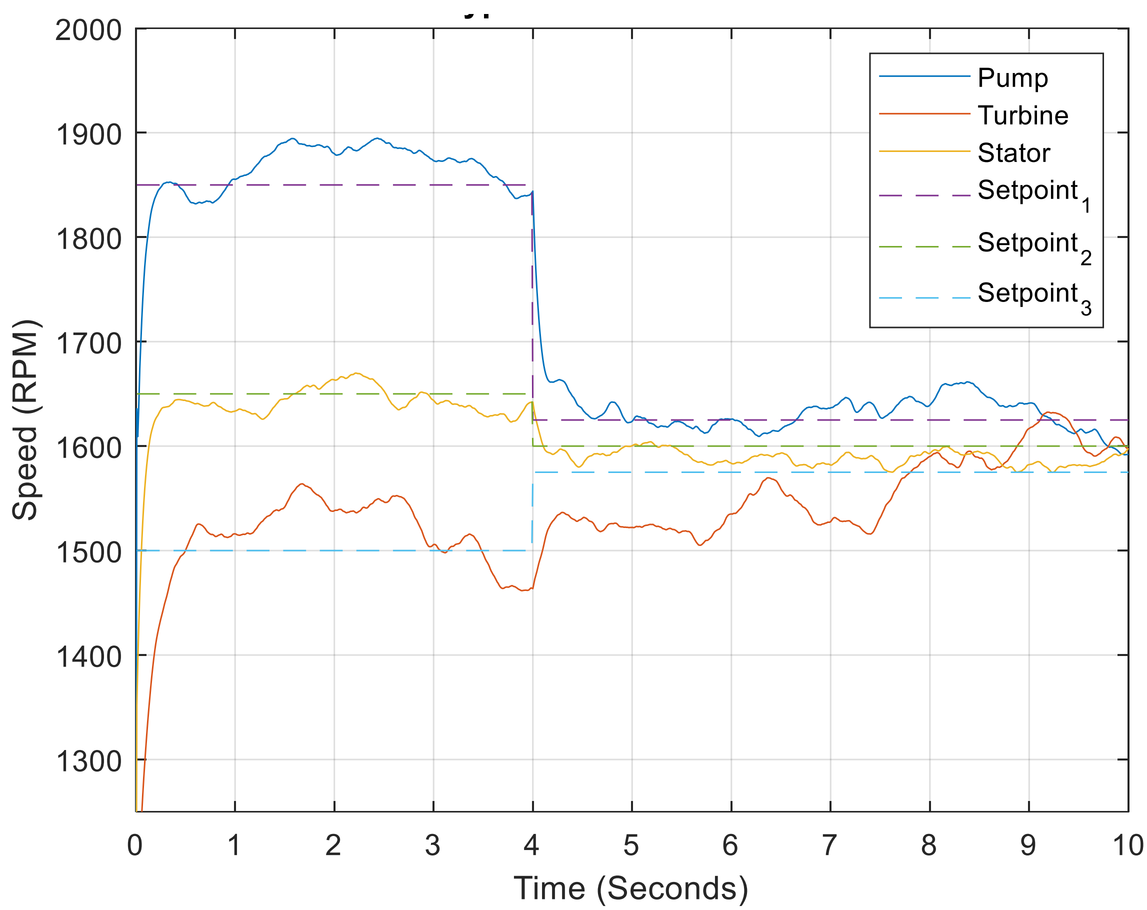

Figure 6.9 - D-DOBC with 100% Disturbance of State RPM

The final controller presented in this dissertation is an I-DOBC controlled TC. The Type control method evaluated both the LMS and RLS method for estimating the disturbance. The LMS method used a fixed step size calculation that only required two simple equations calculations per time step to identify and correct the estimation of the disturbance. The results of these estimates are presented in Figure 6.10. The estimate does an excellent job of tracking the average shape of the disturbance curve however, it is not fast enough to respond to the transient high frequency disturbances. This method would be ideally suited for slowly changing modeling parameter changes opposed to the rapid changes of the ICE torque impulses and measure dropout errors associated with the TC system.

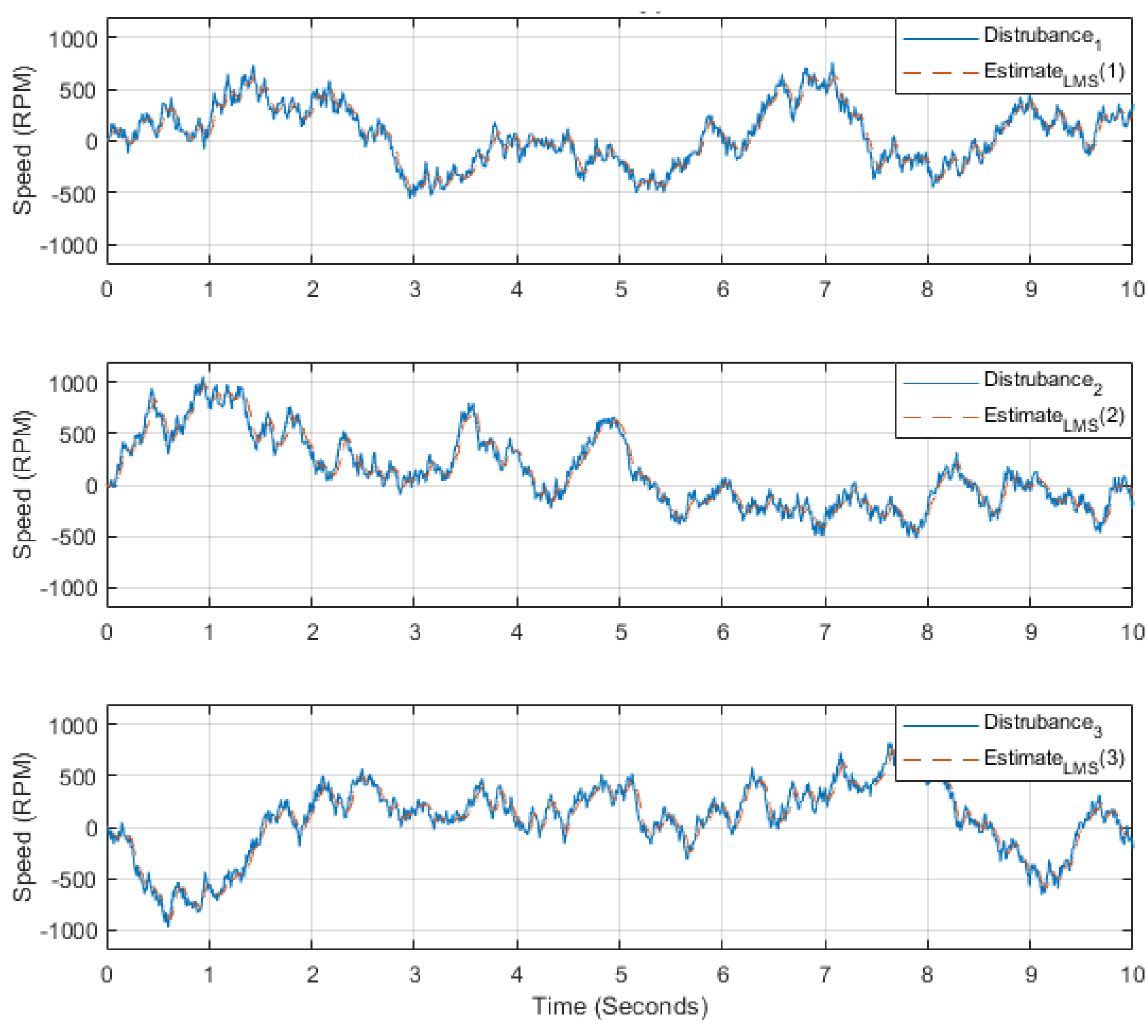

Figure 6.10 - LMS Disturbance Estimates

The second method used to estimate the disturbance on the I-DOBC controller is the RLS method. This method uses a variable gain in updating the error correction allowing the control effort to change fast enough to track the ICE and measurement errors while not use the large control efforts seen in the OSA methods to track the slow-moving changes present in this complex disturbance signal. The results of the RLS method are shown in Figure 6.11. With careful examination it can be seen that the estimate tracks the high frequency changes better than the LMS method. However, the estimate has a few milliseconds time delay from the disturbance.

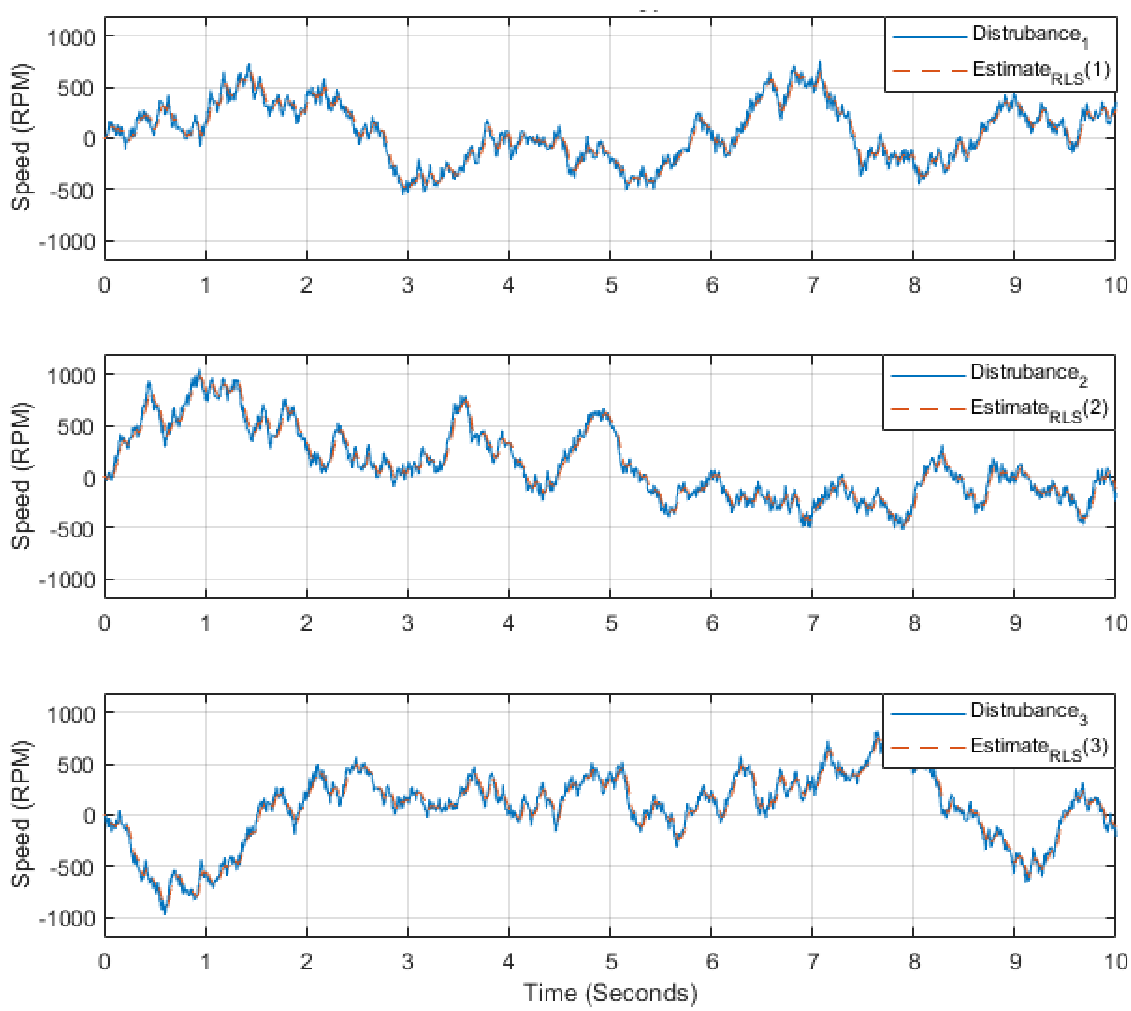

Figure 6.11 - RLS Disturbance Estimate

Because of the dampened hydraulic-mechanical reactions seen in an automotive driveline, this delay would be shorter than the response of a TTC making it appropriate to use in this application. Because of this the RLS estimation method was used though the rest of the I-DOBC simulations.

The I-DOBC results with 10% disturbance shown in Figure 6.12 are remarkably similar to the D-DOBC results shown in Figure 6.6. A notable difference is that the D-DOBC had a noticeable slowly varying ripple of about 1/3 HZ that is not present in the I-DOBC simulation. The amplitude of this ripple is a few percent of the TC's speed while it is unmeasurable on the I-DOBC controller shown in Figure 6.12.

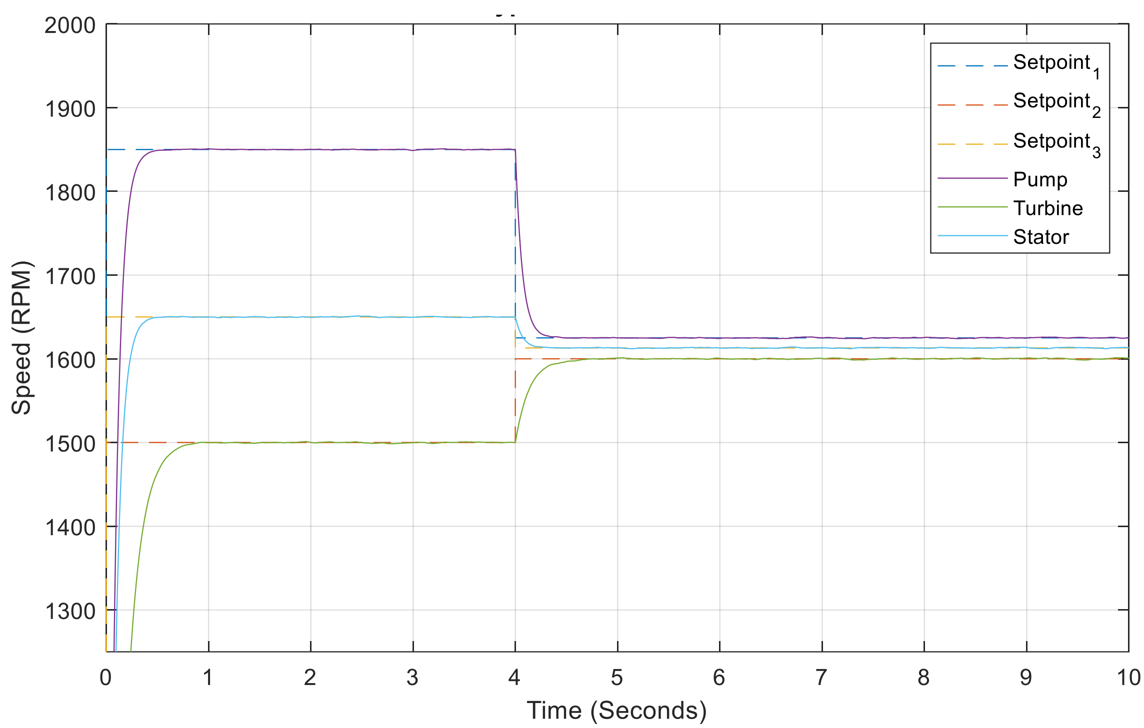

Figure 6.12 - I-DOBC with 10% Disturbance

This trend of little low frequency ripple in the I-DOBC simulation continues when 25%, 50% and 100% disturbance is applied to the TC system as shown in Figures 6.13, 6.14, and 6.15 respectively. However, the high frequency impulses amplitude and occurrences become more pronounced as the disturbance levels are increased. A careful study of the 100% disturbance shown in Figure 6.15 shows a nearly constant amplitude random occurrence disturbance of about +/- 5 RPM cancelation error is independently present on the pump, turbine, and stator speeds. These small errors are within the 25 RPM pump/turbine target slip thus allowing the TCC to remain in slip mode without locking up.

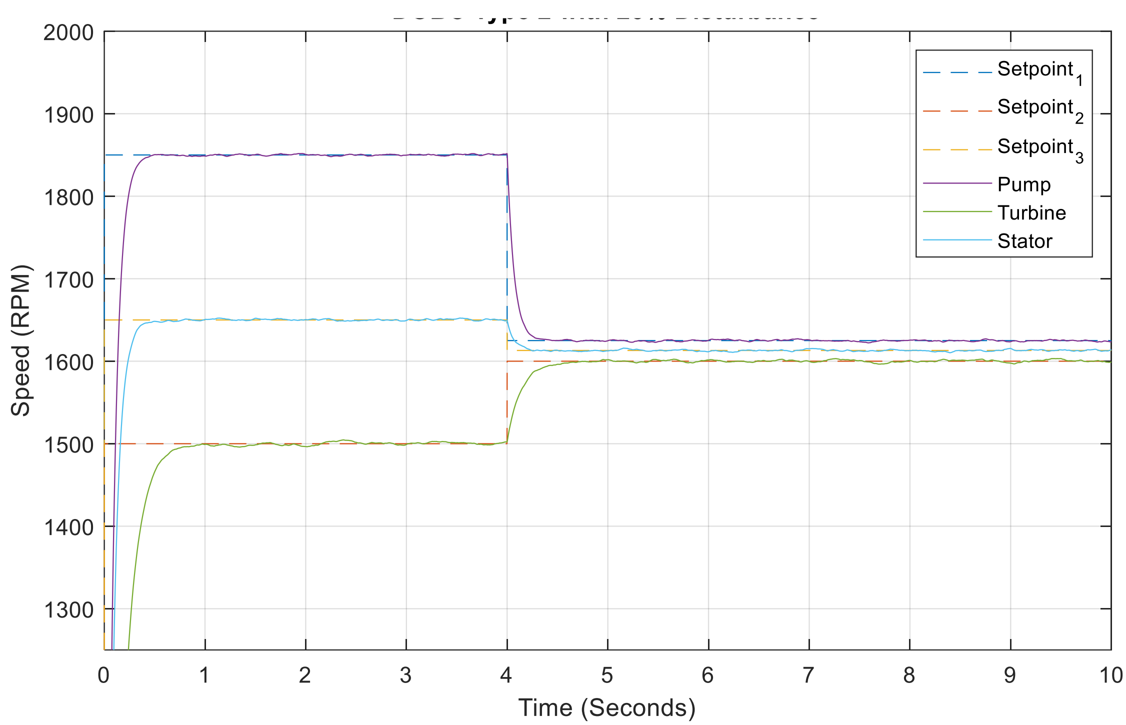

Figure 6.13 - I-DOBC with 25% of State RPM Disturbance

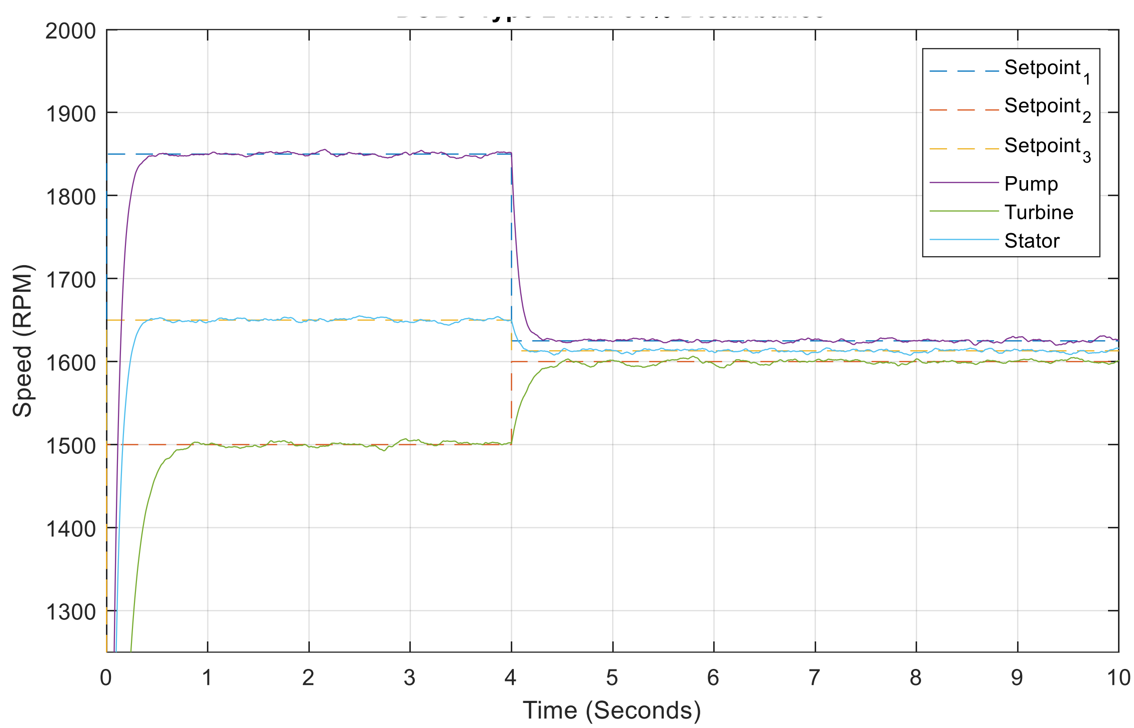

Figure 6.14 - I-DOBC with 50% of State RPM Disturbance

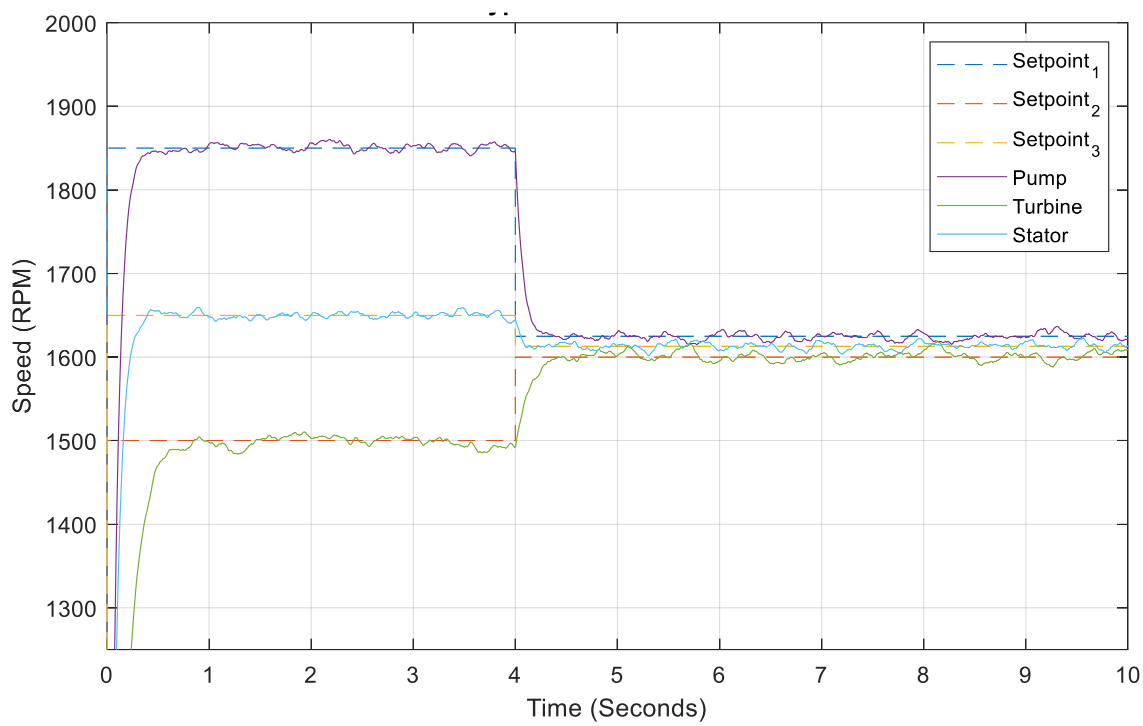

Figure 6.15 - I-DOBC with 100% of State RPM Disturbance

CHAPTER SEVEN

CONCLUSION AND FUTURE WORK

This chapter presents a few concluding remarks about the three controllers presented in Chapters 3, 4, and 5 with the observation and conclusions of the author. These remarks also address the fitment of each controller to the automatic transmission TCC slip mode application. The chapter then presents some possible extensions of the research for future work on the topic.

7.1 Conclusions

This dissertation compared three different controllers on their robustness to following a tracking reference input by simulation of a linearized model of an automotive torque converter system with disturbances added. The first controller presented is OSA based and, as they are known for, it shows a very quick response to changes to the reference input at the cost of high control efforts. Even with their quick tracking responses, they were unable to estimate, and thus anticipate and respond to the high frequency and high amplitude disturbances. This makes them not suitable for the TC TCC control application but more suitable for highly dampened applications with no more than 10% total disturbance. The DOBC controllers excelled at their robustness to disturbances. They both did well at tracking both the slow time varying changes caused by model parameter uncertainty and the rapid changes caused by the ICE torque impulses and measurement uncertainties. Their ability to work with both LMS and RSL generated estimates shows the ability of the Unknow Input Observers to estimate the random disturbances.

The I-DOBC's independent disturbance observer proved to be the most robust to disturbance. Even with 100% random disturbance introduced to the system, it was able to maintain TCC slip mode without locking up the TCC. This was not achieved without a computational cost. Second only to the D-DOBC, the I-DOBC had the highest computational cost requiring complex algorithms to be solved during each step. This powerful control algorithm is well suited to the highly uncertain and changing system parameter world of the TC.

7.2 Future Work

My future work around the control of automatic transmission TCC control will include reducing the computational load required to implement a DOBC Type controller. It is my belief that the number of observers and their strength are not required for this application. Currently UIO are created and updated for the three system speeds, the disturbance, the input, and the plant model during each time. It is my expectation that comparable results can be archived by modeling only the pump speed, corresponding to a single disturbance, and a single TCC input. It is also believed that I-DOBC internal damping is strong enough to filter most of the highly dynamic ICE and measurement errors that a LMS nor RLS estimation of the disturbances would not be necessary. Another area of intended future work would be replacing the random inputs attributed to the ICE torque inputs to the TC with known values from an existing model of an applicable ICE. This would both reduce the amplitude and frequency of this disturbance and allow for better adaptation of the unknown model parameters. This change would allow the TCC to synchronize more or less torque to counteract the combustion cycles of the ICE during each rotation. A final area that I could continue my work is in increasing the fidelity of the linear TC model. The current scope of this dissertation is looking at the effects of highly nonlinear disturbances on the steady state TCC slip mode control while holding the ICE torque applied to the pump constant. I would like to expand the linear model to include ICE and road load, via the turbine, torque inputs. This expansion would allow the TCC to compensate for driver request changes and elevation and aerodynamic changes in real-time. I believe this change would allow for the application of the TCC slip mode to additional driving applications, thus improving comfort and efficiency.

REFERENCES

[1] S. Arun, “Fuel Efficiency Improvement in Automatic Transmissions by Lockup Slip Methodology,” SAE International, 400 Commonwealth Drive, Warrendale, PA, United States, Technical Paper 0148–7191, Oct. 2019. doi: 10.4271/2019-28-0029.

[2] G. Juergen, “Automatic Transmission Systems Beyond 2020 - Challenges and Competition,” SAE International, 400 Commonwealth Drive, Warrendale, PA, United States, Technical Paper 0148–7191, Apr. 2013. doi: 10.4271/2013-01-1273.

[3] W. Thomas, “Impact of the Future Fuel Economy Targets on Powertrain, Driveline and Vehicle NVH Development,” SAE Int. J. Veh. Dyn. Stab. NVH, vol. 1, no. 2, pp. 428–438, Jun. 2017, doi: 10.4271/2017-01-1777.

[4] C. Lee, K. Ahn, J. M. Lee, and W. S. Lim, “Slip Control Strategy for an Automatic Transmission Vehicle,” J. Mech. Sci. Technol., vol. 17, no. 4, pp. 521–527, 2003, doi: 10.1007/BF02984453.

[5] S. F. d. Silva, E. d. M. Fernandes, and W. F. d. A. Junior, “Modeling and Simulation of the Performance and Efficiency of a Sport Utility Vehicle Powertrain with Automatic Transmission through Model-Based Design,” in 2018 13th IEEE International Conference on Industry Applications (INDUSCON), 2018, pp. 1128–1132. doi: 10.1109/INDUSCON.2018.8627243.

[6] D. Robinette, M. Grimmer, J. Horgan, J. Kennell, and R. Vykydal, “Torque Converter Clutch Optimization: Improving Fuel Economy and Reducing Noise and Vibration,” SAE Int. J. Engines, no. Journal Article, 2011, doi: 10.4271/2011-01-0146.

[7] V. Velayudham and S. Ravichandran, “Torque Converter Lockup Clutch Slip Modeling in NVH Simulation,” 0148–7191, 2021. doi: 10.4271/2021-01-0704.

[8] R. Hibino, M. Osawa, K. Kono, and K. Yoshizawa, “Robust and Simplified Design of Slip Control System for Torque Converter Lock-Up Clutch,” J. Dyn. Syst. Meas. Control, vol. 131, no. 1, 2009, doi: 10.1115/1.3023116.

[9] B. Kim, S. B. Choi, and Y. Kim, “Observer-Based Control for a Torque Converter Lock-Up Clutch Utilizing a Steady-State Torque Map,” IEEE Trans. Control Syst. Technol. Control Syst. Technol. IEEE Trans. IEEE Trans Contr Syst Technol, vol. 31, no. 3, pp. 1208–1219, May 2023, doi: 10.1109/TCST.2022.3214720.

[10] R. Hibino, M. Osawa, H. Yamada, K. Kono, and M. Tanaka, “H/sup /spl infin// control design for torque-converter-clutch slip system,” Proc. 35th IEEE Conf. Decis. Control Decis. Control 1996 Proc. 35th IEEE Conf. On, vol. 2, p. 1797, Jan. 1996, doi: 10.1109/CDC.1996.572828.

[11] Y. Umemura and N. Sakamoto, "Optimal Servo Design for Lock-Up Slip Control for Torque Converter-Nonlinear Output Regulation Approach," IEEE Trans. Control Syst. Technol., vol. 23, no. 4, pp. 1587–1593, 2015, doi: 10.1109/TCST.2014.2366077.

[12] A. Singh, S. Bharadwaj, and S. Narayan, "ANALYSIS OF VARIOUS NVH SOURCES OF A COMBUSTION ENGINE.," Anal. Razl. NVH IZVORA Mot. UNUTARNJIM IZGARANJEM, vol. 10, no. 1/2, pp. 29–37, Jul. 2016.

[13] A. J. Kotwicki, Dynamic models for torque converter equipped vehicles. JSTOR, 1982.

[14] J.-H. Lee and H. Lee, "Dynamic Simulation of Nonlinear Model-Based Observer for Hydrodynamic Torque Converter System," 2004. doi: 10.4271/2004-01-1228.

[15] Q. Chen, J. Wang, and Q. Ahmed, "Design and Evaluation of a Structural Analysis-Based Fault Detection and Identification Scheme for a Hydraulic Torque Converter.," Sens. 14248220, vol. 18, no. 12, p. 4103, Dec. 2018.

[16] K. D. Mishra and K. Srinivasan, "On-line Identification of a Torque Converter Model," in 20th World Congress The International Federation of Automatic Control, Toulouse, France,: The International Federation of Automatic Control, 2017, pp. 4763–4768. doi: 10.1016/j.ifacol.2017.08.952.

[17] A. A. Hadi, "Math-Based Modeling and Parametric Sensitivity Analysis of Torque Converter Performance Characteristics," SAE International, 400 Commonwealth Drive, Warrendale, PA, United States, Technical Paper 0148–7191, Apr. 2011. doi: 10.4271/2011-01-0732.

[18] H. Adibi Asl, N. Lashgarian Azad, and J. McPhee, "Modeling Torque Converter Characteristics in Automatic Drivelines: Lock-up Clutch and Engine Braking Simulation," in ASME 2012 International Design Engineering Technical Conferences & Computers and Information in Engineering Conference, Chicago, IL, USA: American Society of Mechanical Engineers, 2012, pp. 359–367. doi: 10.1115/DETC2012-70222.

[19] H. Xia and P. Oh, "A dynamic model for automotive torque converters," Int. J. Veh. Des., vol. 21, no. 4-5 SPEC. ISS., pp. 344–354, Jan. 1999, doi: 10.1504/ijvd.1999.005589.

[20] J. Maguire, H. Peng, and S. Bai, Dynamic Analysis and Control System Design of Automatic Transmissions, 1st ed. Warrendale: SAE International Books, 2013. doi: 10.4271/R-413.

[21] J. D. Jang, I. T. Lee, W. J. Kim, and D. M. Chun, "Effect of a piston hole under the slip control condition of the lock-up clutch in a torque converter," Int. J. Automot. Technol., vol. 16, no. 1, pp. 139–144, 2015, doi: 10.1007/s12239-015-0015-4.

[22] M. Buechel and A. Knoll, “A Parameter Estimator for a Model Based Adaptive Control Scheme for Longitudinal Control of Automated Vehicles,” IFAC Pap., vol. 49, no. 15, pp. 181–186, 2016, doi: 10.1016/j.ifacol.2016.07.729.

[23] S. SEGAWA et al., “Power transmission device having a torque converter with a lockup clutch and lockup control method for torque converter,” no. Generic, 2011.

[24] S. A. Nadeem, “Design of an Anti-Jerk Controller for Both Locked and Slipping Torque Converter Conditions in a Vehicle,” ProQuest Dissertations Publishing, 2020.

[25] B. P. Jagielo, Z. Zhang, Y.-Y. Wang, G. Cimini, H. Atmaram, and J. Zavala Jurado C., “MODEL PREDICTIVE CONTROL OF TORQUE CONVERTER CLUTCH SLIP,” no. Generic, 2020.

[26] B. Gao, H. Chen, H. Zhao, and K. Sanada, “A Reduced-Order Nonlinear Clutch Pressure Observer for Automatic Transmission,” IEEE Trans. Control Syst. Technol., vol. 18, no. 2, pp. 446–453, 2010, doi: 10.1109/TCST.2009.2024758.

[27] W. Wei, “Real-Time Model-Based Estimation of Transfer Case Clutch Parameters and Traction Torque,” ProQuest Dissertations Publishing, 2021.

[28] T. M. Vu, R. Moezzi, J. Cyrus, J. Hlava, and M. Petru, “Automatic clutch engagement control for parallel hybrid electric vehicle,” Energ. Basel, vol. 14, no. 21, p. 7256, 2021, doi: 10.3390/en14217256.

[29] K. Hebbale et al., “Model Based Torque Converter Clutch Slip Control,” 0148–7191, 2011. doi: 10.4271/2011-01-0396.

[30] M. Hirata, F. Iino, Y. Kaneko, and K. Y. Adachi, “Performance Enhancement of Slip Control of a Lock-Up Clutch by Using Gain-Scheduled H∞ Control Method,” Ieej Trans. Ind. Appl., vol. 130, pp. 1139–1146, 2010.

[31] C. Johnson Jr. and E. Tse, “Adaptive implementation of one-step-ahead optimal control via input matching,” IEEE Trans. Autom. Control Autom. Control IEEE Trans. IEEE Trans Autom. Contr, vol. 23, no. 5, pp. 865–872, Oct. 1978, doi: 10.1109/TAC.1978.1101867.

[32] A. J. Ross and M. Das, “Design of an Integrated Weighted One Step Ahead and Fuzzy Yaw Controller for an Electric AWD Powertrain,” 2023 IEEE Int. Conf. Electro Inf. Technol. EIT Electro Inf. Technol. EIT 2023 IEEE Int. Conf. On, pp. 314–321, May 2023, doi: 10.1109/eIT57321.2023.10187285.

[33] Q. Wang, Q. Li, and M. Zhao, “Fast Terrain-Adaptive Motion of Humanoid Robots Based on Model Reference One-Step-Ahead Predictive Control,” IEEE Trans. Control Syst. Technol., vol. 31, no. 6, pp. 2819–2834, Nov. 2023, doi: 10.1109/TCST.2023.3288295.

[34] K. S. Sin and G. C. Goodwin, Adaptive filtering prediction and control. Dover Publications, 2014.

[35] C. Lazar, E. Poli, and F. Schonberger, “Weighted one-step-ahead control for a thermal treatment furnace,” in MELCON, IEEE, 1994, pp. 743–745 vol.2. doi: 10.1109/MELCON.1994.380900.

[36] T. A. Perkins and M. Das, “Modeling and Adaptive Control of an Automotive Torque Converter Clutch System,” in EIT, IEEE, 2018, p. 928. doi: 10.1109/EIT.2018.8500098.

[37] Y. Zhao, X. Shan, W. Bi, Y. Wang, K. Yuan, and K. Zhang, “Extended Disturbance Observer Based Execution Adjustment Estimation Method of Dynamic Demand Response,” 2019 Int. Conf. Control Autom. Inf. Sci. ICCAIS Control Autom. Inf. Sci. ICCAIS 2019 Int. Conf. On, pp. 1–5, Oct. 2019, doi: 10.1109/ICCAIS46528.2019.9074729.

[38] C. D. Johnson, “Accommodation of External Disturbances in Linear Regulator and Servomechanism Problems,” IEEE Trans. Autom. Control, vol. 16, no. 6, pp. 635–644, 1971, doi: 10.1109/TAC.1971.1099830.

[39] C. Johnson, “Correction to ‘Accommodation of external disturbances in linear regulator and servomechanism problems,’” IEEE Trans. Autom. Control, vol. 18, no. 3, p. 326, 1973, doi: 10.1109/TAC.1973.1100278.

[40] E. Sariyildiz, R. Oboe, and K. Ohnishi, “Disturbance Observer-Based Robust Control and Its Applications: 35th Anniversary Overview,” IEEE Trans. Ind. Electron. Ind. Electron. IEEE Trans. IEEE Trans Ind Electron, vol. 67, no. 3, pp. 2042–2053, Mar. 2020, doi: 10.1109/TIE.2019.2903752.

[41] H. Trinh and T. Fernando, Functional Observers for Dynamical Systems, vol. 420. Berlin, Heidelberg: Springer Berlin / Heidelberg, 2011.

[42] M. Darouach, M. Zasadzinski, and S. J. Xu, “Full-order observers for linear systems with unknown inputs,” IEEE Trans. Autom. Control, vol. 39, no. 3, pp. 606–609, 1994, doi: 10.1109/9.280770.

[43] M. Darouach, “Complements to full order observer design for linear systems with unknown inputs,” Appl. Math. Lett., vol. 22, no. 7, pp. 1107–1111, 2009, doi: 10.1016/j.aml.2008.11.004.

[44] Z. Miao, D. He, A.-G. Wu, H. Kong, and M. R. James, “Coherent strong observers for a class of linear quantum stochastic systems with unknown inputs,” Automatica, vol. 146, Dec. 2022, doi: 10.1016/j.automatica.2022.110625.

[45] S. Gómez-Peñate, G. Valencia-Palomo, F. López-Estrada, C. Astorga-Zaragoza, R. A. Osornio-Rios, and I. Santos-Ruiz, "Sensor Fault Diagnosis Based on a H∞ Sliding Mode and Unknown Input Observer for Takagi-Sugeno Systems with Uncertain Premise Variables.," Asian J. Control, vol. 21, no. 1, pp. 339–353, Jan. 2019.

[46] Z. Ding, "Consensus Disturbance Rejection With Disturbance Observers," IEEE Trans. Ind. Electron. 1982, vol. 62, no. 9, pp. 5829–5837, 2015, doi: 10.1109/TIE.2015.2442218.

[47] S. Nazari, "The Unknown Input Observer and its Advantages with Examples," no. Journal Article, 2015.

[48] Y. Yang, D. Yue, and Z. Gu, "Observer-based adaptive fault-tolerant control of a class of nonlinear systems with actuator failures," in 2016 UKACC 11th International Conference on Control (CONTROL), 2016, pp. 1–6. doi: 10.1109/CONTROL.2016.7737605.

[49] P. Tomei and C. M. Verrelli, "Observer-Based Speed Tracking Control for Sensorless Permanent Magnet Synchronous Motors With Unknown Load Torque," IEEE Trans. Autom. Control, vol. 56, no. 6, pp. 1484–1488, 2011, doi: 10.1109/TAC.2011.2121330.

[50] W.-H. Chen, J. Yang, L. Guo, and S. Li, "Disturbance-Observer-Based Control and Related Methods-An Overview," IEEE Trans. Ind. Electron. 1982, vol. 63, no. 2, pp. 1083–1095, 2016, doi: 10.1109/TIE.2015.2478397.

[51] S. O. Omekanda, T. A. Perkins, and M. A. Zohdy, "Robustness Analysis of Linear Time-Invariant Dynamic State Observers," ASCE J., no. Journal Article, 2014.

[52] T. A. Perkins and M. Das, "Modeling and Control of Torque Converter Clutch Using a Disturbance Observer based Tracking Controller," 2023 IEEE Int. Conf. Electro Inf. Technol. EIT Electro Inf. Technol. EIT 2023 IEEE Int. Conf. On, pp. 399–405, May 2023, doi: 10.1109/eIT57321.2023.10187311.

[53] P. Otanez, F. Samie, C. J. Lee, and C.-K. Kao, "Aggressive Torque Converter Clutch Slip Control and Driveline Torsional Velocity Measurements," SAE Int. J. Fuels Lubr., vol. 1, no. 1, pp. 883–892, Jan. 2009.

[54] H. Adibi Asl, N. Lashgarian Azad, and J. McPhee, "Math-based torque converter modelling to evaluate damping characteristics and reverse flow mode operation," Int. J. Veh. Syst. Model. Test. Ijvsmt, vol. 9, no. 1, pp. 36–55, 2014, doi: 10.1504/IJVSMT.2014.059155.

[55] Xi Chen and Liuping Wang, "Discrete-time one-step ahead prediction control (DOPC) of a Quadcopter UAV with constraints," 2016 Aust. Control Conf. AuCC

Control Conf. AuCC 2016 Aust., pp. 180–185, Nov. 2016, doi: 10.1109/AUCC.2016.7868184.

[56] B. Yu, S. Kim, and J. Suk, "Robust Control based on ADRC and DOBC for Small-Scale Helicopter," Elsevier Ltd, 2019, pp. 140–145. doi: 10.1016/j.ifacol.2019.11.183.

[57] K. Ogata, Modern control engineering, 5th ed. London: Pearson, 2010.

[58] Das, Manohar, "Multivariable Adaptive Pole Assignment," Dissertation, Colorado State University, 1984.

[59] H. Garnier and L. Wang, Identification of continuous-time models from sampled data. in Advances in industrial control. Springer, 2008. [Online]. Available: https://search.ebscohost.com/login.aspx?direct=true&AuthType=sso&db=cat09721a&AN=ouc.oai.edge.oakland.folio.ebsco.com.fs00001142.b61364bf.c94f.4435.a243.c93b4eb9c875&site=eds-live&scope=site&authtype=sso&custid=s9275379

[60] D. K. Malav and R. Taparia, "Sliding mode control of yaw movement based on Ackermann's formula," 2017 Int. Conf. Comput. Commun. Electron. Comptelix Comput. Commun. Electron. Comptelix 2017 Int. Conf. On, pp. 628–632, Jul. 2017, doi: 10.1109/COMPTELIX.2017.8004045.

PUBLICATIONS

Journal Publications:

ICGST/ACSE(10-2014) - Nonlinear State Control Optimized by Lyapunov and Riccati via Piecewise Linear ...(Perkins/Zohdy)

ICGST/ACSE(4-2014) - Robustness Analysis of Linear Time-Invariant Dynamic State Observers (Omekenda/Perkins/Zohdy)

Conference Proceedings:

EIT 2023/IEEE (05/2023) - Modeling and Control of Torque Converter Clutch Using a Disturbance Observer based Tracking Controller

EIT 2018/IEEE (05-2018) - Modeling and Adaptive Control of an Automotive Torque Converter Clutch System (Perkins/Das)

Other Publications:

ASEE (4-2013) - When is a Motor More Than an Electromechanical Device: Teaching K-12 STEM Subjects through Hands-on Experiments

Design of a Disturbance Accommodating Discrete One Step Ahead Controller for an Automotive Torque Converter Clutch System (to be submitted).

Design of a Direct Disturbance Observer Based Controller for an Automotive Torque Converter Clutch System (to be submitted).

Design of an Indirect Disturbance Observer Based Controller for an Automotive Torque Converter Clutch System (to be submitted).